European summer weather linked to North Atlantic freshwater anomalies in preceding years

Marilena Oltmanns[1], N. Penny Holliday[1], James Screen[2], Ben I. Moat[1], Simon A. Josey[1], D. Gwyn Evans[1], and Sheldon Bacon[1]

[1]National Oceanography Centre, Southampton, UK
[2]University of Exeter, Exeter, UK

Correspondence: Marilena Oltmanns (marilena.oltmanns@noc.ac.uk)

Abstract. Amplified Arctic ice loss in recent decades has been linked to increased occurrence of extreme mid-latitude weather. The underlying mechanisms remain elusive, however. One potential link occurs through the ocean as the loss of sea ice and glacial ice leads to increased freshwater fluxes into the North Atlantic. Thus, in this study, we examine the ~~role of~~ link between North Atlantic freshwater anomalies ~~in medium-term climate trajectories and specifically assess their links to~~ and European summer weather. Combining a comprehensive set of observational products, we show that stronger freshwater anomalies are associated with a sharper sea surface temperature ~~gradients over the~~ front between the subpolar and the subtropical North Atlantic in winter, ~~destabilising the overlying atmosphere and inducing a~~ an increased atmospheric instability above the sea surface temperature front, and a large-scale atmospheric circulation that induces a northward shift in the North Atlantic Current, ~~In turn,~~ shifting and strengthening the sea surface temperature front. In the following summer, the jet stream ~~over the North Atlantic is deflected northward in the following summers~~ is deflected along the enhanced sea surface temperature front and the European coastline, leading to warmer and drier weather over Europe. ~~Our results suggest that growing freshwater fluxes into the North Atlantic could initiate a chain of ocean-atmosphere feedbacks that increases the risk of heat waves and droughts over Europe , and that could yield~~ Accordingly, we find that stronger freshwater anomalies in the subpolar North Atlantic in winter are followed by warmer and drier weather over Europe in the subsequent summer, with the regions of the warm and dry anomalies being sensitive to the location, strength and extent of the North Atlantic freshwater anomalies in the preceding winter. The identified statistical links are significant on timescales from years to decades and indicate an enhanced predictability of European summer weather ~~, months to years~~ several months in advance.

1 Introduction

Arctic near-surface temperature is currently warming twice as fast as the global average (Cohen et al., 2019), which manifests itself in an average sea ice volume loss of $3.0 \pm 0.2 \cdot 1000$ km^3 decade^{-1}, based on the period 1979 to 2018 (Kumar et al., 2020). Similarly large losses are observed for land ice, particularly from the Greenland ice sheet, amounting to $3.0 \pm 0.3 \cdot 1000$ km^3 decade^{-1}, based on the period 2003 to 2012 (Khan et al., 2015). Earlier studies noticed statistical links between an amplified sea ice loss at high latitudes and an increased occurrence of weather extremes at mid-latitudes (Francis and Vavrus,

2012; Tang et al., 2014; Screen and Simmonds, 2013; Cohen et al., 2014). However, the robustness of these links has been

25 questioned and the underlying mechanisms are poorly understood (Barnes, 2013; Overland et al., 2015; Blackport and Screen, 2020).

One potential connection occurs through the ocean. Specifically, the loss of sea ice and glacial ice in the Arctic and sub-Arctic regions constitutes a source of freshwater for the North Atlantic (Bamber et al., 2018; Carmack et al., 2016). Large North Atlantic freshwater anomalies, moreover, were found to give rise to cold surface anomalies and the development of storms in

30 the subpolar region in winter (Oltmanns et al., 2020). In turn, cold anomalies in the subpolar region in winter were found to precede heat waves over Europe in the subsequent summer (Duchez et al., 2016; Mecking et al., 2019). The heat waves were attributed to a stationary jet stream over the North Atlantic (Duchez et al., 2016) and were successfully reproduced in model simulations initialised with the cold anomaly (Mecking et al., 2019). Thus, by triggering cold anomalies in winter, increased surface freshening could initiate a deterministic chain of events that first leads to cold anomalies and storms in winter and then

35 heat waves in the subsequent summer.

While earlier studies support individual connections between the North Atlantic sea surface temperature (SST) and the jet stream (Woollings et al., 2010), or between shifts in the jet stream and European heat waves (Dong et al., 2013; Gervais et al., 2020), the role of freshwater in initiating this causal chain is unclear. Yet, given that the Arctic and sub-Arctic regions are expected to continue to warm and release freshwater from melting sea ice and glacial ice into the North Atlantic, it is critical

40 to understand how the resulting feedbacks will affect weather in Europe.

The gap in our knowledge around the potential influences of North Atlantic freshwater anomalies on European summer weather arises from the difficulty to ~~observe and~~ simulate salinity. Freshwater ~~is advected into~~ enters the subpolar region through narrow boundary currents and mesoscale eddies requiring a ~~high~~ fine grid spacing of ∼1/12° (Marzocchi et al., 2015; Böning et al., 2016; Müller et al., 2019). Most current coupled global climate models have a coarser grid spacing, giving

45 rise to salinity biases (Mecking et al., 2017; Menary et al., 2015; Wu et al., 2018). ~~Moreover, in-situ~~ From an observational perspective, estimating freshwater variations is also difficult. In-situ observations of sea surface salinity mostly stem from Argo floats ~~and cannot capture the high~~ which cannot fully capture the large spatial variability at high temporal resolution. ~~Lastly~~Moreover, satellite observations of sea surface salinity are associated with large uncertainties and only available since 2009 (Bao et al., 2019; Xie et al., 2019).

50 Given the limitations associated with ~~the~~ currently available model and observational products of sea surface salinity, we use a new approach to estimate freshwater variations, taking advantage of a dynamical constraint of the sea surface salinity on the SST. In the subpolar region in ~~winter, surface~~ autumn and winter, the air is colder than the ocean surface. Thus, the surface water is cooled by the atmosphere, becomes denser, and sinks. Enhanced surface freshening reduces the surface density and ~~thus~~ requires additional cooling before the surface water is dense enough to ~~be mixed down. When salinity changes are the~~

55 ~~dominant driver of stratification changes, this~~ sink. This constraint of freshwater on the ~~SST~~ surface cooling can be used to infer its variability using a mass balance analysis (Oltmanns et al., 2020).

In the following, we describe the involved data products (Section 2)~~and~~. We then explain the approach to estimate freshwater variability from a surface mass balance (Section 3). ~~We then use the approach to identify freshwater anomalies, examine~~

2

~~the associated~~ In Section 4, we examine the ocean-atmosphere evolution associated with freshwater anomalies, and assess their links with European summer weather based on statistical analyses (Section 4). We conclude by discussing the dynamical ~~contribution~~ role of freshwater anomalies ~~to the identified chain of events and their implications~~ in the identified ocean-atmosphere evolution and the implications for predictability (Section 5).

2 Data

First, we describe the ~~data~~ observational products involved in this study ~~. To examine the ocean-atmosphere feedbacks associated with freshwater anomalies,~~ and describe any processing steps. Since the analyses are based on statistical methods, a high data quality is important. Thus, we focussed on the period since 1979, motivated by the increased data quality associated with the onset of satellite observations in 1979. ~~For assessing longer-term variations in North Atlantic freshwater variability, we also considered the period since 1950.~~

2.1 Datasets

2.2 ~~Observations~~

The analysis of ocean variability includes a merged SST product consisting of Hadley Centre HadISST1 data (Rayner et al., 2003; Hurrell et al., 2008) and optimal-interpolated, remote sensing-based SST data from NOAA (Reynolds et al., 2002). The merged Hadley – NOAA data product has a monthly temporal resolution, a 1° x 1° spatial resolution and is available from https://gdex.ucar.edu/dataset/158_asphilli.html.

~~We further employed~~ To assess changes in surface currents, we further used absolute dynamic topography data since 1993, derived from altimetry (Le Traon et al., 1998). Absolute dynamic topography represents the sea level anomaly with respect to the geoid and thus, the stream function of the geostrophic surface flow. ~~It is used to assess changes in surface currents.~~ The monthly, gridded, absolute dynamic topography dataset has a spatial resolution of 0.25° x 0.25° and is distributed by the Copernicus Marine Environment Monitoring Service (https://marine.copernicus.eu/).

~~In addition, we included in-situ hydrographic observations from a mixed-layer database derived from Argo float profiles (Holte et al., 2017),~~ Geostrophic surface velocities were calculated from the absolute dynamic topography using $u_g = -\frac{g}{fR_E}\frac{\partial \eta}{\partial \theta}$ and ~~raw Argo profiles. The data is used~~ $v_g = \frac{g}{fR_E cos(\theta)}\frac{\partial \eta}{\partial \phi}$, where u_g and v_g are the zonal and meridional velocities, η is the absolute dynamic topography, g is the gravitational acceleration, f is the Coriolis parameter, R_E is the Earth's radius, and θ and ϕ are the latitude and longitude respectively.

Moreover, to compare freshwater anomalies, estimated from the surface mass balance analysis, with in-situ observations ~~and to assess the vertical extent of air-sea coupling processes in summer. Argo data is available at~~ from the subpolar North Atlantic, we included a hydrographic, mixed layer database. The dataset provides mixed layer depths, mixed layer salinities, and mixed layer temperatures, derived from Argo float profiles (Holte et al., 2017). It is freely available at http://mixedlayer.ucsd.edu.

The ocean data is complemented by monthly output from the ERA5 atmospheric reanalysis model from the European Centre for Medium-Range Weather Forecasts since 1979 (Hersbach et al., 2018). In addition to the standard variables from ERA5, we estimated the maximum Eady growth rate. The maximum Eady growth rate is used to assess the baroclinic instability in the atmosphere over increased meridional SST gradients. Following earlier studies (Lindzen and Farrell, 1980; Dierer et al., 2005), we estimated the maximum Eady growth rate in the 1000 hPa to 750 hPa layer with $\sigma_E \approx 0.31 \frac{f}{N} \mid \frac{u_{750}-u_{1000}}{z_{750}-z_{1000}} \mid$, where f is again the Coriolis frequency, u is the zonal wind, z the height, N the Brunt-Väisälä frequency and the subscripts refer to the associated pressure levels.

A key parameter, used to derive freshwater indices, is the mean North Atlantic Oscillation (NAO)in summer, obtained from the National Oceanic and Atmospheric Administration (NOAA) Climate Prediction Center. The NAO index was calculated using Rotated Principal Component Analysis, applied to the monthly standardised 500 hPa geopotential height anomalies between 20°N and 90°N (Barnston and Livezey, 1987) and identified as the dominant mode of variability in the northern hemisphere. A detailed derivation can be found at https://www.cpc.ncep.noaa.gov/products/precip/CWlink/pna/nao.shtml.

2.2 Model simulations

While the study is based on observationsLastly, we included model simulations to address specific processes. Thus, we used data from the Greenland climate model MAR to assess potential causes of freshwater anomalies. We used version 3.12, run at a resolution of 20 km forced by the ERA5 reanalysis (Fettweis et al., 2017) and distributed by the Laboratory of Climatology at the University of Liège. For the purpose of this study, we considered the runoff over the full ice sheet from 1950 through to the end of 2022 at monthly resolution. The dataset is available at ftp://ftp.climato.be/fettweis/MARv3.12.

To investigate the role of the SST in driving the atmospheric circulation, we employed SST-forced simulations from ECHAM5 (Roeckner et al., 2003) and CAM5 (Neale et al., 2012), obtained from the Facility of Climate Assessments repository (Murray et al., 2020). The simulations were performed with the prescribed, observed SST and sea ice cover and time varying greenhouse gases and ozone. Further details on the experimental setup can be obtained from . ECHAM5 was run with a horizontal grid spacing of 0.75° x 0.75°, 31 vertical levels and 50 ensemble members, and CAM5 was run with a horizontal grid spacing of 1° x 1°, 30 vertical levels and 40 ensemble members. We excluded other models from the repository that do not cover the period 1979–2018 or that do not include all investigated parameters.

2.2 Removing greenhouse gas effects

2.2 Preprocessing

The recent period was characterised by a significant trend of increasing greenhouse gas concentrations, implying that the warming trend Over the investigated period, the climate has been characterised by increasing greenhouse gas concentrations, leading to enhanced surface warming (Lashof and Ahuja, 1990). Over the last two decades, moreover, the freshening has also been increasing (Tesdal et al., 2018), particularly because of increased runoff and melting from Greenland (Bamber et al., 2012, 2018). Thus, the surface warming resulting from increased greenhouse gases could superimpose on a potential warming trend due

~~to freshwater anomalies and distort their effect on European air temperatures. To~~ potential surface cooling or warming signals resulting from changes in the ocean or atmospheric circulations associated with increased North Atlantic surface freshening. This superposition could distort the interpretation of the statistical analyses when assessing the specific influences of changes in the ocean and atmospheric circulations associated with increased North Atlantic freshening.

Considering that the freshening trend is an important part of the signal we are investigating, removing trends at each location (or grid point) would remove an important part of a signal that we are interested in. Thus, to reduce the influence of increasing greenhouse gas concentrations on European air temperatures, we ~~subtracted~~ subtract regionally averaged trends from the air temperature~~, both in ERA5 and the model simulations. By using regional averages, we assumed that the trend of the direct, greenhouse gas-induced warming over Europe is distributed relatively uniformly~~. The method of subtracting regionally averaged trends is motivated by the observation that greenhouse gases are distributed comparatively uniformly in the atmosphere (Reuter et al., 2020) whereas the observed surface warming exhibits large regional differences (Simmons, 2022). These regional differences in surface warming result from changes in the ocean and atmospheric circulations, which are redistributing the excess heat. Since, in this study, we are specifically interested in these dynamic processes associated with changes in the ocean and atmospheric circulations, we are subtracting a spatially uniform warming trend associated with increasing greenhouse gases.

We tested different regions and found that the results are not sensitive to the exact area that is used for the averaging, as long as it is sufficiently large. Here, we averaged over the main area of investigation from 25 °N to 65 °N and from 60 °W to 60 °E, resulting in an average trend of ~~~0.03~~ ~ 0.04 °C year^{-1} in the 2-m air temperature from ERA5. Extending the region in any direction does not appreciably change this trend, nor the subsequent results, consistent with the assumption that the direct warming trend that is solely due to increasing greenhouse gases is distributed relatively uniformly.

~~Since the freshening of the subpolar North Atlantic exhibited a trend over the recent period (Tesdal et al., 2018), trends are part of the signal we are interested in. In contrast to greenhouse gas induced warming , however, we do not expect the freshwater trend to cause any net imbalance in the net surface energy budget. Instead, considering the delineated links between fresh and cold anomalies, the jet stream, and European summer weather, we expect freshwater anomalies in the North Atlantic to be linked to baroclinic instabilities in the atmosphere, which equally produce warming regions and cooling regions. Thus, by subtracting regionally-averaged signals, we filter out the uniform warming effect of increasing greenhouse gases from those associated with baroclinic wave activity.~~

~~Indeed, when we remove the~~ While the summer air temperature is strongly affected by a spatially uniform warming trend, the other variables exhibit no or only minor trends after they have been averaged over a large area. Thus, after removing the trend in the air temperature prior to the analyses, we obtain a signal that is dynamically consistent across all investigated variables. If, on the other hand, we do not remove the trend in the air temperature, we still obtain the same patterns throughout the results but there would be a large-scale, uniform warming signal superimposed over the full domain.

We did not apply any other averaging, smoothing, filtering, or further preprocessing steps to the datasets.

3 Estimation of freshwater anomalies

155 The objective of this study is to investigate feedbacks initiated by freshwater anomalies. However, high-quality global salinity measurements have only been routinely available since 2002, and mostly in the open ocean from Argo floats. Moreover, satellite observations of the sea surface salinity are of relatively low accuracy and only available since 2009 (Bao et al., 2019; Xie et al., 2019). Considering the limitations associated with currently available salinity products, we use a surface mass balance analysis to estimate the variability of freshwater.

160 ### 3.1 Mass balance

~~We start with a surface mass balance for the~~

The mass budget for the surface mixed layer in the subpolar region in winter ~~(Fig. 1):~~ can be expressed as:

$$\frac{\partial}{\partial t}\left(\int_{-h(t)}^{0}\frac{\partial \rho}{\partial t}^{\eta} \rho\, dz\right) = -\frac{B}{g} + A + M - \nabla \cdot \left(\int_{-h(t)}^{\eta} \rho \boldsymbol{u}\, dz\right), \tag{1}$$

where ρ is the mixed layer density, h is the mixed layer depth, ~~A corresponds to horizontal mass transports~~ η is the surface
165 elevation above the geoid (which is equivalent to the absolute dynamic topography), g is the gravitational acceleration, B is the buoyancy flux through the surface, and ~~M is the mass flux entrained through the base of~~ $\boldsymbol{u}$ corresponds to the velocity vector (Gill, 2016; Griffies and Greatbatch, 2012). The term $-\nabla \cdot \left(\int_{-h(t)}^{\eta} \rho \boldsymbol{u}\, dz\right)$ represents the convergence of mass, which we separate into an active component A and a passive component E. The passive component is defined as the entrainment of mass into the mixed layer ~~(Gill, 2016).~~ that results from mixed layer deepening as the mixed layer density increases. The
170 active component results from externally forced, horizontal and vertical mass fluxes, such as wind-driven Ekman transports and upwelling. The passive component can only change the mixed layer depth, but not its density, while the active component does change the mixed layer density.

Next, we assume that the density is homogeneous in the mixed layer and that η in winter is much smaller than the mixed layer depth h. After integrating Eq. (1) ~~over the mixed layer~~ from summer to winter ~~, we obtain:~~ and neglecting the contribution
175 of the surface elevation η relative to the mixed layer depth on the lefthand side of Eq. (1), we thus obtain:

$$\rho h \underset{=}{\approx} h_0 \rho_0 + \left(-\frac{B}{g} + A + \underline{M}\underline{E}\right) \cdot \underline{dt}\Delta t, \tag{2}$$

where h_0 and ρ_0 represent a mixed layer depth and density ~~before the winter,~~ at the end of the summer (for instance in September), h and ρ refer to the depth and density in winter (January to March), and ~~dt~~ Δt is the corresponding integration interval from summer to winter.

180 ~~Mass budget for a mixed layer of depth h in the subpolar region, taking into consideration horizontal advection A, the density flux from beneath the mixed layer M, and the density contribution from the surface buoyancy flux $\frac{B}{g}$.~~

While the climatological mean mixed layer density increases during the winter, the mixed layer deepens. Thus, before the winter, the mixed layer is several tens of metres deep while during the winter, it reaches several hundred metres. Since the

density anomaly in the initial shallow mixed layer becomes distributed over a much larger depth range, the first term on the righthand side is negligible compared to the other terms. Any density anomalies beneath the initial, shallow mixed layer are ~~included in M.~~ still included in E. Eq. (2) thus simplifies to:

$$\rho h \approx \left(-\frac{B}{g} + A + E \right) \cdot \Delta t. \tag{3}$$

We further separate each term into a mean and an anomaly n, with n referring to the n'th winter of an arbitrary subset of N winters and the mean representing the mean over these winters. ~~Assuming that the~~ Since we have defined E as a passive component that can only change the mixed layer depth, not its density, we can write it as $E_n \cdot \Delta t = h_n \cdot (\rho_n + \rho_{mean})$. Moreover, assuming that the mean state is in balance, we subtract the mean values from ~~the resulting equation:~~ Eq. (3), resulting in:

$$\rho_n h_{mean} + \rho_{mean} h_n + \rho_n h_n \underline{=} \approx \left(-\frac{B_n}{g} + A_n \right) \cdot \Delta t + \underline{M} h_n \cdot \underline{dt.} \left(\rho_n + \rho_{mean} \right), \tag{4}$$

where the terms involving h_n cancel each other.

~~Next, we linearise the equation of state~~ Lastly, we express the density as a function of temperature and salinity by considering variations in the density around a reference ~~state~~, which we choose to be the mean over the N selected winters. Since local density variations due to pressure are several orders of magnitude smaller than those, due to changes in salinity and temperature (Talley, 2011), we only consider temperature and salinity variations: $\rho_n \approx \rho_{mean} \left(-\alpha \cdot T_n + \beta \cdot S_n \right)$, where T is the temperature, S is the salinity, α and β are the thermal and haline expansion coefficients. ~~After plugging the linearised equation of state into the first term of~~ Plugging this expression into Eq. (~~3~~4), we obtain:

$$\rho_{mean} \left(-\alpha \cdot T_n + \beta \cdot S_n \right) \cdot h_{mean} \underline{+\rho_{mean} + \rho_n \cdot h_n} \approx \left(-\frac{B_n}{g} + A_n \underline{+M_n} \right) \cdot \underline{dt} \Delta t. \tag{5}$$

The objective of ~~this~~ the following analysis is to find conditions ~~(referred to as 'c'),~~ in which the density anomalies associated with temperature anomalies are much larger than the effect of potential, active drivers of density anomalies on the righthand side of Eq. (~~4): $\rho_{mean} \cdot h_{mean} \cdot |\alpha \cdot T_c| \gg |\left(-\frac{B_c}{g} + A_c \right)| \cdot dt.$ With the surface buoyancy and advective fluxes being negligible, and hence without an anomalous thermal or mechanical forcing, the mixed layer can only entrain water of the same density as that in the mixed layer, such that $M_n \cdot dt \approx (\rho_{mean} + \rho_n) \cdot h_n$, cancelling the corresponding term on the lefthand side of Eq. (4).~~ 5): $\rho_{mean} \cdot h_{mean} \cdot |\alpha \cdot T_n| \gg |\left(-\frac{B_n}{g} + A_n \right)| \cdot \Delta t.$ Under these conditions, the temperature and salinity anomalies must compensate each other in their influence on density, allowing us ~~, under these conditions,~~ to estimate the salinity anomalies from the associated temperature anomalies: $\beta S_n \approx \alpha T_n$.

The idea that such conditions exist is motivated by the observation that salinity changes are not only a response to surface fluxes and entrainment but can, in turn, constrain the drivers of density anomalies. Large freshwater anomalies ~~, in particular,~~ in winter can impede convection and entrainment ~~(M)~~ and thus limit the oceanic heat release to the atmosphere (B). At the same time, a stronger surface cooling is required to mix freshwater down, influencing the ~~surface temperature (~~mixed layer temperature T~~).~~. Considering the competing influences of salinity and temperature on stratification, the conditions in which

215   freshwater may impact the temperature, can only occur in autumn and winter, when surface water is cooled by the atmosphere, becomes denser and sinks. In summer, the temperature and salinity do not compete in their influence on stratification and thus, do not constrain each other.

    To exploit this constraint of salinity on temperature ~~,~~ and identify these potential conditions, we ~~derive~~ assume that the surface mixed layer in winter is relatively well mixed, so we can approximate the mixed layer temperature T with the SST.

220   We then search for potential freshwater indices that exhibit a strong ~~relationship to subpolar temperature anomalies. We then take advantage of these relationships by regressing~~ linear relationship with subpolar SST anomalies, regress Eq. (~~4) onto the indices. Since the drivers are (by construction) not connected to the indices, they are likely~~ 5) onto these indices, and compare the magnitude and spatial characteristics of the resulting terms. If enhanced surface freshening substantially affected the SST, we expect the terms A_n and B_n to drop out of Eq. (5) after the regression~~such that the density changes implied by the~~

225 ~~temperature anomalies must be balanced by density changes associated with salinity anomalies.~~ In essence, the indices serve as filters that ~~detect the conditions c in which stratification has been controlled by salinity, allowing us, under these conditions, to infer the variability of freshwater from the SST.~~help us to identify conditions in which freshwater anomalies have been sufficiently large to influence the heat exchange between the ocean and the atmosphere, either within the subpolar region or before entering it. Later (in Section 4.5), we will further assess if these conditions in which the air-sea heat exchange and in

230   turn the SST have been affected by freshwater anomalies hold generally over the North Atlantic or only for selected indices.

3.2   Derivation of freshwater indices

~~To identify suitable indices for freshwater anomalies~~The challenge in detecting the conditions in which freshwater anomalies may have affected the SST, consists in the complexity of SST and freshwater variability in the subpolar region. In theory, changes in surface freshwater can be influenced by river runoff, sea ice and glacial melting, evaporation and precipitation,

235   mixing, and ocean currents. Considering that multiple factors can contribute to freshwater variations over a range of timescales and spatial scales, it may not be possible to reduce the complexity of freshwater variability in space and time into a single, one-dimensional index.

    To overcome this challenge, we construct indices over subsets of years that allow us to closely constrain the variability of the SST, over the selected subset. Thus, this approach is different to traditional methods in which the dynamical mechanisms

240   are known a priori, and statistical methods are used to assess the significance of these mechanisms. Here, we first select indices with a strong and significant statistical relationship with the SST, and then look for potential freshening mechanisms that can explain the relationship, assuming that these mechanisms exist but may be masked by other drivers.

    As a first, educated guess to identify suitable freshwater indices, we start with the NAO ~~in summer (Fig. 1a), which has previously been linked to potential drivers of freshwateranomalies in the subpolar North Atlantic~~index in summer, motivated

245   by its dynamical links to freshwater. On the one hand, a lower NAO phase in summer ~~is~~ has been associated with enhanced runoff and melting over Greenland (Hanna et al., 2013, 2021), which is a source of freshwater to the North Atlantic (Bamber et al., 2018; Dukhovskoy et al., 2019). On the other hand, a higher NAO phase ~~is~~ has been associated with an intensified subpolar gyre circulation, leading to enhanced freshwater imports into the subpolar region (Häkkinen et al., 2011a, 2013;

8

Holliday et al., 2020). ~~While the choice of the NAO index is motivated by these dynamical links, we here use it for a purely~~ ~~statistical purpose and make no assumptions on the dynamical underpinnings~~ Yet, even if the freshening occurs in summer (when melting and runoff is strongest), the effect of the freshwater on the SST would only become visible in autumn and winter (when the freshwater impedes the sinking of surface water). Thus, we focus on the SST in winter to infer the possible existence of freshwater anomalies.

~~(a,b) Regression of the SST in winter (January through to March) onto two NAO$_S$ subsets below and above 0.5, where NAO$_S$ is the NAO index of the preceding summer (July and August). The corresponding years are shown by the strong red and blue colours in panels c and d, excluding the transparent years, which were selected to minimise the signal-to-noise ratio. Thus, F$_E$ includes 8 years while the regression on F$_W$ is based on 17 years. Contours encompass regions that are significant at the 95% confidence level. The '+1' in the title refers to the time lag of the SST signal since it appears in the winter after the summer index. Please note the different colour scales. (c) Variability of the NAO index in July and August (NAO$_S$), with the colour coding matching that in d. (d) Relationship between NAO$_S$ and the subsequent winter SST, where ΔSST corresponds to the SST difference between the red, subtropical and blue, subpolar 95% confidence regions in panels a (red years) and b (blue years) respectively, relative to the climatological mean.~~

Consistent with the existence of multiple possible drivers of freshwater and ~~associated~~ SST anomalies in winter, we obtain a qualitatively different relationship between the summer NAO index in July and August (NAO$_S$) and the ~~meridional SST~~ ~~gradient across ∼45 °N~~ temperature difference between the subpolar and subtropical gyres in the subsequent winter below and above a threshold of ~ -0.5 in NAO$_S$ ~~.~~ (Fig. 1a and b). Below this threshold, there is a progressively larger SST difference between the northern subtropical region and the southern subpolar region for ~~lower~~ decreasing NAO$_S$ ~~states~~ phases in the preceding summer ~~.~~ (Fig. 1a). Above this threshold, there is a progressively larger SST difference for ~~higher~~ increasing NAO$_S$ ~~states~~ phases in the preceding summer ~~(Fig. 2d, with the corresponding regions shown in Figure 2a and b and the corresponding~~ ~~years shown in Figure 2c.~~ Also, the associated cold, subpolar SST anomaly is weaker and displaced further to the northwest (Fig. 1b).

~~To improve the capability of the identified subsets to filter out the conditions c that allow us to estimate freshwater anomalies~~ ~~from the temperature~~ Next, we strengthen the identified relationships between the two NAO subsets ~~and the meridional SST~~ ~~gradient~~ (above and below -0.5) and the subsequent SST anomalies through subsampling. ~~The subsampling is motivated by~~ ~~the objective of achieving a steep regression slope between the subsampled~~ Specifically, if x_i corresponds to the NAO$_S$ ~~index~~ ~~and~~ subset years, and y_i corresponds to the SST anomaly in the ~~subsequent SST anomaly , implying that small changes in~~ ~~the subsampled index correspond to large changes in the subsequent SST anomaly. In turn, this highsensitivity implies that~~ subsequent winter, we strive to derive a linear relationship $y = ax + b$, where a and b are constants and in which $|a|$ is high. The higher the magnitude of ~~the temperature term~~ a is, the higher is the magnitude of αT on the lefthand side of Eq. (~~4)~~ ~~becomes very large after regressing it onto the NAO subsets.~~ 5) after regressing Eq. (5) onto the index. Thus, we aim to select NAO years for which the magnitude of the slope $a = \frac{y_i - y}{x_i - x_0}$ is large, where $x_0 = x|_{y \approx \bar{y}_i}$ and $\bar{y}_i$ represents the mean over y_i. At the same time, we strive to obtain a high correlation between the subset and the subsequent SST anomalies. Thus, we aim
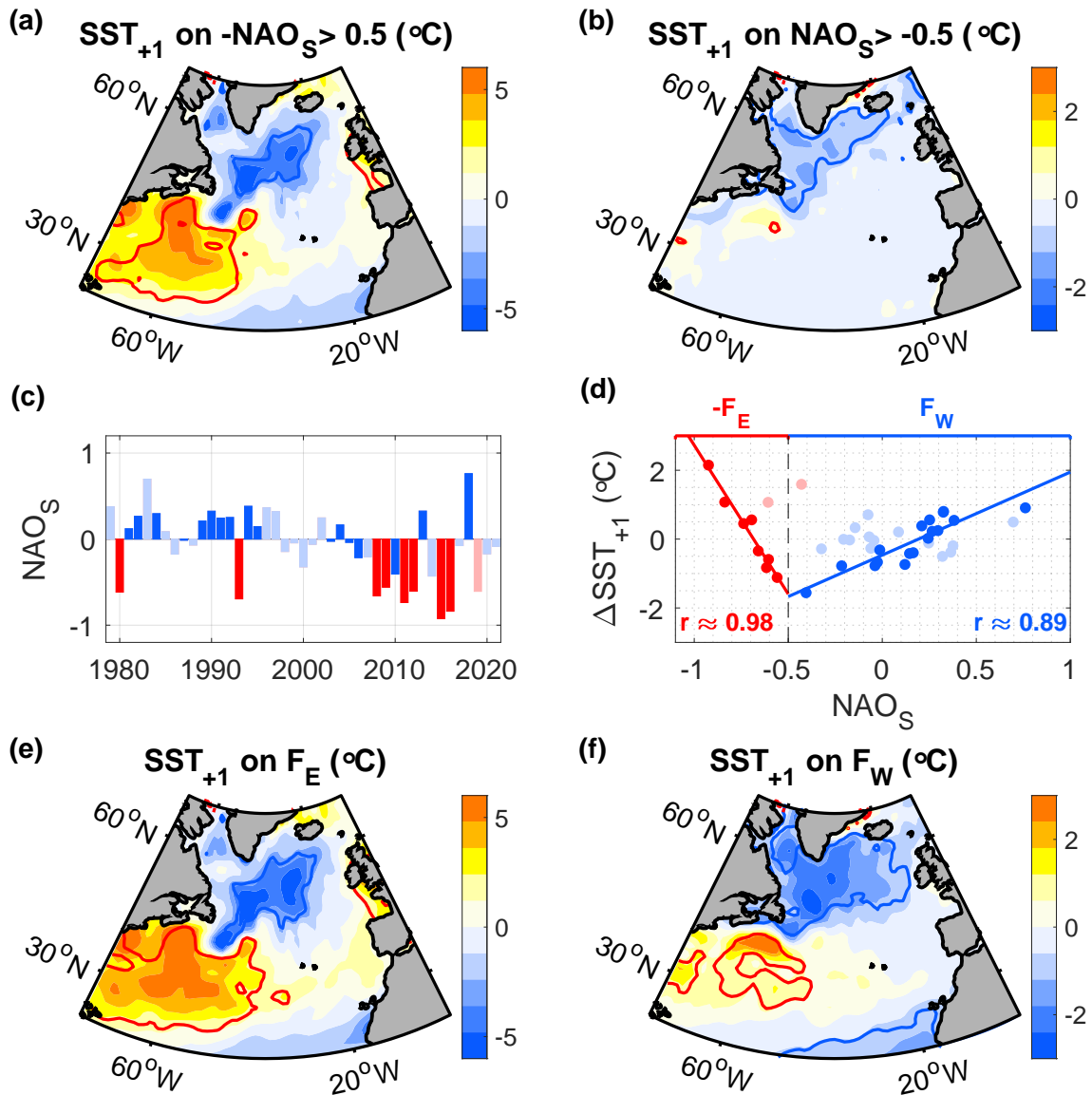
Figure 1. (a,b) Regression of the SST in winter (January through to March) onto (a) $-\mathrm{NAO}_S$ in all years in which $\mathrm{NAO}_S < -0.5$ and (b) $+\mathrm{NAO}_S$ in all years in which $\mathrm{NAO}_S > -0.5$, where NAO_S refers so the NAO index of the preceding summer (July and August). The '+1' in the title refers to the time lag of the SST signal since it appears in the winter after the summer index. (c) Variability of the NAO index in July and August (NAO_S), with the colour coding matching that in d. (d) Relationship between NAO_S and the subsequent winter SST, where ΔSST corresponds to the SST difference between the red, subtropical and blue, subpolar 95% confidence regions in panels e (red years) and f (blue years) respectively, relative to the respective means. (e,f) Regression of the SST in winter onto the two freshwater indices, obtained after the subsampling. The corresponding years are shown by the strong red and blue colours in panels c and d, excluding the faint years. Thus, F_E includes 8 years while the regression on F_W is based on 17 years. Contours encompass regions that are significant at the 95% confidence level. Please note the different colour scales.

to select NAO years where $(x_i - x_0)^2$ is large, since this increases the variance of the SST anomalies that can be explained by the index.

285 ~~For the cold anomalies associated with lower states of the summer NAO, we select the years in which NAO~~The values x_i included in each subset directly correspond to the respective NAO~~$_S < -0.5$, excluding the outliers in 2014 and 2019. The threshold of ~ -0.5 and the outliers were identified through visual inspection of the relationship between the summer NAO and the meridional SST gradient in the subsequent winter~~ values (Fig. ~~2d) . The resulting correlation of the selected subset with~~ 1c) without scaling them, while the values y_i correspond to the SST difference between the ~~warm subtropical warm and~~

290 ~~cold subpolar regions, enclosed within 95% confidence lines, is ~ -0.98 ($p \approx 2.8 \cdot 10^{-5}$). Here, we specifically selected the 95% confidence regions as a means~~ subpolar and the subtropical gyres, rather than only the SST anomaly at a single location. Using the SST difference has the advantage that we filter out any spatially uniform, radiative warming signals due to increasing greenhouse gas concentration and base the analysis on larger regions. In addition, we only consider regions in which the SST anomalies are significant, allowing us to directly inspect the robustness of the underlying correlations and ensure that they are

295 not due to outliers or clusters. ~~Another advantage of using spatial differences is that we filter out any potential, spatially uniform, radiative warming signals. However, the identified relationships are not sensitive to the exact regions~~Thus, we identified two outliers, corresponding to the NAO summers in 2014 and 2019 (faint red years in Figure 1d), which we excluded from the subsequent subsampling to obtain a faster convergence of the results.

~~For higher values of the preceding summer NAO state, the correlation with the subsequent SST gradient is weaker, amounting~~

300 ~~to ~ 0.64 ($p \approx 0.001$). Thus, to optimise our method of inferring freshwater variations from Eq. (3),~~Following the above objectives to maximise the slope and variance of the subsampled index, we select the ~~years that most lead to an increase in the correlation and regression. Considering the~~ N years where the term $(y_i - y) \cdot (x_i - x_0)$ is highest. Here, the subscript i refers to all years in the two sets where the NAO$_S$ is above or below 0.5 respectively, excluding the two outliers, and y is the associated, linear regression of y_i on x_i. Graphically, the subsampling is equivalent to increasing the slope of the regression

305 line while keeping a high variance (Fig. 1d). It represents a powerful method for increasing the statistical relationship between two variables and thus identifying dynamical links, based on the assumption that noise, and other mechanisms, can mask these links. Once a strong statistical connection has been established, the physical basis will be assessed by investigating the potential, underlying dynamical links.

There is a trade-off between the number of years ~~included~~ N included in each subset and the resulting ~~correlation, we~~

310 correlations between the NAO subset and subsequent SST pattern. Considering that the number of years is already low for the cold anomalies preceded by strongly negative NAO summers ($N = 8$), where NAO$_S$ is smaller than -0.5, we do not apply any further subsampling. For the other subset, we selected $N = 17$ years as a reasonable compromise for obtaining a high correlation of ~ 0.90 while keeping a relatively large sample size, reflected in ~~low p-values ($p \approx 2.6 \cdot 10^{-6}$). However,~~ the low p-value of $\sim 1.8 \cdot 10^{-6}$.

315 In Section 4.5 and Appendix B, we show that the results are not sensitive to ~~this choice.~~ the subsampling or the number of years included. However, having a close relationship between the index and the SST results in reduced uncertainties when estimating the associated freshwater anomalies. In addition, the high correlations help us to identify and assess potential

dynamical links more clearly: Freshwater indices that are only poorly correlated with freshwater are only of limited use when assessing links between freshwater and other ocean or atmospheric parameters. Since the indices will be used as a tool for representing freshwater anomalies, high correlations between the indices, the SST and potential freshwater anomalies are a prerequisite, not a conclusion, and we make no assumptions on the suitability of both subsets outside the selected years.

~~Since the~~ Through the subsampling, we have derived two subsets with close, linear relationships with the SST (Fig. 1d, e and f). To distinguish the two subsets from each other, we name them according to the location of the associated cold SST anomalies. Since the maximum cold anomalies associated with ~~higher NAO states extend over the western subpolar region~~ lower NAO states ($NAO_S < -0.5$) are strongest over the southeastern subpolar region (Fig. 1e), we refer to the selected ~~years as 'F$_W$' subset. Thus, we distinguish these cold anomalies from those associated with~~ 8 years as F$_E$ index — shown by the clear red coloured bars in Figure 1c and listed. For the other subset, ~~which we refer to as 'F$_E$' subset, for eastern subpolar cold anomalies~~ the maximum cold anomalies extend over the full subpolar gyre, including the western part (Fig. ~~2). Given their close relationships with the SST, the two subsets have optimal chances of describing the conditions c that allow to estimate freshwater anomalies from Eq. (4). While the choice of the subsets is thus motivated by their potential to represent freshwater anomalies, the focus of this study is on the link between freshwater anomalies and their downstream effects. The subsets are only used as a tool. High correlations between the subsets,~~ 1f). Thus, we refer to the ~~SST and, potentially, the associated freshwater anomalies are a prerequisite, not a conclusion, and we make no assumptions on the suitability of both subsets outside the selected years.~~ selected 17 years as F$_W$ index — shown by the clear blue coloured bars in Figure 1c. The corresponding years included in each index are additionally listed in Table A1. In the following analyses, we will examine the dynamical links of both indices to freshwater anomalies and the associated air-sea feedbacks.

4 Results

Having selected two NAO subsets, we ~~next~~ will first assess their suitability for representing freshwater anomalies. Thus, we evaluate the associated mass balance ~~, determine the accuracy of the obtained freshwater estimates~~ to estimate freshwater anomalies and examine their ~~links with European summer weather. To increase the robustness of the analyses, independent of the indices , we further construct composites of the~~ potential causes. We will then use the indices to investigate links between the estimated freshwater anomalies and the large-scale ocean and atmospheric conditions ~~associated with the~~ in winter and summer, and test if the identified links hold generally by using an un-subsampled index. Lastly, we will assess the role of North Atlantic freshwater anomalies as a predictor for Europe's warmest summers by constructing composites of the 10 ~~warmest and coldest European summers over the last 40 years and compare the preceding freshwater anomalies. Finally, we analyse the long-term variability of freshwater anomalies, estimate the role of ocean-atmosphere feedbacks, and discuss their implications for the predictability of European summer weather~~ warmest relative to the 10 coldest summers between 1979 and 2022 and comparing the preceding freshwater anomalies.

4.1 Estimation of freshwater anomalies

Taking advantage of the strong relationships between the selected NAO_S subsets and subsequent SST anomalies, we regress each term in Eq. (45) on the ~~two subsets~~corresponding indices F_E and F_W. We then evaluate the surface mass balance over the ~~cold~~ subpolar cold SST anomaly regions within the regions enclosed by the 95% confidence lines. ~~When using different regions, for instance the full subpolar region where the SST anomaly is negative, the results do not change appreciably.~~ In the following, we present the key analysis steps and results while a detailed evaluation and comparison with in-situ observations is provided in Appendix A.

~~First, we estimated~~

~~To estimate~~ the temperature term ~~. Assuming~~ αT_n, we again assume that the mixed layers are relatively ~~homogeneous, we~~ homogenous and approximate the mixed layer temperature with the SST, averaged over the winter (January through to March). Even if the SST is slightly warmer or colder than the mixed layer temperature, the relationship between the mixed layer temperature and the mixed layer salinity ~~still remains~~ will still remain the same as that between the SST and the sea surface salinity, due to having a constant density profile in the mixed layer. To estimate the mean mixed layer depth h_{mean}, moreover, we averaged the mean mixed layer depth, obtained from Argo floats (Holte et al., 2017), over the same regions and months as the SST, resulting in a mean mixed layer depth of $\sim$250 m for the F_E subset and $\sim$280 m for the F_W subset.

We further compute α and β using the Gibbs Seawater Routines (McDougall et al., 2009), in accordance with the highest standards of current knowledge. Noting that the effects of salinity and pressure on α and β are small and only affect the second decimal place or less, we use nominal values of 35 g kg^{-1} and 10 db for the subpolar region in winter to compute α and β. The dependence of α and β on temperature is larger, however. For instance, α can vary from $5 \cdot 10^{-4}$ to $18 \cdot 10^{-4}$ °C^{-1} across the subpolar ocean surface. Thus, for an enhanced accuracy, we allow α and β to vary with the SST.

~~We then estimated the~~ Next, we estimate the terms on the righthand side of Eq. (~~4), including the~~ 5). On the timescales and spatial scales considered, oceanic flows are predominantly in geostrophic balance, redistributing heat and freshwater. However, geostrophic flows cannot contribute to a net mass input. Over the open ocean, away from topographic boundaries, on interannual timescales, the winds and air-sea fluxes represent the largest energy sources that can result in vertical mixing or horizontal mass convergence (Ferrari and Wunsch, 2009; Wunsch and Ferrari, 2004). Other sources of energy include pressure loading by the atmosphere, geothermal heating, biological activity, and the tides but we estimate them to be negligible over the investigated timescales and spatial scales. Thus, the terms on the righthand side of Eq. (5) are confined to the surface buoyancy fluxes, ~~vertical~~ horizontal Ekman transports and ~~advection. Overall, we found~~wind-driven vertical fluxes, all of which are estimated using the atmospheric reanalysis ERA5. Considering the nonlinearity within the individual terms of Eq. (5), we first evaluate each term before regressing it onto the indices.

After estimating the density anomalies associated with the cold anomalies, and the buoyancy fluxes, the horizontal Ekman transports and the vertical Ekman velocity, and regressing them onto the freshwater indices (Appendix A), we find: Regardless of the exact region and mean mixed layer depth, and regardless of which month is selected as starting month of the integration, the density increase implied by the cold anomalies associated with F_E and F_W is always more than an order of magnitude

larger than the density changes associated with A_n or B_n. Moreover, neither of these fluxes is significantly correlated with the subsets, and their spatial patterns are inconsistent with the obtained SST patterns~~(Appendix A)~~, regardless of whether we

385 include the full subpolar region where the SST anomaly is negative or only the region enclosed by the 95% confidence lines, or whether we start the integration in October or only consider the winter months January to March.

With the buoyancy fluxes, vertical Ekman transports and horizontal advection being negligible, ~~there cannot be an anomalous density flux through the base of the mixed layer. The mixed layer can only entrain water of the same density as that at the surface. Thus, M_n can only change the mixed layer depth, not the density . When integrated over the winter period, it can~~

390 ~~be approximated with $(\rho_{mean} + \rho_n) \cdot h_n$ canceling the corresponding term on the lefthand side of Eq. (4). We are left with $\rho_{mean}(-\alpha \cdot SST_n + \beta \cdot SSS_n) \cdot h_{mean} \approx 0$,~~ we conclude that the density increase associated with the cold anomalies must be balanced by a density decrease associated with freshwater anomalies: $\alpha SST_E \approx \beta SSS_E$, and $\alpha SST_W \approx \beta SSS_W$, where SSS is the sea surface salinity and ~~n now refers~~ the subscripts refer to the anomalies obtained from the regressions ~~.~~ onto the respective index. This result implies a close connection between freshwater and SST anomalies included in each subset. A

395 demonstration of the connection between SSS and SST anomalies with hydrographic observations shows that, even in winters with most intense air-sea fluxes, freshwater anomalies can still be inferred from the SST with reasonably small uncertainties (Appendix A).

~~With none of the terms on the righthand side of Eq. (4) being able to account for the the density increase, independent of the exact integration period, region, and mixed layer depth, we conclude that the density increase associated with the cold anomalies~~

400 ~~must be balanced by a density decrease associated with freshwater anomalies: $\alpha SST_E \approx \beta SSS_E$, and $\alpha SST_W \approx \beta SSS_W$. Physically, this density compensation implies that the freshwater anomaly determines the temperature that the surface water is required to have before it is mixed down.~~

~~The estimated surface freshwater anomalies~~ Using the obtained density compensation between SSS and SST anomalies, we estimate SSS anomalies from the two NAO subsets. Thus, we find that the maximum freshwater anomalies (or minimum SSS anomalies)

405 associated with F_E ~~are strongest over the eastern~~ occur over the central subpolar region (~~Fig. 3a)~~ , while corresponding to the southeastern subpolar gyre) and are spatially more confined than the maximum freshwater anomalies associated with F_W ~~also extend over the western subpolar region~~ (Fig. 2a and b). Moreover, the significant area of F_W freshwater anomalies extends further eastward, westward, and northward compared to F_E freshwater anomalies and the anomalies have a smaller amplitude, consistent with the associated cold, subpolar SST anomalies (Fig. ~~3b)~~ 1e and f).

410 Since the buoyancy fluxes represent the largest term on the righthand side of Eq. (~~4~~5), they determine the uncertainty of the obtained salinity estimates, amounting to 4% for the F_E subset and ~~7~~6% for the F_W subset ~~. Another~~ (Appendix A). These uncertainties apply to the cold anomaly regions, enclosed by the 95% lines. Uncertainties at each individual grid point can differ. Moreover, if the freshwater forcing is very large, the surface mass balance may underestimate the freshening because freshwater anomalies can (in theory) increase up to a salinity threshold of zero, while SST anomalies cannot drop below the

415 air temperature. Still, we find that even during the strong observed freshwater anomalies in 2015 and 2016, the surface mass balance provided a good approximation (Appendix A), suggesting that a potential underestimation is only small.
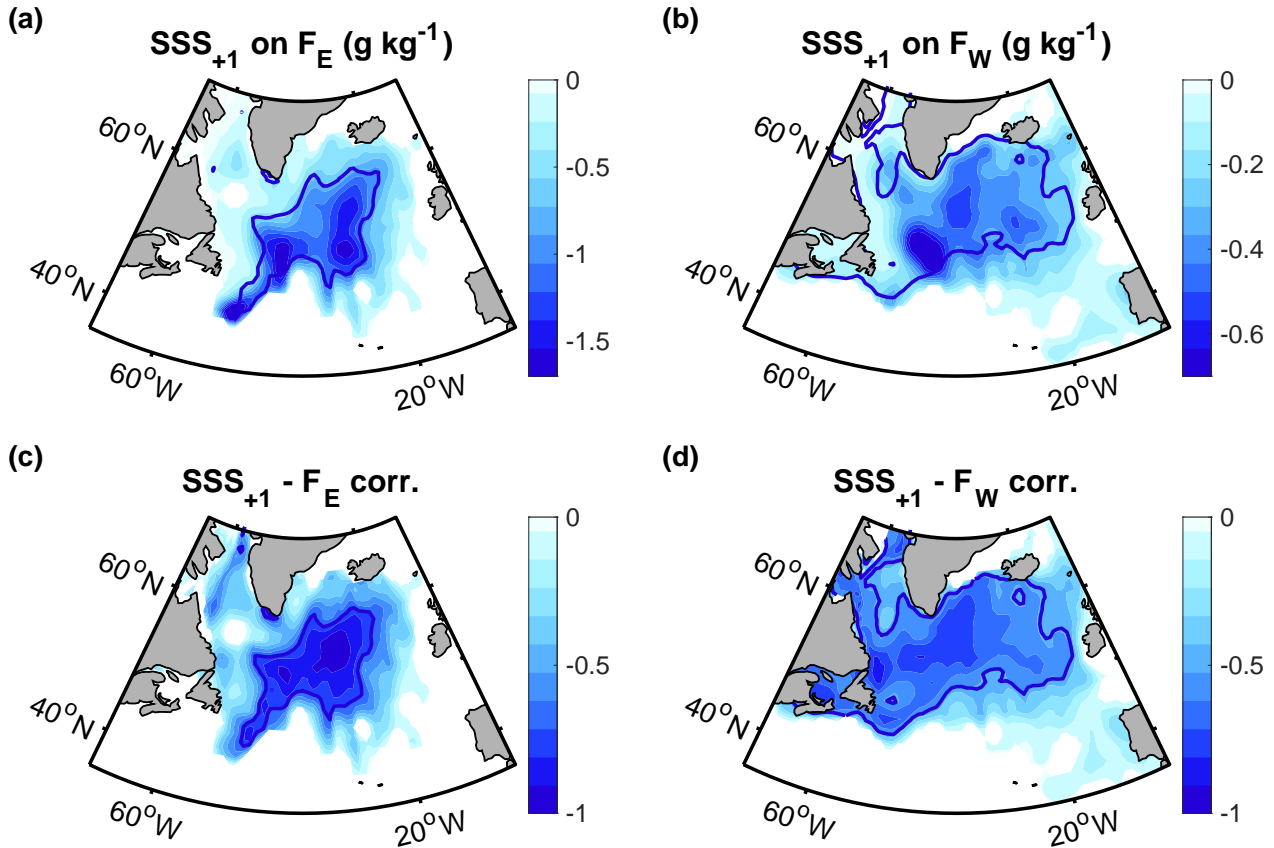
Figure 2. (a,b) Regression of the sea surface salinity in winter (January through to March) on the two freshwater indices from the preceding summer (Fig. 1c). The contours delineate the regions that are significant at the 95% confidence level. (c,d) Correlations between the sea surface salinity in winter and the freshwater indices from the preceding summer, with the thick contours delineating the regions that are significant at the 95% confidence level, assessed by means of two-sided t-tests. The underlying sea surface salinity variability has been estimated from the surface mass balance by assuming density compensation with the SST anomalies.

In addition to the low overall uncertainties of the SSS estimates, another implicit advantage of the selected ~~subsets~~ NAO subsets F_E and F_W is that they are, by construction, highly correlated with the obtained freshwater estimates in the subsequent winter, with the ~~correlations~~ magnitude of the correlations between the SSS anomalies and the freshwater indices exceeding 0.9 ~~over large parts of the subpolar region~~ (Fig. ~~3c~~ 2c and d).

~~(a,b) Regression of the sea surface salinity in winter (January through to March) on the two freshwater indices from the preceding summer (Fig. 2). The contours delineate the regions that are significant at the 95% confidence level. (c,d) Correlations between the sea surface salinity in winter and the freshwater indices from the preceding summer, with the thick contours delineating the regions that are significant at the 95% confidence level, assessed by means of two-sided t-tests. The sea surface salinity has been estimated from the mass balance.~~

The SSS correlations with the F_E subset reach their highest magnitude over the southeastern subpolar gyre while the highest magnitudes of the SSS correlations with F_W occur over the central and northern subpolar region, covering an overall larger area, like the corresponding regressions. Considering the low uncertainties of the obtained freshwater estimates, and their high correlations with the two NAO subsets, we conclude that both subsets represent suitable freshwater indices. ~~This result implies a close connection between freshwater and SST anomalies. A demonstration of this connection with hydrographic observations shows that, even in winters with most intense air-sea fluxes, freshwater anomalies can be inferred from the SST with reasonably small uncertainties (Appendix A).~~

4.2 Causes of freshwater anomalies

~~The preceding derivation revealed two types of cold and fresh anomalies, which are associated with opposite atmospheric circulation patterns in the previous summer, characterised by high and low NAO states respectively. To better understand this nonlinear relationship between the NAO state in summer and the freshwater anomalies in the subsequent winter, we review potential large-scale drivers of the obtained freshwater anomalies.~~

Freshwater anomalies may result from enhanced sea ice or glacial melt, river runoff, surface fluxes (precipitation minus evaporation), and circulation changes. After investigating the surface fluxes from ERA5, glacial runoff from the Greenland climate model MAR, and the regional gyre circulation from altimetry, we find a ~~significantly enhanced freshening in lower summer NAO states only for~~ significant negative relationship between the summer NAO and runoff (Fig. ~~4a). This is in agreement with earlier~~ 3a), pointing to runoff as potential freshwater source for the F_E freshwater anomalies, associated with a strongly negative NAO_S index. While other sources of meltwater, such as sea ice, may also contribute enhanced freshening, the correlation between runoff and the summer atmospheric circulation is consistent with other studies evaluating individual links between the summer atmospheric forcing ~~,~~ and glacial runoff (Hanna et al., 2013, 2021), and the resulting freshwater input into the North Atlantic (Bamber et al., 2018; Dukhovskoy et al., 2019).

~~To further support the relationship between surface melting and subpolar freshwater anomalies we take advantage of the pronounced seasonality of the melting and runoff, being largest in summer (July and August).~~

With the majority of ~~the seasonal freshwater~~ seasonal runoff arriving in the subpolar gyre during autumn (Fratantoni and McCartney, 2010; Schmidt and Send, 2007), the ~~surface mass balance has previously been evaluated for the period from~~
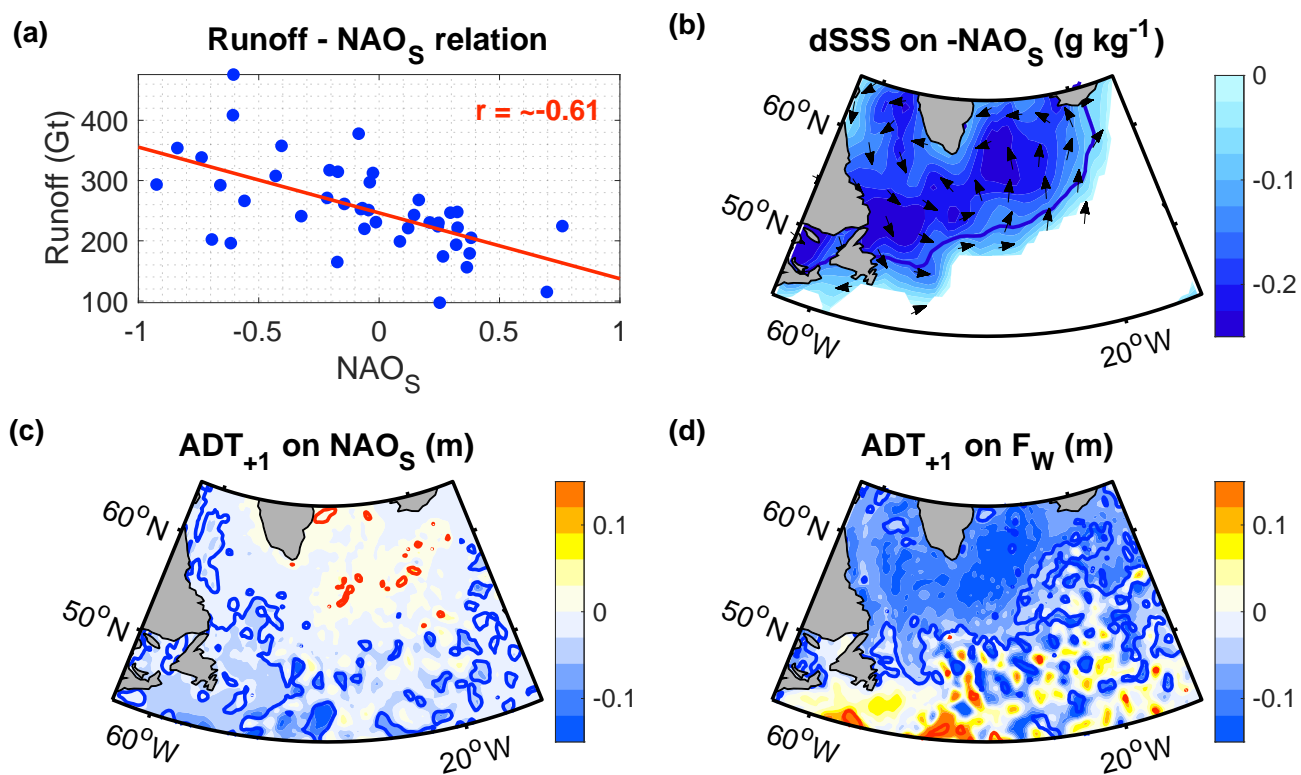
Figure 3. (a) Relationship between the NAO in July and August (NAO_S) and the ~~total~~ runoff integrated over the Greenland ice sheet ~~, also~~ ~~in~~ and over July and August. (b) Regression of the newly arriving, seasonal surface freshening ~~from~~ between summer (August) ~~to~~ and winter (January to March) onto $-NAO_S$ from the preceding summer. dSSS corresponds to the SSS change from summer and winter, estimated using a mass balance analysis (Oltmanns et al., 2020). The arrows represent the mean geostrophic surface flow, obtained from the absolute dynamic topography, averaged from August to March (the period of the freshening). Multiplying the summer NAO by '-1' serves the purpose of ~~obtaining~~ using an index that is positively correlated with the surface freshening. ~~The seasonal surface freshening has been estimated from a surface mass balance (Oltmanns et al., 2020).~~ (c,d) Regression of the absolute dynamic topography in winter (January to March) onto (c) NAO_S and (d) F_W from the preceding summer. Contours encompass regions that are significant at the 95% confidence level.

~~summer to winter~~ change in the surface salinity from summer (August) to winter (January to March) has previously been estimated by evaluating Eq. (1) for a shallow surface layer (Oltmanns et al., 2020). Thus, the summer NAO, multiplied by '−1' was identified as a suitable index for the seasonal freshwater that ~~is newly added to~~ reaches the subpolar region ~~in the subsequent autumn~~ between August and winter (Fig. ~~4b~~3b). The timing of the ~~freshwater input, arriving between summer and~~

455 ~~winter, thus~~ increased seasonal freshwater input associated with $-NAO_S$ supports the role of seasonal runoff and melting for the ~~identified freshwater anomalies~~F_E freshwater anomalies, since they are preceded by a strongly negative summer NAO.

While the full, un-subsampled summer NAO is a suitable indicator of the seasonal freshwater input from summer to winter, it is not necessarily correlated with ~~the absolute surface freshwater anomaly in winterbecause smaller, seasonal freshwater anomalies are mixed down before a significant cold anomaly develops. Only when the seasonal freshwater release is sufficiently~~

460 ~~large does it lead to surface fresh and cold anomalies in winter (Fig. 2a and 3a). Otherwise~~absolute SSS anomalies in winter. Once a seasonal mixed layer is eroded, the SST and surface salinity ~~in winter are increasingly~~ are expected to be influenced by other factors~~.~~, consistent with the nonlinear relationship between the summer NAO and subsequent winter SST anomalies (Fig. 1d).

Among the dominant drivers of deeper freshwater anomalies is the subpolar gyre circulation. Specifically, a stronger subpo-

465 lar gyre circulation, particularly in the northwestern subpolar region, has been found to lead to enhanced inflow of fresh and cold polar water from the coastal Labrador Current into the subpolar gyre ~~(Häkkinen, 2002; Häkkinen and Rhines, 2009; Häkkinen et al., 2011a,~~ (Häkkinen and Rhines, 2009; Häkkinen et al., 2011a, 2013; Koul et al., 2020). Since the subpolar gyre circulation is, in turn, largely forced by the wind stress (Häkkinen et al., 2011b; Spall and Pickart, 2003), earlier studies have identified a significant link between a stronger wind stress curl over the subpolar North Atlantic and a reduced salinity in the subpolar gyre

470 ~~(Häkkinen and Rhines, 2009; Häkkinen et al., 2011a, 2013; Holliday et al., 2020)~~(Häkkinen and Rhines, 2009; Häkkinen et al., 2011a, 20 .

~~Inspection of the~~

To assess the role of the wind stress curl and subpolar gyre circulation for the cold and fresh anomalies associated with higher summer NAO states, we inspect the associated absolute dynamic topography in ~~winters after higher NAO states in~~

475 ~~summer confirms an intensified subpolar gyre~~ winter. The full, un-subsampled summer NAO only displays a weak and mostly non-significant relationship with the geostrophic surface circulation in the ~~Labrador Sea~~southwest subpolar region (Fig. ~~4c),~~ ~~implying an enhanced geostrophic advection of cold and fresh polar water off the coast of Newfoundland into the subpolar region. This is expected as higher NAO phases imply an increased wind stress curl in the subpolar North Atlantic. After the subsampling, the signal becomes stronger~~ 3c). When using the sub-sampled summer NAO corresponding to the F_W subset,

480 however, the absolute dynamic topography north of 50 °N in winter is significantly reduced, implying a more cyclonic and hence, stronger subpolar gyre circulation in the northwest subpolar region ~~(Fig. 4d), supporting the subsampling and the identified, increased freshwater correlations with~~ 3d). The strengthened relationship between the subsampled summer NAO and the subpolar gyre circulation thus supports the subsampling by providing a physical explanation ~~.~~for the freshwater anomalies associated with F_W (Fig. 2b).

While a detailed quantification of freshwater budget is beyond the scope of this study, the proposed physical causes of the obtained freshwater estimates are supported by their spatial characteristics and intensities. F_W freshwater anomalies are largest over the western subpolar region, where the subpolar gyre circulation is strongest and where the surface heat fluxes are largest, ~~mixing~~ and can erode seasonal freshwater anomalies ~~down~~more easily. F_E freshwater anomalies are largest over the southeastern part of the subpolar region where surface fluxes and the subpolar gyre circulation are weaker, and where the mixed layer depths are shallower. ~~Consequently, freshwater anomalies associated with F_E are expected to be shallower and hence, more intense compared to freshwater anomalies associated with F_W, as they are distributed over a smaller depth range.~~

We also examined the associated surface fluxes (precipitation minus evaporation) but found that they were too small to account for freshwater anomalies~~after both higher and lower NAO phases in summer~~. In autumn and winter, moreover, the surface freshwater fluxes were evaluated as part of the buoyancy fluxes in the surface mass balance and found to be negligible.

~~Moreover, on decadal timescales, freshwater releases in the subpolar region have been attributed to switches of the Arctic Beaufort gyre circulation (Proshutinsky et al., 2015). While these periodic, Arctic freshwater releases may have contributed to the low-frequency variability of the North Atlantic SST variability, we here focus on the higher-frequency variability of freshwater and the SST that is naturally extracted by subsampling the summer NAO.~~

~~Consistent with the observations and earlier studies, we conclude that, in most years (when $NAO_S \gtrsim -0.5$), the freshwater anomalies are responding to changes in the subpolar gyre circulation. In those years, the seasonal freshening is mixed down and too small to affect the absolute SST anomaly in winter. However, F_E freshwater anomalies have a higher sensitivity to the summer NAO than the F_W freshwater anomalies, which is reflected in steeper regressions (Figs. 2 and 3) and can be explained by shallower, seasonal mixed layers. As a result, freshwater anomalies, linked to enhanced seasonal melting, change faster with the summer NAO and at some point (when $NAO_S \lesssim -0.5$) become the dominant signal. The implication that seasonal runoff and melt can cause absolute freshwater anomalies in winter is new and suggests that many recent fresh and cold anomalies in the subpolar North Atlantic were forced by a different mechanism to those in earlier decades.~~

4.3 Atmosphere-ocean ~~feedbacks~~ circulation in winter

~~Having identified two~~

Next, we examine the large-scale atmosphere circulation associated with both types of freshwater anomalies~~, we next examine their evolution in winter~~. We focus on the anomalies that are represented by the F_E subset (Fig. ~~3a~~2a) due to their sharper SST signals. However, freshwater anomalies associated with the F_W subset show qualitatively similar atmospheric responses, both in winter (not shown) and in summer (Section 4.4).

Since the meridional SST gradient is increased in winters after stronger freshwater anomalies, there is a sharper SST front between the subtropical and the subpolar gyre, pariticularly over the western North Atlantic (Fig. ~~2a~~1e). Directly above this sharper SST front, we observe an amplified baroclinic instability in the atmosphere, indicated by an enhanced Eady growth rate (Fig. ~~5a~~4a).

The amplified baroclinic instability manifests itself in a distinct circulation anomaly. When an air parcel travels northward across the SST front, it rises because it is warmer than the surrounding air masses. By rising, the air column stretches, acquiring
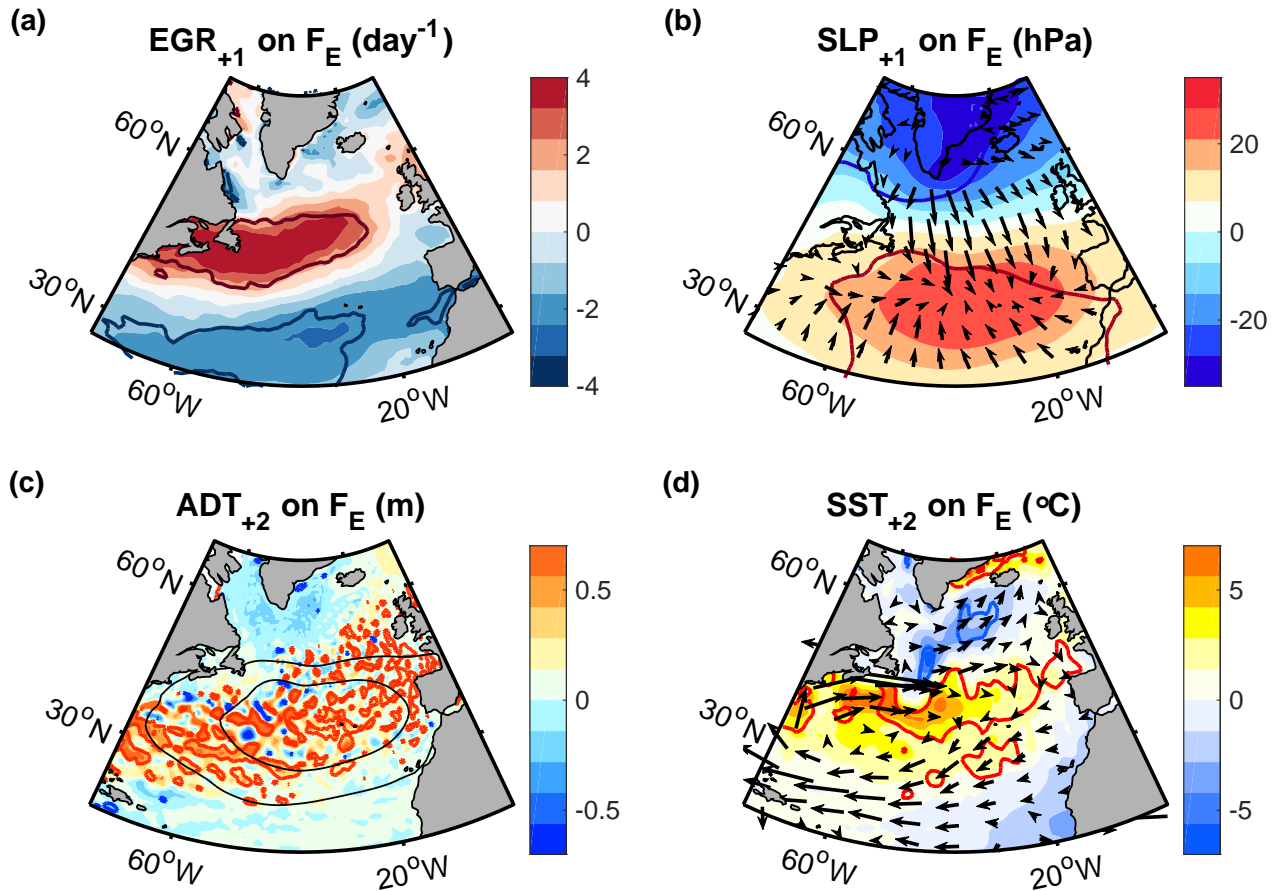
Figure 4. Regressions of (a) the maximum Eady growth rate, (b) the sea level pressure, (c) the absolute dynamic topography (ADT) and (d) the SST in winter (January through to March) on F_E. (a) and (b) are in the first winter after the anomalies whereas (c) and (d) are in the second winter after F_E (indicated by the '+1' and '+2' in the title). The arrows in (b) show the direction of the associated Ekman transports. The arrows in (d) represent the smoothed geostrophic flow implied by the ADT anomaly. The thin black contours in (c) show the region of Ekman flow convergence from (b). Thick contours in all panels encompass regions that are significant at the 95% level.

positive vorticity. The opposite occurs when an air parcel travels southward across the front. Consistent with the resulting enhanced baroclinic wave activity, the observations show a cyclonic anomaly ~~to~~ north of the SST front and an anticyclonic anomaly to the south (Fig. ~~5b~~4b), representative of a positive NAO phase. Thus, the observed atmospheric circulation anomaly is consistent with the underlying SST pattern and the observation that, after strong F_E anomalies, the NAO anomaly switches sign ~~. While a detailed investigation of the associated diagnostics is beyond the scope of this study, the observed atmospheric circulation anomalies are reproduced by SST-forced model simulations, albeit at lower amplitudes, supporting that the SST significantly contributes to these anomalies (Appendix B)~~from being strongly negative in summer to being strongly positive in winter.

The obtained atmospheric circulation anomaly drives a convergent Ekman transport between the subtropical and subpolar gyre (Fig. ~~5b~~4b), leading to an increase in sea level. This Ekman transport is ~~an instantaneous response~~ a direct response to the associated wind forcing but the resulting increase in sea level and ~~horizonal~~ horizontal pressure gradients can have longer lasting repercussions. Indeed, the increased sea level and associated ocean instabilities ~~,~~ manifest themselves in a broad band of anti-cyclonic eddies that extends into the second winter after the freshwater anomalies (Fig. ~~5c~~4c). The eddies are not visible in the SST due to the coarser 1° x 1° ~~resolution~~ grid spacing of the SST product, compared to the 0.25° x 0.25° ~~resolution~~ grid spacing of the absolute dynamic topography product.

Considering that the mean flow along the eddies is eastward, representing the North Atlantic Current, the integrated effect of the anti-cyclonic eddies is a reduced eastward speed at the southern edge of the band and an increased eastward speed at the northern edge (Fig. ~~5d~~4d). This circulation pattern has been referred to as inter-gyre gyre circulation (Marshall et al., 2001) and is equivalent to a northward shift of the North Atlantic Current (Kostov et al., 2021; Zhao and Johns, 2014).

The northward shift of the North Atlantic Current implies a large-scale warm SST anomaly to the south of the subpolar cold anomaly, not because the water inside the current is anomalously warm but because the current occurs at an anomalously northward location. ~~It~~ This warm SST anomaly is seen in the first, and the second winter after freshwater anomalies (Fig. ~~2a and 5d~~1e and 4d). However, in the first winter, the northward shift is partially obscured by the wind-driven, southward expansion of the cold SST anomaly over the eastern North Atlantic, potentially driving enhanced mixing and erosion of the SST front. The spatial distribution of the surface heat fluxes, on the other hand, does not match the SST field (Fig. A1d), indicating that ~~their influence may be limited.~~ the contribution of the surface heat fluxes to the warm SST anomaly is limited. While this mechanism has been demonstrated using the F_E subset, the signals for the F_W subset are qualitatively the same but confined to only the first winter.

We summarise that freshwater anomalies are ~~linked to~~ associated with cold anomalies in the subpolar region in winter (Fig. ~~2~~1e and f). The cold anomalies ~~contribute to~~ form part of an enhanced meridional SST gradient, implying a sharper SST front between the subpolar gyre and the subtropical gyre. The sharper SST front is associated with an amplified baroclinic instability in the atmosphere (Fig. ~~5a~~4a) that is characterised by a more cyclonic circulation anomaly over the subpolar gyre and a more anticyclonic anomaly to the south (Fig. ~~5b~~4b). This atmospheric circulation anomaly sets up ~~pressure gradients, which in turn,~~ surface pressure gradients through Ekman transports, which drive a geostrophic flow that contributes to the warm anomaly ~~to the~~ south of the subpolar cold anomaly (Fig. ~~5c~~ 4c and d). ~~The warm anomaly reinforces the SST anomalies, amplifying~~

The overall effect of the ~~air-sea coupling is an increased SST front~~ ocean-atmosphere coupling is a sharper SST gradient between the subtropical warm anomaly and the subpolar cold anomaly, ~~representative of the characteristic~~ which is characteristic of the large-scale SST tripole pattern ~~(Czaja and Frankignoul, 2002). The cold anomaly off the coast of western Africa can be explained by the large-scale atmospheric circulation anomaly over the subtropical region, leading to southward winds along the African coast and enhanced upwelling. Given the associated air-sea feedbacks~~ and associated feedbacks (Czaja and Frankignoul, 2002; Mar̶. By being highly correlated with the SST anomalies, the freshwater indices serve as valuable tools for visualising the associated ocean and atmospheric circulations, reinforcing each other (Figs. 1 and 4). However, we do not causally attribute ~~this large-scale SST signal~~ the SST pattern to freshwater anomalies~~alone~~, and we do not infer that the freshwater anomalies act as a trigger for the characteristic tripole SST pattern.

4.4 ~~**Implications for European summer weather**~~

4.4 **Links to European summer weather**

The preceding analysis revealed a close statistical link between freshwater anomalies and associated winter conditions. Next, we investigate the SST and atmospheric conditions in subsequent summers. In the first summer after stronger freshwater anomalies (again represented by F_E), we find that the SST is characterised by an enhanced ~~meridional SST gradient with the subpolar cold~~ subpolar cold SST anomaly covering part of the North Atlantic Current ~~, as in the preceding winter~~ in the central North Atlantic (Fig. ~~6a~~5a). In the second summer, the northward shift of the North Atlantic Current is the most pronounced signal, ~~implying that the region of the enhanced meridional SST gradient is shifted northward compared to the first summer~~ visible by a band of increased SST that extends northeastward across the North Atlantic from Nova Scotia towards the British coast (Fig. 5b).

The SST signal in both summers after the freshwater anomalies implies an increased SST difference between the warm subtropical gyre and the cold subpolar gyre. The exact location of the SST front between the subtropical gyre and the subpolar gyre can differ between the years included in the subset and is therefore poorly constrained, resulting in reduced significances at individual grid points. However, the increased SST gradient — which is of greater dynamical relevance than absolute SST anomalies — is highly significant. For instance, the SST difference between the region in which the SST anomaly exceeds 2 °C and the region in which the SST anomaly falls below -2 °C, includes a substantial area of the extra-tropical North Atlantic (Fig. ~~6b) .~~ 5a and b) and is significantly correlated with the F_E index with a correlation coefficient well above 0.7 in both summers ($r \approx 0.76$ and 0.84 in the first and second summer respectively), with p-values well below 0.05.

As in the preceding winters, ~~the SST fronts destabilise the overlying atmosphere, resulting in an enhanced jet stream along the front~~ we find that the atmospheric circulation is aligned with the underlying SST in both the first and second summer after the freshwater anomalies, with the winds at 700 hPa circulating cyclonicly around the subpolar cold SST anomalies (Fig. ~~6a~~ 5a and b). In summer, ~~moreover~~however, there is an additional ~~surface temperature gradient~~ temperature contrast across
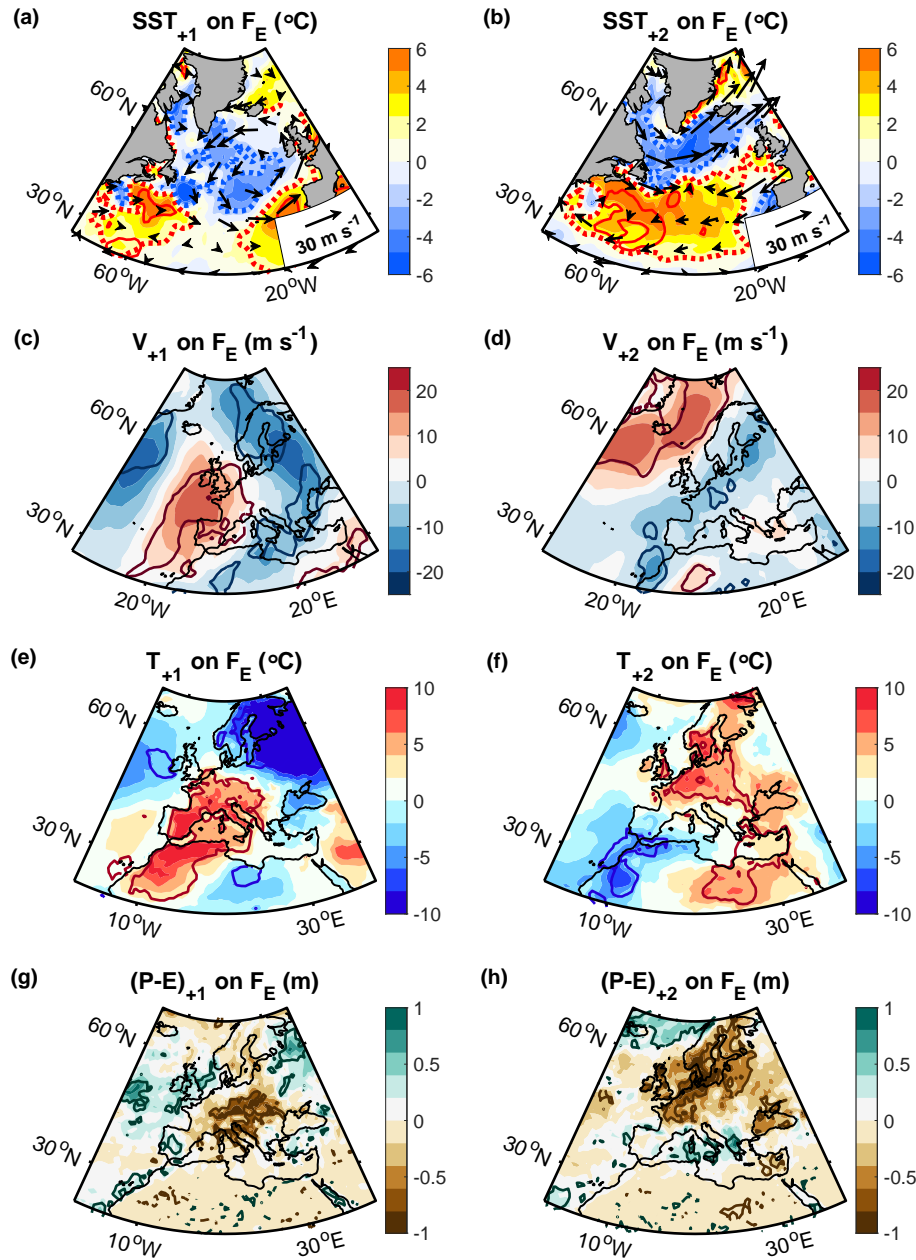
Figure 5. Regressions of (a,b) the SST ~~with the 700-hPa~~ (colour shading) and 700 hPa winds (arrows), (c,d) the meridional winds at 700 hPa, (e,f) the 2-m air temperature and (g,h) the accumulated precipitation minus evaporation on F_E in (a,c,e,g) the first and (b,d,f,h) the second summer (May through August) after the freshwater anomalies (indicated by the '+1' and '+2' in the titles). We removed large-scale trends from the air temperature to reduce the direct warming effect of greenhouse gases (Section 2), and we excluded the anomaly in ~~2015~~ 2016 since its responses were covered by the ~~2016~~ 2017 anomaly (not shown). Thick contours encompass regions that are significant at the 95% confidence level and the red and blue dotted lines in panels a and b delineate the regions in which the the SST anomalies exceed $2\,°C$ and fall below $-2\,°C$.

23

the European coast~~, so the anticyclonic circulation anomaly is, in part rotated over the continent, and~~ . Thus, we observe a northward deflection of the jet stream downstream of the cold SST anomaly along the coast (Fig. 5c and d). In the first summer, the ~~jet stream is deflected northward~~ northward deflection occurs west off northern Africa, Spain, Portugal, France and the British coastline (Fig. 5c). In the second summer, the northward deflection of the jet stream occurs further north to the northwest of the Scandinavian coastline (Fig. ~~6c and d). Thus, in~~ 5d), consistent with the more northerly SST front over the North Atlantic (Fig. 5a and b).

In line with the more northerly SST front and jet stream locations in the second compared to the first summer, we observe relatively warmer and drier air over northern Africa and southwest Europe in the first summer after stronger freshwater anomalies, and relatively warmer and drier air over northwest Europe in the second summer (Fig. ~~6e-h).~~ 5e-h). In the first summer the maximum warm anomalies extend from Morocco and Algeria northward to France and southern Germany, while the maximum dry anomalies occur further to the east covering large parts of southwest Europe, including Italy and Greece. In the second summer after the freshwater anomalies, the maximum warm anomalies occur over central to northern Europe, including Germany, France, the UK, Poland and southern Sweden, while the maximum dry anomalies again extend further eastward, including Finland and the Baltic countries. Considering that precipitation anomalies preferentially occur along trailing cold fronts and are shifted southward relative to cyclone centres (Booth et al., 2018; Kodama et al., 2019), the observed displacement of the dry anomalies relative to the warm anomalies is expected from their locations within individual weather systems and consistent with other studies (Yu et al., 2023).

~~Regressions of (a) the SST with the 700-hPa winds, (b) the meridional winds at 700 hPa, (c) the 2-m air temperature and (d) the precipitation minus evaporation in summer (July and August) on F_W from the preceding summer, again after subtracting large-scale trends from the air temperature. The thick contours encompass regions that are significant at the 95% confidence level.~~

~~Freshwater anomalies~~ Similar to the F_E freshwater anomalies, freshwater anomalies associated with the F_W subset are also followed by a cold SST anomaly in the subsequent summer. However, compared to F_E freshwater anomalies, the cold SST ~~anomaly after~~ anomalies associated with the F_W ~~freshwater anomalies is more confined in the central North Atlantic~~ index are smaller and confined to the central and western North Atlantic off the coast of Newfoundland, with the regressions peaking in July and August (Fig. ~~7a~~ 6a). Consequently, we observe a sharp northward deflection of the jet stream ~~(Fig. 7b), leading to more westerly warm and dry anomalies over Europe~~ just eastward of the cold anomaly, and further west compared to the F_E subset (Fig. ~~7c and d). While the warm anomalies after the F_E freshwater anomalies extend across the Iberian Peninsula all the way to northern Africa~~ 6b). Likewise, the warm ~~anomalies following the F_W freshwater anomalies are centred around over France~~ air temperature anomalies over Europe also occur further west and are centred over France, Great Britain, Belgium and northern Spain, extending westward of the coast, while the dry anomalies extend eastward to the Baltic Sea region and northern Poland (Fig. 6c and d).

~~Moreover,~~

Overall, we find that the regressions of the SST and atmospheric circulation on F_W are weaker compared to those on F_E, consistent with weaker freshwater anomalies (Fig. ~~3~~2) and smaller regression slopes (Fig. ~~2d). Physically,~~ 1d), implying weaker
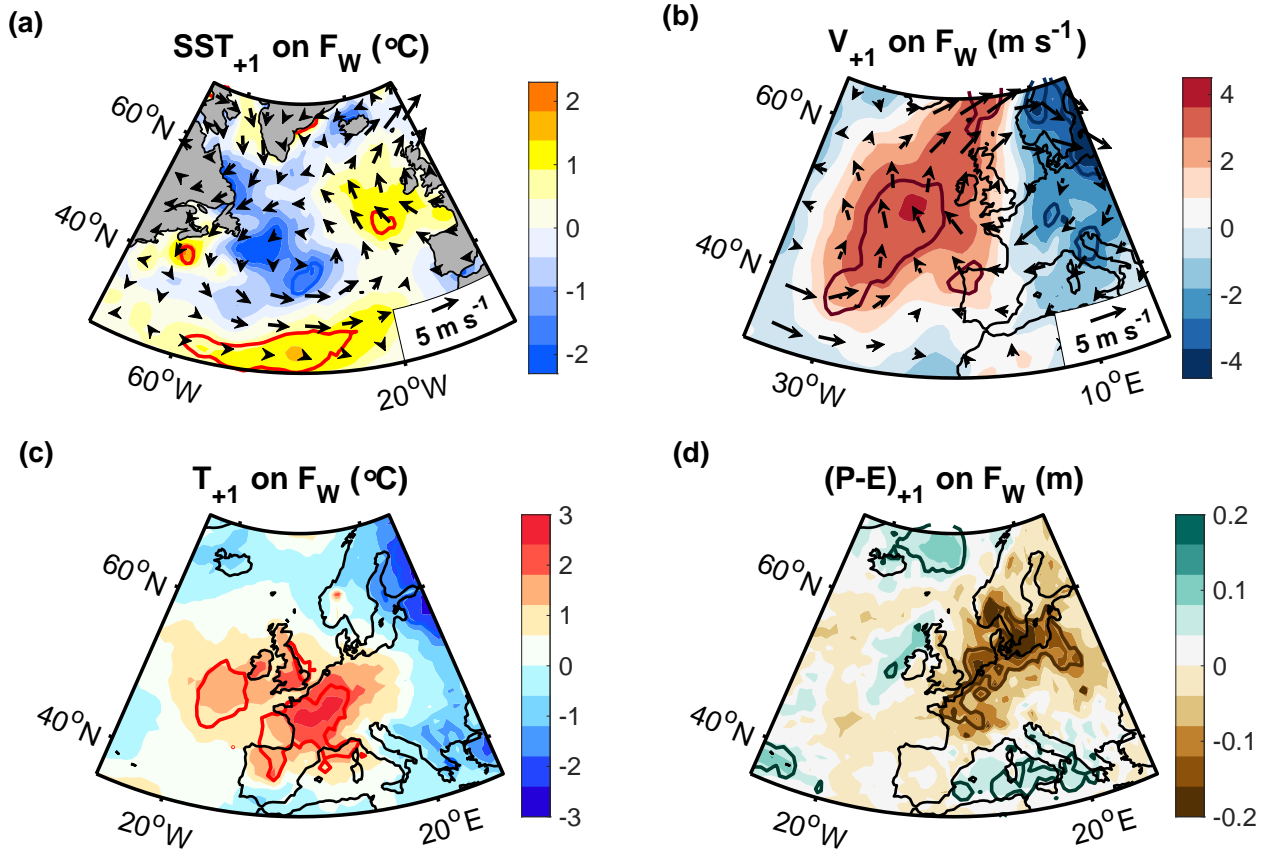
Figure 6. Regressions of (a) the SST (colour shading) and the 700-hPa winds (arrows), (b) the meridional winds at 700 hPa, (c) the 2-m air temperature and (d) the precipitation minus evaporation in summer (July and August) on F_W from the preceding summer, again after subtracting large-scale trends from the air temperature. The thick contours encompass regions that are significant at the 95% confidence level.

sensitivities to the freshwater index and associated atmospheric circulation in the preceding summer. Yet, despite differences in the location and magnitude of ~~the higher regressions on the F_E subsets imply a higher sensitivity of the ocean and atmospheric conditions to F_E~~ freshwater anomalies. ~~Once the seasonal freshening exceeded a critical threshold (corresponding to a threshold of ~ −0.5 in the NAO_S index), a relatively small further increase was linked to substantially warmer and drier summers.~~

~~Despite these individual differences,~~ anomalies, the overall patterns are qualitatively similar after F_E and F_W freshwater anomalies: Both types of freshwater anomalies are characterised by a cold SST anomaly and northward deflection of the jet stream ~~around the cold anomaly~~ over the North Atlantic in the subsequent summer. In both cases, the northward deflection of the jet stream reduces the advection of moist, maritime air masses over ~~different~~ parts of Europe, resulting in warmer and drier weather over parts of Europe.

4.5 ~~Warm summers in Europe~~ Significance and robustness

The ~~preceding analyses showed that two types of freshwater anomalies with opposite atmospheric drivers (characterised by a high and a low NAO states in the preceding summer) are followed by cold anomalies over the North Atlantic in winter, shifts in the jet stream and warmer, drier weather over Europe in the subsequent summers. Next, we investigate if warm European~~

635 ~~summers can, in turn, be linked back to a freshwater anomaly in the preceding year.~~ significance of the relationships between the freshwater indices and the ocean and atmospheric conditions in the subsequent winter and summer was assessed by Student t-tests, noting that the subsampling does not affect the significance of the relationship between the indices and any variable that is statistically independent of freshwater. If there is no connection to freshwater anomalies, the probability for randomly obtaining a significant statistical link by chance remains the same.

640 ~~Based on composites, we~~ Thus, we obtained significant links above the 95% confidence level, indicating that the probability for randomly obtaining the identified links is less than 5%. To ensure that the results are robust, we repeated the regressions by changing the number of years included in the subsampling, and by excluding anomalies in consecutive years (Appendix B). In all cases, we find that the ~~10 warmest relative to the 10 coldest summers in Europe were associated with a pronounced cold anomaly over the North Atlantic, and an atmospheric circulation anomaly that is characterised by a northward deflection of~~

645 ~~the jet stream (Fig. 8a-e). Using a surface mass balance (Appendix A), we again trace the cold anomaly back to a freshwater anomaly in the preceding winter~~ identified links are robust, which is consistent with the scatter diagram (Fig. ~~8f). Selecting different regions for the temperature variability over Europe shifts the location of the obtained anomalies but does not qualitatively alter these results~~1d), showing that there are no outliers or clusters of values responsible for the high correlations.

~~This analysis of Europe's warmest and coldest summers supports the statistical link between freshwater anomalies and~~

650 ~~European summer weather. It demonstrates that the link is robust to the analysis technique and independent of the indices. While the regressions on the freshwater indices showed that freshwater anomalies can constrain the variability of the subsequent European summer weather, the composites additionally show that, on interannual timescales, Europe's largest temperature anomalies were preceded by freshwater anomalies. This indicates that enhanced freshwater anomalies are not only a sufficient but also a necessary condition for warmer European summers.~~

655 ~~(a) Variability of the de-trended 2-m air temperature anomaly over land within the box shown in (b) during summer (July and August). (b,c,d,e) Composites of (b) the 2-m air temperature, (c) the meridional winds at 700 hPa, (d) the sea level pressure, and (e) the SST with the 700 hPa wind anomalies for the ten warmest minus the ten coldest summers, shown in (a). (f) Same as in (b-e) but for the sea surface salinity anomaly in the preceding winter, obtained from a surface mass balance (Appendix A). Contours delineate the regions that are significant at the 95% confidence level, assessed by means of two-sample t-tests.~~

660 ## 4.6 ~~Variability of freshwater over the last 70 years~~

~~Next, we assess the longer-term variability of surface freshwater over the period since 1950. Following a surface mass balance analysis (Appendix A), we identify a significant freshwater trend accompanying a cooling trend in the subpolar region (Fig. 9a~~

26

and b). The spatial SST pattern bears a high resemblance to the SST trend in summer (Fig. 9c), and the summer SST anomalies associated with increased runoff in the preceding year (Fig. 9d).

To investigate the variability of the SST pattern more closely, we project the SST variability each summer onto the pattern obtained from the SST trend. We use the region between 10° W, 65° W, 30° N and 60° N to focus on the area of reduced cooling A limitation of F_E and F_W is that they only cover a limited set of years, raising the question if the relationship between the SST, SSS and subsequent atmospheric anomalies holds generally or only over the selected subsets. To address this question, we use an un-subsampled SST-based index covering all years. As before, we avoid potential influences of a spatially uniform warming trend by using the spatial SST differences between the subpolar and the subtropical gyre ('ΔSST'), rather than absolute cold anomalies. Specifically, we use the SST difference between regions enclosed by the 95% lines, obtained after regressing the SST on F_E (Fig. 9c and d). However the results are not sensitive to the exact region. Closer examination of the time evolution of the SST pattern reveals a high interannual variability, superimposed on the long-term trend (Fig. 9e and f). Moreover, the interannual variability of the SST pattern is significantly linked to the summer NAO and runoff from the preceding year. For instance, the correlation of the pattern with runoff is ∼0.52 (p ≈ 3 · 10^{-6}), which remains significant after subtracting the trend (7a). Using the regions obtained from F_W does not appreciably change the results, as the associated ΔSST time series (obtained from F_E and F_W) are highly correlated with each other (r ≈ 0.31; 0.96, p ≈ 0.01 10^{-23}).

Apart from seasonal runoff and melt-driven freshening, there are currently no conceivable, physical mechanisms in the tropics, stratosphere or outside the North Atlantic which, at the same time, have a significant trend over the last 70 years, exhibit a similarly high interannual variability, can explain the occurrence of freshwater anomalies in the subpolar region in the subsequent winter, and are significantly correlated with the characteristic summer SST pattern a year before it occurs. This suggests that seasonal freshening may not only be a predictor of the SST pattern but also a trigger, investigated next.

(a,b,c) Linear trend of (a) the SSS, obtained from a surface mass balance (Appendix A), and (b,c) the SST in winter (January to March) and summer (July and August) over the last 70 years. (d) Regression of the SST in summer onto the total (normalised) runoff from the preceding summer (July and August). Contours delineate the regions that are significant at the 95% confidence level. (e) Variability of the SST trend pattern in summer (blue bars) and the de-trended time series (red bars), obtained by (1) projecting the spatial variability of the SST in summer onto the trend pattern in (c) between 35° and 65° N and 10° and 70° W (shown by the box in c), and by (2) de-trending the resulting time series. (f) Autocorrelations of the time variability of the trend pattern (blue bars in e), the detrended time series (red bars in e) and the summer NAO in July and August.

4.6 Role of air-sea coupling

To assess the role of freshwater in triggering the SST signal, and thus, future implications of increased melting and runoff, we investigate the associated air-sea coupling processes. Therefore, we use the full, un-subsampled summer NAO as predictor. Using the summer NAO as predictor has the advantage that it occurs exactly one year before the summer SST pattern and European summer weather, has a high, interannual variability, a negligible trend and low autocorrelations. In addition, it is ubiquitously used, freely available, and does not include any processing. Still, we point that the subsequent results do not

~~change appreciably if, instead of the summer NAO, we use runoff from the Greenland climate model MAR, or the variability of the SST trend pattern in summer (Fig. 9c).~~

~~Using the full , un-subsampled summer NAO as predictor, we find that, the cold anomaly one year after reduced NAO states in summer is associated with an enhanced atmospheric baroclinic instability across the European coastline and a cyclonic atmospheric circulation anomaly near the cold SST anomaly~~ Evaluating the surface mass balance associated with the new ΔSST index, we again find that none of the terms on the righthand side of Eq. (5) can account for the mass increase, implied by the associated cold, subpolar SST anomaly (Appendix A). Thus, we conclude the cold anomaly can only be explained by the simultaneous existence of a freshwater anomaly, allowing us to infer the variability and spatial distribution of surface freshwater with an overall uncertainty of $\sim$6% that results from assuming density compensation. The correlation of the estimated freshwater variability with the ΔSST index extends over the full subpolar region, with maximum amplitudes of up to $\sim$0.8 occurring in the eastern subpolar gyre (Fig. ~~11a-c~~7b). This ~~circulation anomaly is associated with a northward deflection of the jet stream along the European coastline and warmer, drier weather over parts of southern and southeastern Europe (Fig. 11d-f).~~ correlation is slightly smaller than those obtained for the other two freshwater indices but the index now includes 44 years.

~~While a detailed heat budget of the mixed layers from winter to summer is beyond the scope of this study, we qualitatively~~ Considering the significant link between the ΔSST index and surface freshwater in the supolar region, we use it as a new freshwater index and examine the ocean and atmospheric ~~processes, that may contribute to the SST development. Like in winter, we find that the surface heat fluxes have only a limited contribution to the subpolar cold anomaly and mostly in spring (Appendix C). However, the atmospheric circulation anomaly after lower NAO states in summer implies a more cyclonic wind field over the cold anomaly. This circulation anomaly leads to upwelling in the centre of the cyclone~~ conditions in the subsequent summer. Inspection of the SST shows that a stronger ΔSST index in winter is associated with pronounced cold SST anomaly over the central subpolar region in the subsequent summer (Fig. ~~10)and thus increases the temperature contrast between the surface water, that is heated by solar radiation, and the deeper, upwelled water in the cyclone centre, that has been in contact with the atmosphere in the preceding winter and spring. Moreover, the warm anomaly region to the southeast~~ 7c). The atmospheric circulation is aligned with the underlying SST field, with the winds at 700 hPa circulating cyclonicly around the cold, subpolar SST anomaly (Fig. 7c). To the east ~~of the cold anomaly region corresponds to a region of convergent Ekman transports and hence, downwelling~~ SST anomaly, the winds are deflected northward along the European coastline (Fig. ~~10). The consistency of the SST signal with the regions of wind-driven up- and downwelling suggests that the atmospheric forcing may contribute to the development of the SST field.~~ 7d), leading to warm and dry atmospheric anomalies over Europe. The warm anomalies extend over Spain, Italy France, the Netherland and parts of Germany eastward to Austria, Hungary and Slovakia, while the dry anomalies occur further northeastward, covering France, the Netherlands, Denmark, and parts of northern Germany, Poland and Ukraine (Fig. 7e and f).

~~The importance of the air-sea coupling is further supported by the evolution of SST signal, which intensifies from spring to summer and reaches its peak in July, when the temperature contrast between the upwelled water and the newsummer water is largest. In addition, closer inspection of hydrographic observations from the cold anomaly region show that~~ Unlike the summer
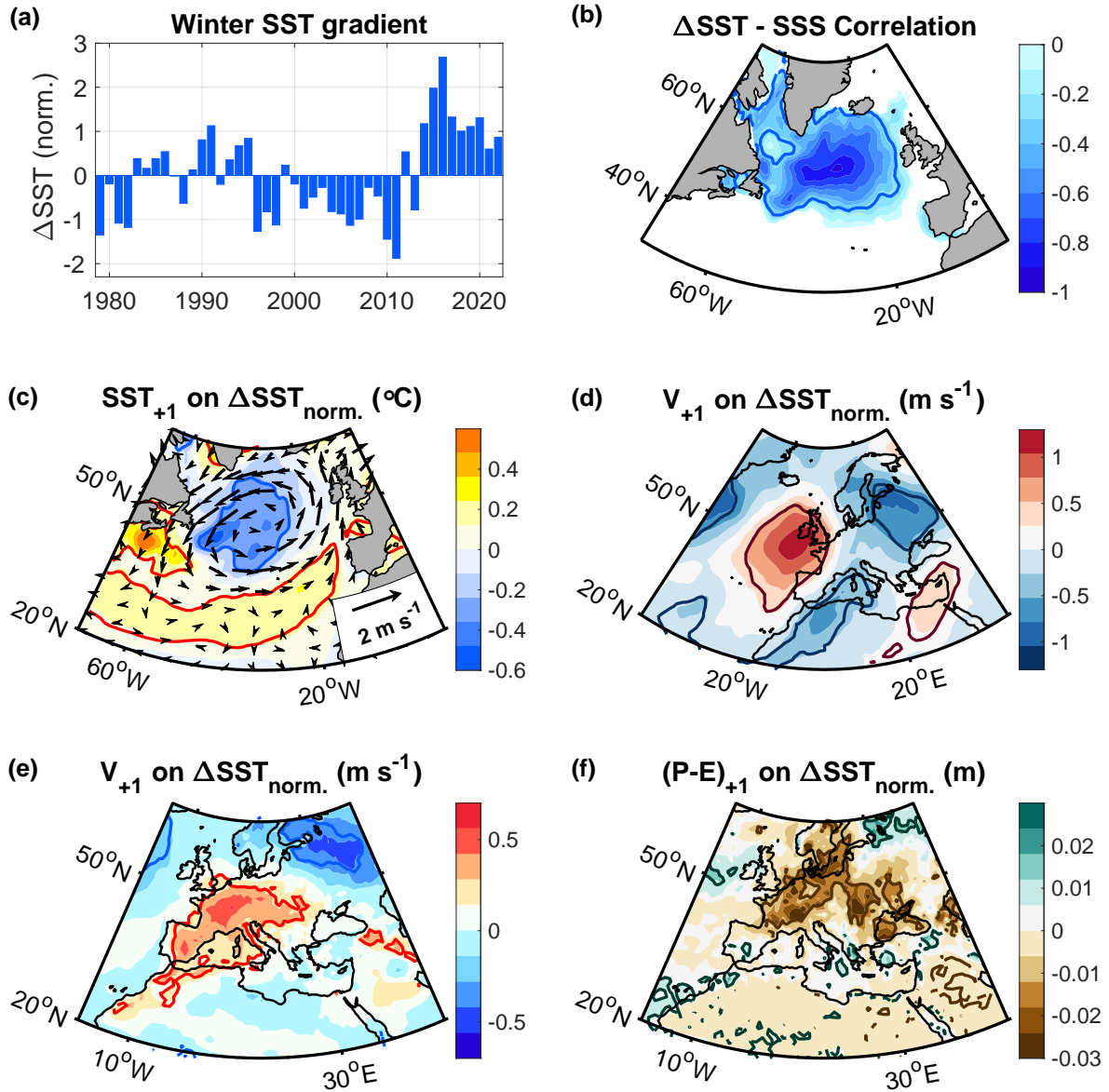
Figure 7. ~~Regression of~~ (a) ΔSST index corresponding to the normalised SST ~~, with arrows indicating~~ difference between the ~~direction of~~ subtropical warm anomaly and the ~~Ekman transports~~subpolar cold anomaly, enclosed within the 95% confidence lines in Figure 1e. (b) Correlation between the ~~maximum Eady growth rate~~ΔSST index, shown in panel a, and the sea surface salinity anomaly in the same winter (January through March), estimated from the surface mass balance. (c-f) Regressions of (c) the ~~sea level pressure~~SST (colour shading) and 700 hPa winds (arrows), (d) the meridional ~~component of the~~ winds at 700 hPa, (e) the 2-m air temperature ~~,~~and (f) the precipitation minus evaporation ~~from May through to August onto~~ ~~NAO~~$_S$ in summer (July and August) onto the ΔSST index from the preceding ~~year.~~ ~~Again~~winter (panel a), ~~we subtracted~~ again after subtracting the large-scale trends from the air ~~temperatures~~temperature. ~~Contours delineate the~~ The thick contours encompass regions that are significant at the 95% confidence level.

NAO, the ~~hydrographic signal is relatively shallow, in line with the idea that it is forced by the atmosphere and contradicting the idea that it is caused, for instance, by a~~ new, SST-based index has higher autocorrelations (Fig. 8a), which we attribute to enhanced low-frequency ~~change in~~ variability of the ~~large-scale ocean circulation (Appendix C).~~

~~The previous analyses suggest that the atmospheric forcing and, specifically, the wind-driven transports play a key role in the development of the SST pattern. To assess, in turn, the role of the SST pattern in driving the atmospheric instability and warm and dry anomalies over Europe, we next define an SST index that captures the time variability of the cold anomaly pattern ('SST_{FW}'). For consistency with the observational analysis, we project the SST each summer onto the observed SST pattern after the summer NAO between 10° W, 65° W, 30° N and 60° N. However, selecting the SST trend pattern~~ North Atlantic climate in winter. We still assume that interannual variability substantially contributes to the correlations, due to the high, interannual variability of European summer weather, reflected in low autocorrelations (Fig. 8b). Nonetheless, to assess the contribution of low-frequency variability to the obtained links, we lowpass filter European summer weather with a hanning filter, using a window size of 3 summers to approximate the higher autocorrelations of the ΔSST index (Appendix B). After accounting for the reduced number of independent samples in the significance tests with $N^* = \frac{N\Delta t}{2T_e} - 2$, where N here refers so the number of data points, Δt is the time interval between them, and T_e is the e-folding timescale of the autocorrelations (Leith, 1973), we still obtain statistically significant relationships but the amplitudes of the regressions are reduced (Fig. ~~9e), or the pattern obtained from runoff~~ B8), indicating that high-frequency, interannual variability substantially contributed to the relationship obtained from the unfiltered timeseries (Fig. ~~9d), yields qualitatively the same results.~~ 7).

~~Next, we regress the~~ To further assess the timescales on which the identified relationship holds and is significant, we carry out a multi-taper coherence analysis. Specifically, we calculate the coherence between the ΔSST index and the temperature and precipitation ~~anomalies, obtained from 90 ensemble simulations over 40 years, performed with prescribed observation-based SSTs, onto this newly-defined SST_{FW} index~~ minus evaporation anomalies in the regions in which we identified a significant link from the regressions (Fig. ~~11a and b). We obtain a significant link between the prescribed SST pattern and the~~ 7e and f). Inspection of the coherence estimate shows that both, temperature and precipitation ~~anomalies~~ minus evaporation over Europe, ~~both in the observations~~ are significantly linked to freshwater variations in the subpolar region on timescales from a few years to decades (Fig. ~~11c and e)and in the simulations~~ 8c and d). The coherence between the ΔSST index and the precipitation minus evaporation anomaly is particularly high and well above the 95% significance line (Fig. ~~11d and f). Overall, the observed and simulated atmospheric responses agree qualitatively well but the simulated responses are weaker and cover a larger area (Fig. 11e-f~~8d). The associated phase shifts are relatively constant at 0° for the air temperature (indicating a positive correlation) and 180° for precipitation minus evaporation (implying anti-correlation). We ~~attribute this underestimation of the obtained atmospheric anomalies in the simulations to potential model biases (Osborne et al., 2020) and the lack of air-sea coupling~~used 8 tapers, which is a standard value. However, the results are not sensitive to this choice.

We conclude that the ~~atmospheric forcing contributes to the development of the SST field but is in turn, forced by it. On the one hand, the consistency of the spatial SST pattern with the wind-driven transports, the intensification of the SST signal in mid-summer, and the vertical extent of the hydrographic anomaly point to the relevance of the atmospheric forcing in driving the SST signal over the North Atlantic. On the other hand, model simulations, forced with the prescribed, observed SST,~~
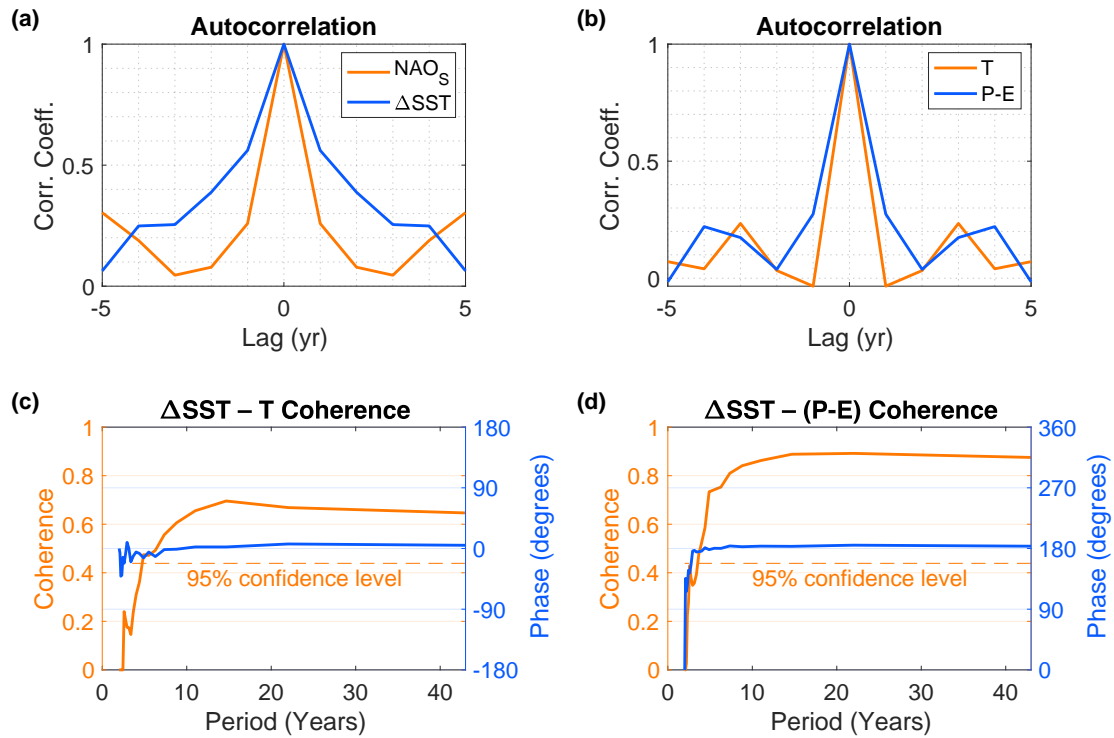
Figure 8. (a) ~~Variability and (~~,b) ~~distribution~~ Autocorrelations of (a) the ~~SST pattern one year after the summer~~ NAO ~~, obtained by projecting index in summer (July and August) and the ΔSST ~~pattern~~ index in ~~the box in~~ winter (January to March), (b) ~~each~~ the 2-m air temperature and precipitation minus evaporation anomalies in summer (~~May through~~ July and August)~~on that after~~, averaged over the ~~summer NAO~~ ~~(Fig~~regions enclosed by the 95% confidence lines in Figure 7e and f. ~~10a).~~ (c,d,~~e,f~~) Regressions of~~ Multi-taper coherence and phase shift estimates for the ΔSST index in winter (~~e,e~~January to March) ~~the observed~~ and (d,f~~c~~) ~~simulated~~ the 2-m air temperature and (d) precipitation minus evaporation in ~~summer onto~~ the ~~normalised SST$_{FW}$ index~~subsequent summer (July and August), again ~~after subtracting~~ within the ~~large-scale trend from~~ regions enclosed by the ~~air temperature. The simulations were acquired from 50 ensemble simulations from ECHAM5~~ 95% confidence lines in Figure 7e and ~~40 ensemble simulations from CAM5 over the period 1979–2018, performed with the pre-scribed, observed SST~~f. ~~Shown is the mean of the regressions from the ensemble members, not the regression of the mean~~We used 8 tapers. ~~Arrows indicate the observed and simulated 700 hPa winds respectively.~~ The ~~thick contours encompass regions that are significant at the~~ 95% confidence ~~level~~estimates are based on Amos and Koopmans (1963) after correcting for the bias inherent in coherence estimates (Priestley, 1982).

~~reveal the importance of the SST field for the large-scale atmospheric circulation, including for European summer weather. The underlying SST pattern covers the entire North Atlantic with the strongest signal occurring in the subpolar region (Fig. 11b). While further studies are necessary to confirm the dynamical contribution of freshwater anomalies to the large-scale SST pattern, its~~ link between cold, fresh ocean anomalies in the subpolar North Atlantic region in winter and warm, dry atmospheric anomalies over Europe in the subsequent summer is robust, significant at both higher and lower frequencies, and independent of the spatial and temporal characteristics ~~, and the time lag of one year, indicate that enhanced surface freshening from the preceding year may have initiated the chain of air-sea feedbacks~~ of the freshwater index that is used.

4.6 Predictability of European summer weather

The preceding analyses revealed significant links between North Atlantic freshwater anomalies and European summer weather in subsequent years. This raises the question to what extent this link can be ~~exploited~~ used to predict European summer weather in advance. Thus, ~~in this last analysis, we~~ we next assess the predictability based on the explained variance in the observations, estimated by means of the squared correlation coefficient with the freshwater indices.

The variance of the near surface temperature and precipitation minus evaporation anomalies, explained by the F_E subset, reaches and even exceeds 80% over large parts of Europe (Fig. ~~12a-d~~9a-d). For the F_W subset, the explained variance drops to ~50% (Fig. ~~12e~~9e and f), and for the ΔSST index, the explained variance drops further to ~20% (Fig. 9g and h), as expected from the ~~reduced correlation between the F_W~~ trade-off between the number of years included in the index and the ~~corresponding freshwater anomalies. In both cases, the explained variance is largest in the regions that show the strongest links with the temperature and precipitation minus evaporation anomalies (Figs. 6 and 7). Given the high interannual variability of European summer weather and the summer NAO, reflected in low autocorrelations, we do not expect these explained variance to be significantly affected by a long-term trend.~~ associated correlations with freshwater anomalies in the subpolar North Atlantic region in winter and European weather anomalies in the subsequent summer.

~~A disadvantage of estimating predictability from the freshwater indices is the small sample size. If, instead, we approximate the freshwater variability by the meridional SST gradient in winter as an alternative freshwater index that covers the full period of investigation (Fig. 2d), or if we replace it by the full, un-subsampled summer NAO to only represent the contribution from the seasonal runoff- or melt-driven freshening component, the explained variance of European summer weather decreases to ~20% and extends over a broader area (not shown).~~

Overall, we find: The higher the correlation is between the initial freshwater anomaly and its index, the higher is also the variance of European summer weather that the index subsequently explains. The F_E index, in particular, has an extremely high correlation with the initial freshwater anomaly of over ~0.9 (Fig. ~~3e~~2c) and explains over 80% of the variance of European summer weather. Notwithstanding the small sample sizes ~~,~~ — in the case of F_E and F_W — or the reduced correlations — in the case of the ΔSST index — these results indicate that accurate ~~observations of surface freshwater~~ estimates of the sea surface salinity in the subpolar region can serve as valuable constraints for ~~seasonal to interannual weather~~~~forecasts~~predictions of European summer weather.
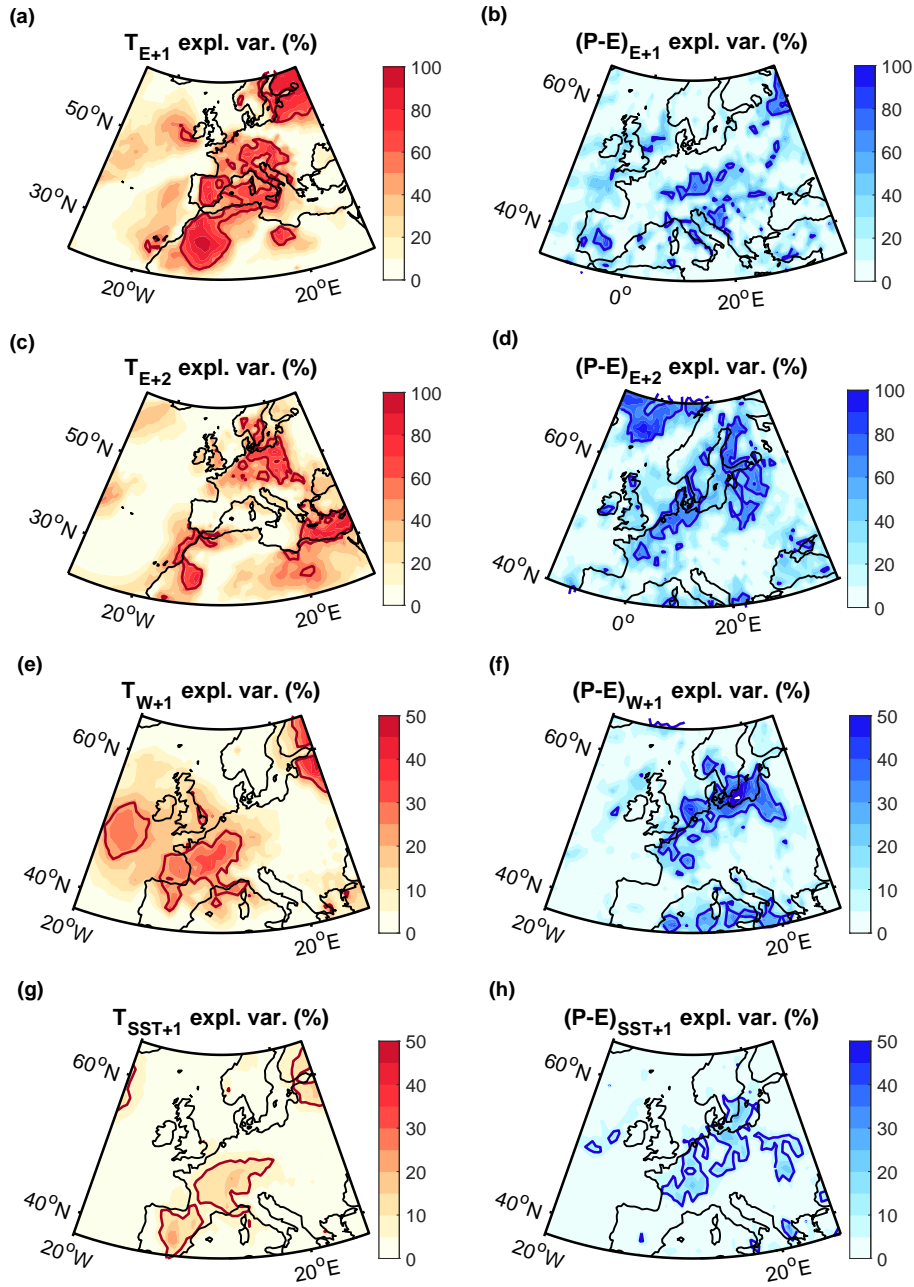
Figure 9. Variances explained by (a-d) F$_E$~~and~~, (e,f) F$_W$ <u>and (g,h) the ΔSST index</u> of (a,c,e,g) the 2-m air temperature and (b,d,f,h) precipitation minus evaporation after freshwater anomalies. '+1' and '+2' in the titles refer to the first and second summer after the ~~NAO subsets~~<u>freshwater anomaly. We again excluded the 2016 freshwater anomaly from F$_E$ since its responses were covered by the 2017 anomaly.</u> Thick contours delineate the regions ~~,~~ in which the correlation is significant at the 95% confidence level, assessed by means of two-sided Student t-tests. The explained variances were obtained from the squared correlation coefficients. Please note the different colour scales.

4.7 Warm summers in Europe

The preceding analyses showed that two types of freshwater anomalies with opposite atmospheric drivers (characterised by a high and a low NAO states in the preceding summer) are followed by cold anomalies over the North Atlantic in winter, shifts in the jet stream and warmer, drier weather over Europe in the subsequent summers. Lastly, we investigate if warm European summers can in turn be linked back to a freshwater anomaly in the preceding year. Thus, we assess the extent to which enhanced freshwater anomalies are not only a sufficient but also a necessary condition for warmer European summers.

Based on composites, we find that the 10 warmest relative to the sensitivity of European summer weather to seasonal melting rapidly increases. While this rapid increase in predictability provides new opportunities, 10 coldest summers in western Europe were associated with a dry anomaly to the east of the higher sensitivity also raises caution that a further increase in seasonal melting and runoff may lead to a more frequent crossing of the critical freshwater threshold and initiate a chain of feedbacks with substantial effects on warm air temperature anomaly, a northward deflection of the jet stream west of Portugal, France and Britain, and a pronounced cold SST anomaly over the North Atlantic (Fig. 10a-e). Using a surface mass balance (Appendix A), we again trace the cold SST anomaly back to a freshwater anomaly in the preceding winter, with the freshwater anomaly covering a large part of the subpolar North Atlantic (Fig. 10f). Selecting different regions for the temperature variability over Europe shifts the location of the obtained jet stream and SST anomalies but does not qualitatively alter the results.

In conclusion, this composite analysis of Europe's warmest and coldest summers supports the statistical link between freshwater anomalies and European summer weather .with an index based on air temperature. While the SST and NAO-based indices suggest that freshwater anomalies in the subpolar North Atlantic in winter are followed by warm and dry anomalies over Europe in the subsequent summer, the composite analysis additionally shows that the 10 warmest relative to the 10 coldest European summers have been preceded by significantly increased freshwater anomalies in winter.

5 Conclusions

In this study, we examined the link between North Atlantic freshwater anomalies and European weather in subsequent summers. Given the limitations of currently available salinity observations, we derived two freshwater indices that were highly correlated with subpolar freshwater anomalies. Taking advantage of the high correlations both indices were used to detect links between the freshwater anomalies, the subsequent ocean-atmosphere evolution, estimated the variability of freshwater based on a surface mass balance analysis. To identify statistical connections between the obtained freshwater estimates and European summer weather. We further supported the identified links by starting from European summer weather and examining its relation to preceding freshwater anomalies. Lastly, we investigated the freshening trend over the last 70 years, the associated ocean-atmosphere feedbacks and their implications for European summer weather, we further applied regression and correlation
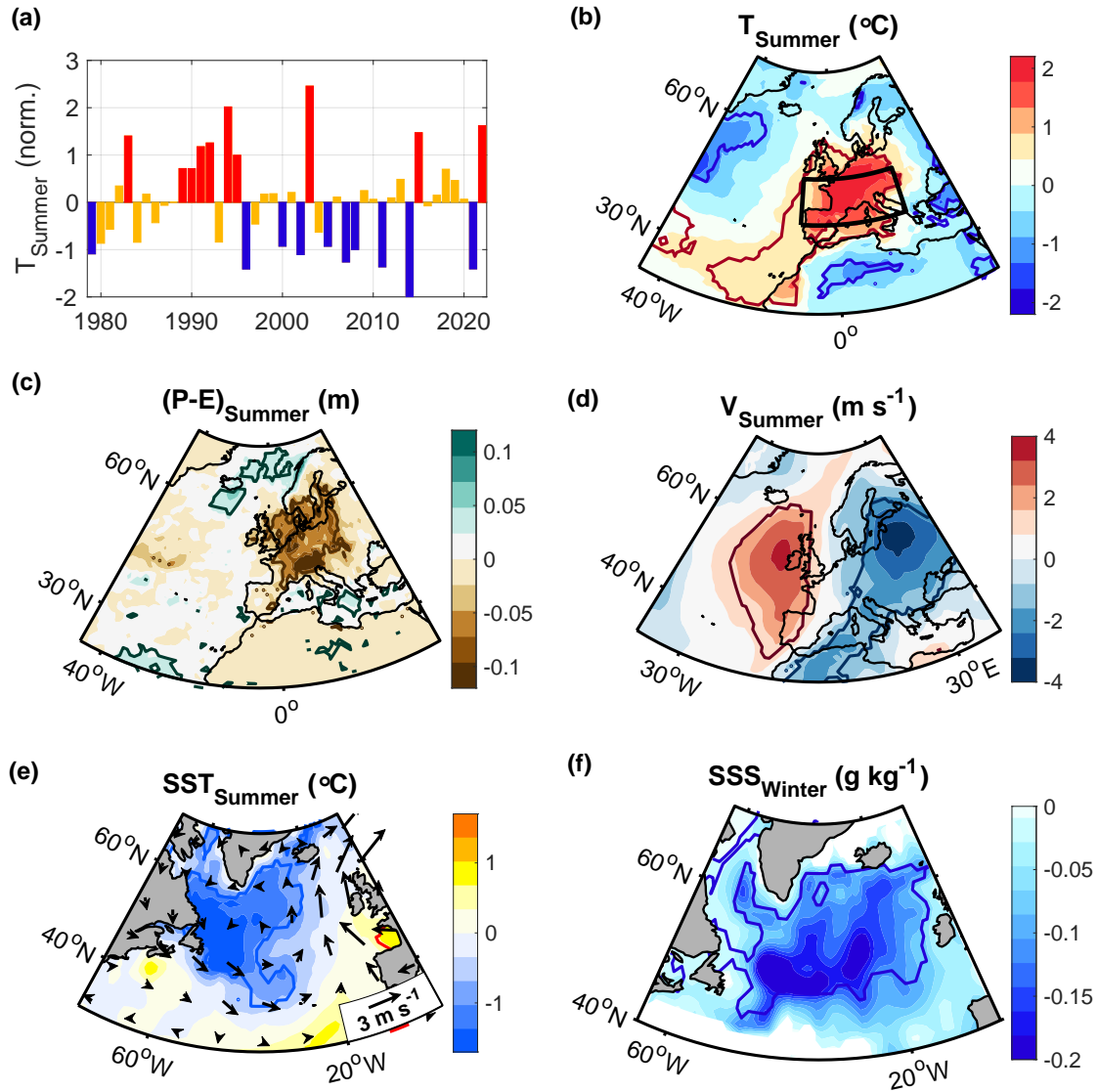
Figure 10. (a) Variability of the de-trended 2-m air temperature anomaly over land within the box shown in (b) during summer (July and August). (b,c,d,e) Composites of (b) the 2-m air temperature, (c) precipitation minus evaporation, (d) the meridional winds at 700 hPa, and (e) the SST (colour shading) and the 700 hPa winds (arrows) for the 10 warmest minus the 10 coldest summers, shown in (a). (f) Same as in (b-e) but for the sea surface salinity anomaly in the preceding winter, obtained from a surface mass balance (Appendix A). Contours delineate the regions that are significant at the 95% confidence level, assessed by means of two-sample t-tests.

830 analyses, composite analyses and multi-tapered coherence analyses. Combined, these analyses reveal a statistically significant relationship between freshwater anomalies in winter and European weather in the subsequent summer.

~~The analyses jointly reveal~~ To understand the physical link between the identified, statistical connections, we examined the associated ocean and atmosphere circulations. Thus we found that enhanced freshwater anomalies are associated with subpolar cold SST anomalies and an increased ~~meridional SST gradient~~ SST front between the warm subtropical and the cold subpolar

835 gyre in winter. The increased meridional SST gradient is linked to an amplified atmospheric instability and a large-scale atmospheric circulation anomaly with a more cyclonic circulation over the subpolar region and an anticyclonic anomaly to the south. This atmospheric circulation anomaly induces a northward shift in the North Atlantic Current which contributes to a warm anomaly to the south of the subpolar cold anomaly, amplifying the meridional SST gradient. In subsequent summers, the jet stream is deflected northward over the North Atlantic, aligned with the underlying SST fronts, leading to warmer and drier

840 weather over Europe.

~~The observed~~

The obtained evolution of freshwater anomalies follows the chain of events ~~predicted by theory. Specifically, the link between freshwater and cold anomalies is constrained by conservation of mass. The subpolar cold anomaly increases the meridional SST gradient leading to an increased meridional temperature gradient which promotes an amplified baroclinic instability~~

845 ~~(Eady, 1949; Davies and Bishop, 1994). Moreover, the ocean's response to the resulting atmospheric circulation is expected from Ekman transports and geostrophy (Munk, 1950; Stommel, 1948; Vallis, 2017). These theoretical underpinnings support the identified statistical relationships and point to~~ expected from theory, indicating a coherent, deterministic mechanism that links North Atlantic freshwater anomalies to European summer weather.

~~Notwithstanding the importance of freshwater as a useful predictor of European summer weather, the evolution and intensification~~

850 ~~of the associated SST patterns through winter and summer can only be explained by a chain of ocean-atmosphere feedbacks. Further studies are needed~~ Yet, further studies are required to quantify the relative contributions of different ocean and atmospheric drivers and their uncertainties, and the role of freshwater as potential trigger of the ~~feedback chain . To date, no conceivable alternative trigger in the tropics, stratosphere or outside the North Atlantic region can explain the high-frequency, interannual variability, the trend, the spatial characteristics of the SST signal, its relationship with the summer NAO and~~

855 ~~runoff and hence, the initiation of the feedback chain a full year before the~~ identified chain of events. This study identified statistically significant links and thus indicates an enhanced predictability of European summer weather arising from freshwater anomalies in the North Atlantic, without attributing the variability of European summer weather ~~as convincingly as freshwater~~ to freshwater anomalies as a mechanical trigger.

Current numerical weather prediction systems show very limited to no forecast skill for European summer weather (Arribas

860 et al., 2011; Dunstone et al., 2018). Thus, the existence of a link between North Atlantic freshwater anomalies and European summer weather indicates new potential to enhance the predictability of European summer weather a year in advance. Further studies that improve the representation of North Atlantic freshwater variations in models, and that quantify the predictability arising from them, are therefore desirable. In addition, targeted observational networks that monitor the variability of freshwater anomalies may help improve current forecast systems~~and circumvent the use of indices in future~~.

36

865　　The melting of ice and runoff are expected to further increase in the coming decades (Notz and Stroeve, 2018; Briner et al., 2020), resulting in an enhanced freshwater discharge into the North Atlantic. With stronger freshwater anomalies, our results indicate ~~a rapid~~ an increase in the risk of warm, dry European summers and of heat waves and droughts accordingly. Unfortunately, global climate models have difficulties in capturing the hydrographic structure in the subpolar North Atlantic, including the distribution of freshwater (Menary et al., 2015; Heuzé, 2017; Liu et al., 2017; Sgubin et al., 2017; Mecking et al., 2017;

870　　Wu et al., 2018). Considering the identified links between freshwater anomalies and the subsequent ~~ocean and atmospheric evolution~~ocean-atmosphere circulation, our results suggest that models may miss a key source of climate variability and potential long-range predictability.

Appendix A: Mass balance analyses

The following sections include the evaluation of the mass balances obtained from the freshwater indices F_E, F_W and ΔSST (A1), ~~those~~ the surface mass balance obtained from the SST composite ~~and trend~~ (A2), and a demonstration of the mass balance with hydrographic observations (A3).

885 ## A1 Surface mass balance for freshwater indices

Taking advantage of the strong relationships between the NAO_S subsets ~~and~~ (F_E and F_W) and the subsequent SST anomalies, we regress each term ~~in~~ of Eq. (45) onto the indices and evaluate the surface mass balance over the subpolar cold anomaly regions within the 95% confidence lines (Figs. A1a and A2a).

Considering that mean mixed layer deepens from summer to winter, reaching its maximum in late winter, the integrated
890 anomalies in the surface heat and buoyancy fluxes during autumn are predominantly driven by existing anomalies in the density profile. For instance, an anomalously warm and light layer of water will lead to increased ocean heat and buoyancy losses once it has been entrained (Timlin et al., 2002). Thus, given that the anomalies in B_n and M_n are expected to largely compensate for each other when integrated over autumn (the period of rapid mixed layer deepening), we focussed on the winter period (January through to March), when the amplitude and variability of the surface fluxes is largest. However, if we integrate
895 the terms on the righthand side of Eq. (45) over autumn and winter, instead of only winter, the magnitude of the integrated anomalies does not appreciably change and their signs remain the same.

First, we estimate the ~~horizontal transports~~ convergence of mass (A). On the timescales and spatial scales considered, the strongest horizontal velocities result from the geostrophic surface flow (including eddies and the subpolar gyre circulation). These surface flows do not contribute to a net mass increase as they occur along lines of constant density and pressure. The
900 largest ageostrophic surface flow in the open ocean results from the wind forcing, which we evaluate using the wind stresses from the atmospheric reanalysis ERA5. Integrated over the winter period (January through to March), we find that neither the horizontal Ekman transports nor the vertical Ekman pumping can account for the density increase associated with the cold anomaly. They are not significantly correlated with the freshwater indices, their amplitudes are too small, and their directions are inconsistent with the cold anomaly (Figs. A1a, b and A2a, b).

905 Next, we estimate the buoyancy flux anomalies $B = \frac{g\alpha}{c_p}Q + g\beta S(P - E)$, where c_p is the heat capacity, Q is the heat flux (positive downward) and $P - E$ is the freshwater flux in kg m^{-2} s^{-1} (Gill, 2016). After evaluating the buoyancy fluxes with 6-hourly ERA5 output and regressing them on the freshwater indices, we find that they do not match the distribution of the SST (Figs. A1c and A2c). The surface heat fluxes, which have the largest contribution to the buoyancy fluxes, are also not significantly correlated with the indices (Figs. A1d and A2d). When averaged over the cold anomaly regions, enclosed by the
910 95% confidence lines, and integrated over the winter, the buoyancy flux anomaly associated with the F_E subset reflects an anomalous mass decrease of $\sim$7 kg m^{-2} whereas the cold anomaly implies a mass increase of $\sim$204 kg m^{-2}. Likewise, the buoyancy flux anomaly associated with the F_W subset reflects a mass decrease of $\sim$~~5~~ 4 kg m^{-2}, whereas the cold anomaly implies a mass increase of $\sim$~~74~~ 69 kg m^{-2}, using a mean density of $\rho_{mean} \approx 1000$ kg m^{-3}.
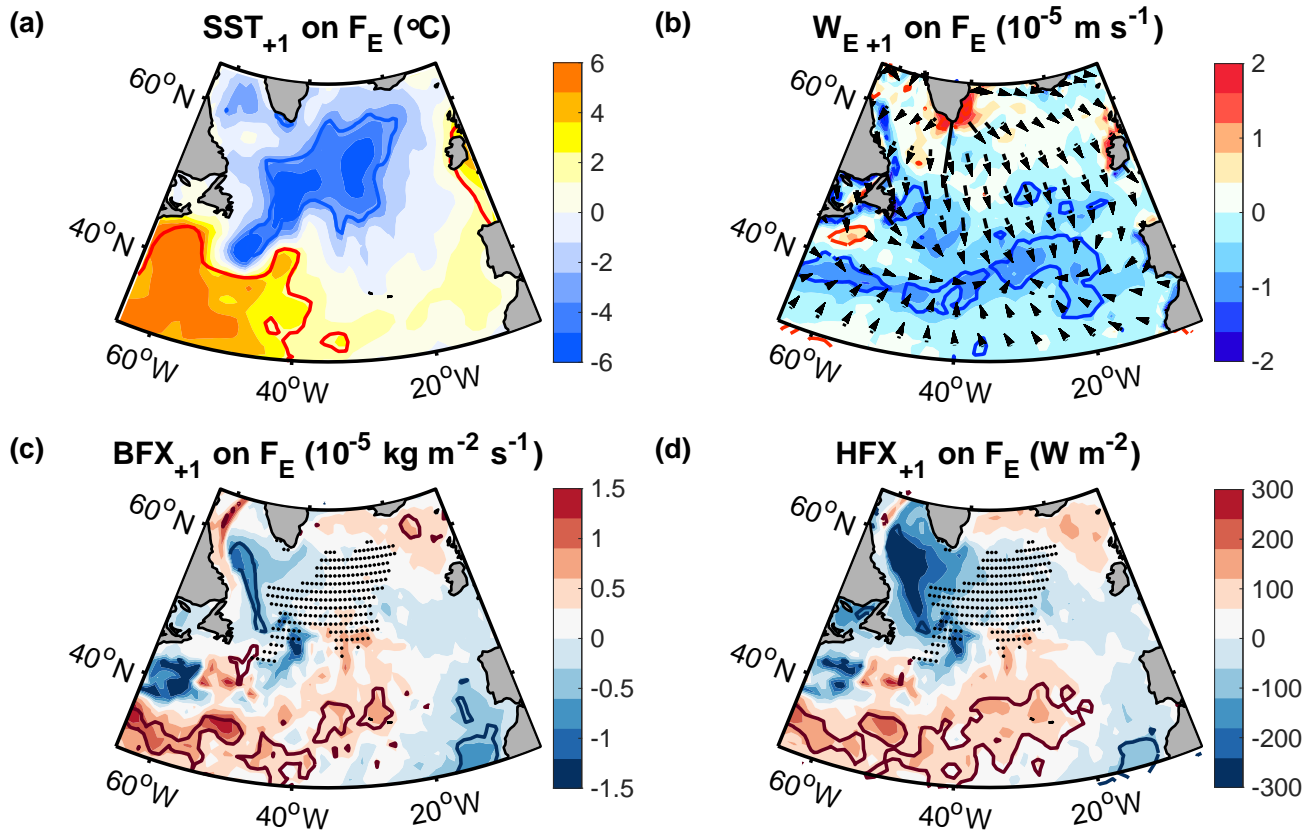
Figure A1. Regression of (a) the SST, (b) the vertical Ekman velocity (positive upward), (c) the buoyancy flux anomaly (positive downward) and (d) the surface heat fluxes (also positive downward) in winter (January through March) on F_E from the preceding summer. The arrows in (b) indicate the direction of the horizontal Ekman transports and the dots in (c) and (d) show the region used for the mass balance calculations, corresponding to the cold anomaly region. Contours encompass regions that are significant at the 95% confidence level.

915 ~~With the buoyancy fluxes, vertical Ekman transports and horizontal advection being negligible, there cannot be an anomalous density flux through the base of the mixed layer. The mixed layer can only entrain water of the same density as that at the surface (Section 4.1). If anomalously cold water from below is entrained, it must also be anomalously fresh. Thus, it drops out of Eq. (4).~~

Since none of the potential, active drivers of density anomalies on the righthand side of Eq. (45) can account for the density increase associated with the cold anomalies, we conclude that the density increase associated with the cold anomalies must be

920 balanced by a density decrease associated with freshwater anomalies. The buoyancy fluxes represent ~~by far~~ the largest term on the righthand side of Eq. (45), and thus determine the uncertainty of the obtained salinity estimates, amounting to $\sim$4% for the F_E subset and $\sim$76% for the F_W subset.
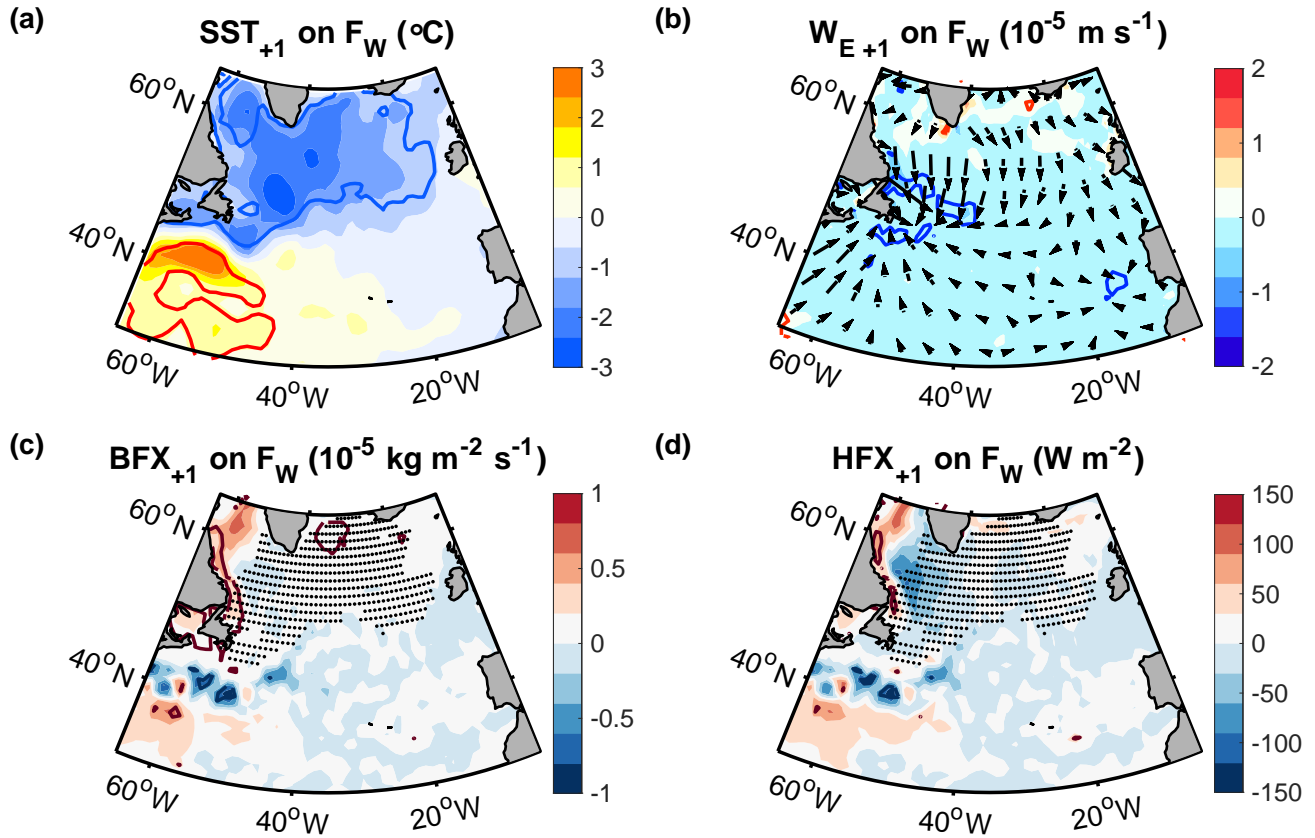
Figure A2. Regression of (a) the SST, (b) the vertical Ekman velocity (positive upward), (c) the buoyancy flux anomaly (positive downward) and (d) the surface heat fluxes (also positive downward) in winter (January through March) on F_W from the preceding summer. The arrows in (b) indicate the direction of the horizontal Ekman transports and the dots in (c) and (d) show the region used for the mass balance calculations. Contours encompass regions that are significant at the 95% confidence level.

~~In the calculations, we used a mean density of $\rho_{mean} \approx 1000$ kg m^{-3}, and a climatological mean winter mixed layer depth~~ ~~h_{mean} of ~250 m and ~280 m in the F_E and F_W cold anomaly regions respectively, obtained from Argo float profiles~~ 925 ~~(Holte et al., 2017). While the results are not sensitive to these values, the positive correlation of density and mixed layer depth~~ ~~anomalies can lead to an underestimate (but not overestimate) of the freshwater anomalies, due to the involved nonlinearity in~~ ~~the regressions.~~

To verify the robustness of the results, we tested different integration periods and regions for the mass balance calculations. For instance, we also integrated the transports and surface fluxes from September to March instead of January to March, and 930 we extended the investigated region over the full cold anomaly region, over which the SST anomaly is negative. In each case, the results did not change appreciably.
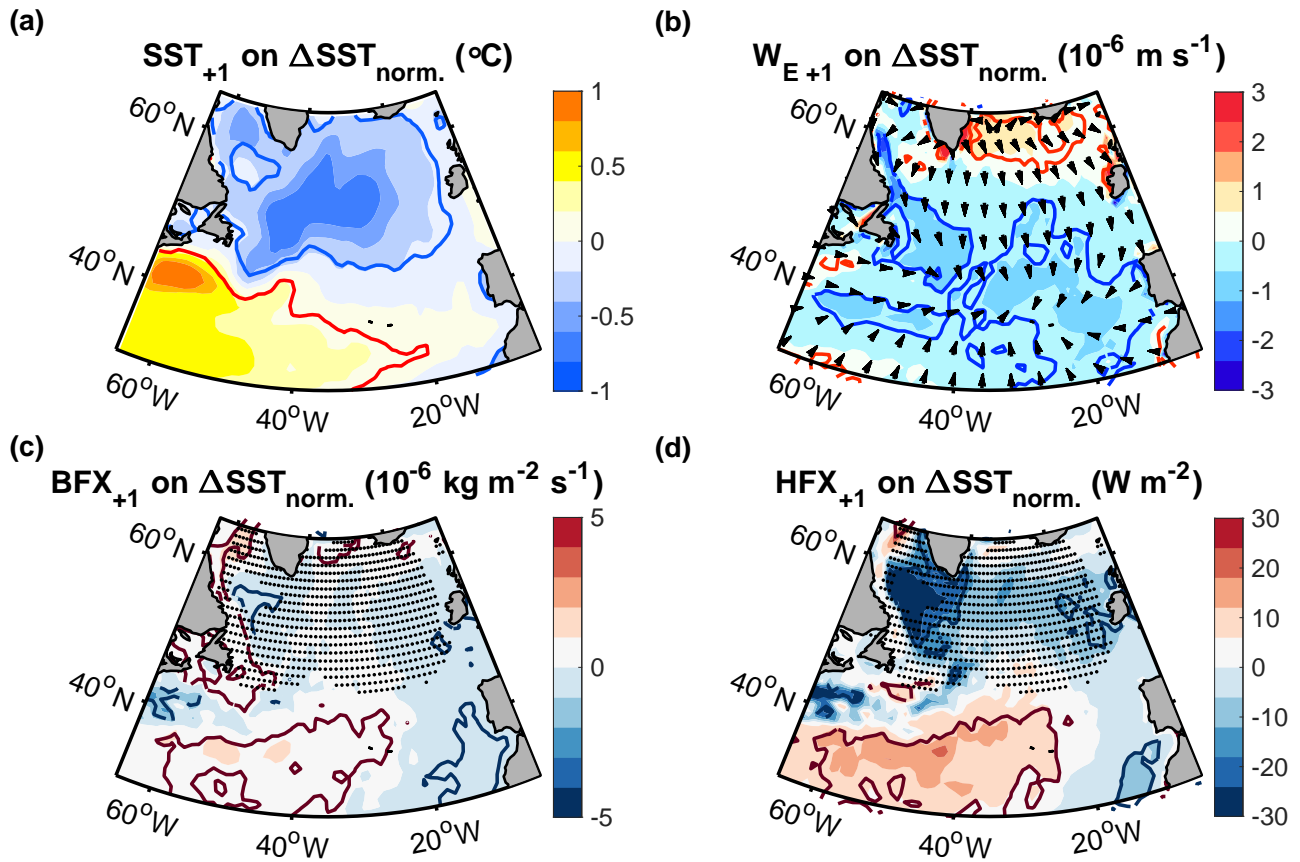
Figure A3. Regression of (a) the SST, (b) the vertical Ekman velocity (positive upward), (c) the buoyancy flux anomaly (positive downward) and (d) the surface heat fluxes (also positive downward) in winter (January through March) on the normalised ΔSST index (Fig. 7a). The arrows in (b) indicate the direction of the horizontal Ekman transports and the dots in (c) and (d) show the region used for the mass balance calculations. Contours encompass regions that are significant at the 95% confidence level.

In addition, we repeated the analyses for the un-subsampled ΔSST index (Fig. A3). In this case, we obtain a mean mixed layer depth of ~ 250 m, a negative mass anomaly of ~ -1 kg m^{-2} resulting from the surface buoyancy fluxes and a positive mass anomaly of $\sim +18$ kg m^{-2} associated with the cold SST anomaly. Thus, estimating the sea surface salinity anomaly by assuming density compensation, we obtain a sea surface salinity of ~ -0.10 g kg^{-1}, averaged over the cold anomaly region enclosed by the 95% confidence lines with an overall uncertainty of 6% that results from neglecting the terms on the righthand side of Eq. (5).

A2 Surface mass balance of the SST composite and trend

We further carried out a mass balance analysis for the composites of the cold anomaly in the winters preceding the 10 warmest relative to the 10 coldest summers over Europe (Fig. ~~8~~10). Thus, we again evaluated the terms in Eq. (~~4~~5) over the cold anomaly region and the winter, where now, the subscript n refers to anomalies associated with the composites.

After evaluating ~~the terms~~ each term in the mass balance equation, we obtain similar patterns compared to those associated with the two NAO subsets (~~not shown~~Fig. A4). Again, we find that none of the density drivers on the righthand side of Eq. (~~4~~5) show a significant signal over the cold anomaly region, and their amplitudes cannot account for the density increase implied by the cold anomaly. The mean mixed layer depth in the cold anomaly region is now $\sim$290 m, the surface buoyancy flux, which is the largest term on the righthand side of Eq. (~~4~~5), amounts to $\sim +$~~1.3~~1.2 g kg^{-1} while the density anomaly implied by the cold anomaly is $\sim -$~~40~~44 g kg^{-1}. Thus, the uncertainty of the estimated freshwater anomaly (Fig. ~~8e) is~~10e) amounts to $\sim$~~3%.~~3%.

~~Lastly, we performed the surface mass balance analysis for the SST trend over the last 70 years (Fig. A3). When averaged over the cold anomaly region, enclosed by the 95% confidence lines, the density increase implied by the cold anomaly amounts to ~ -0.42 kg m^{-2}. The terms on the righthand side of the mass equation are negligible, except for the surface buoyancy fluxes, which amount to $\sim +0.048$ kg m^{-2}, implying an uncertainty of $\sim$11%for the estimated freshwater anomaly (Fig. 9a).~~

A3 Comparison with in-situ observations

To demonstrate the density compensation between temperature and salinity anomalies, we use mixed layer profiles from Argo floats in the subpolar region (Holte et al., 2017). We focus on the extreme winters 2015 and 2016, which were characterised by particularly large surface fluxes and deep convection (Yashayaev and Loder, 2017; Piron et al., 2017).

In both winters, the temperature and salinity anomalies are well-correlated with each other ($r \approx 0.72$, $p \approx 5 \cdot 10^{-242}$, based on 1532 profiles). Moreover, the observed salinity anomalies are well-aligned with the estimated salinity anomalies, obtained by assuming density compensation (Fig. ~~A4~~A5). The root mean square error associated with the mass balance estimate amounts to $\sim$0.09 g kg^{-1}, which is smaller than that of currently available salinity products (Bao et al., 2019; Xie et al., 2019).~~This suggests that even under particularly intense surface fluxes, the additional temperature change achieved by the surface fluxes is still significantly smaller than the temperature anomalies implied by the freshwater anomalies.~~
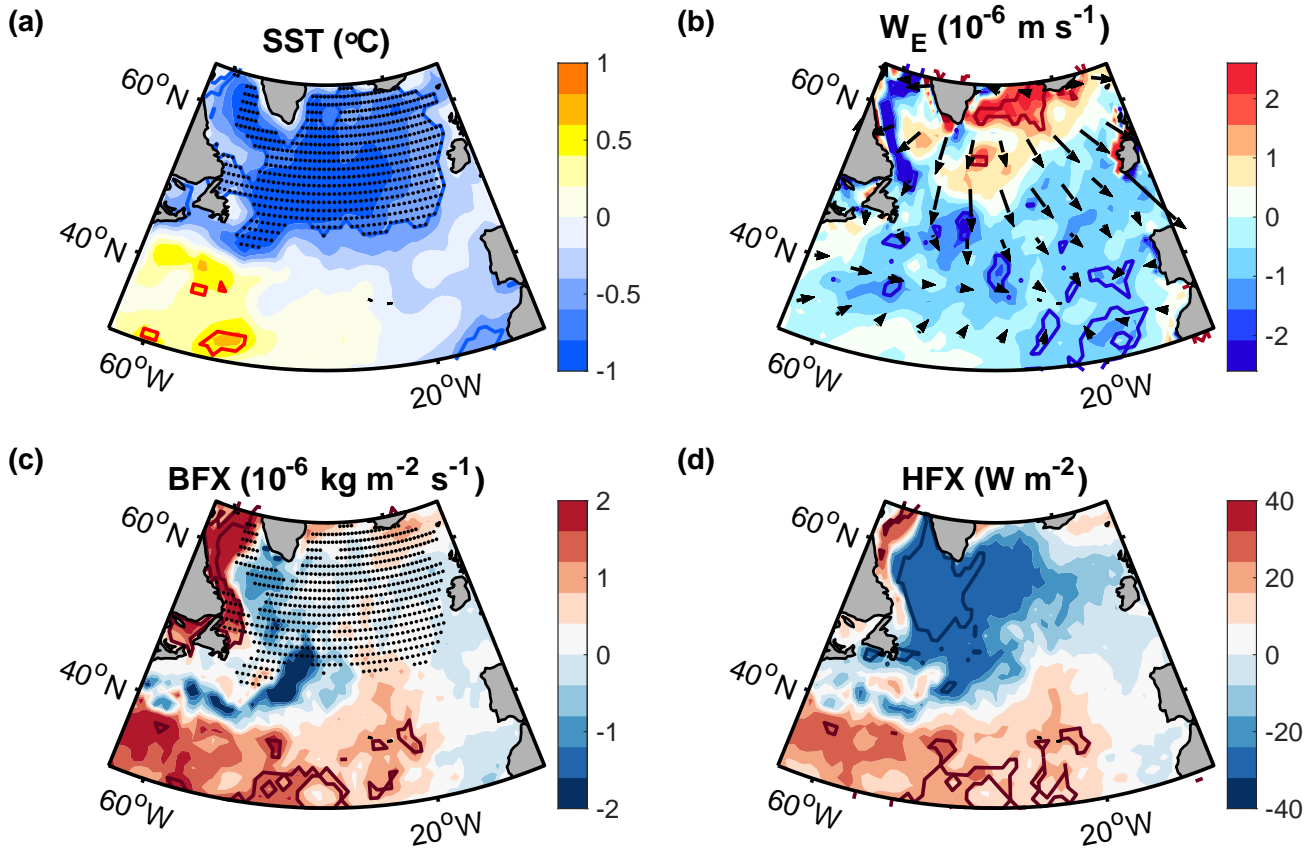
Figure A4. ~~Trends~~ (a,b,c) Anomaly of (a) the SST, (b) the vertical Ekman velocity (positive upward), (c) the buoyancy ~~fluxes~~ flux anomaly (positive downward), and (d) the surface ~~fluxes~~ heat flux (also positive downward) in ~~winter~~ the 10 winters (January through March) before the warmest summers minus the 10 winters before the 10 coldest summers (Fig. 10). The arrows in (b) indicate the direction of the horizontal Ekman transports and the dots in (~~e~~a) and (~~d~~c) mark the region of the mass balance ~~calculation~~calculations.~~Contours delineate the regions that are significant at the 95% confidence level.~~
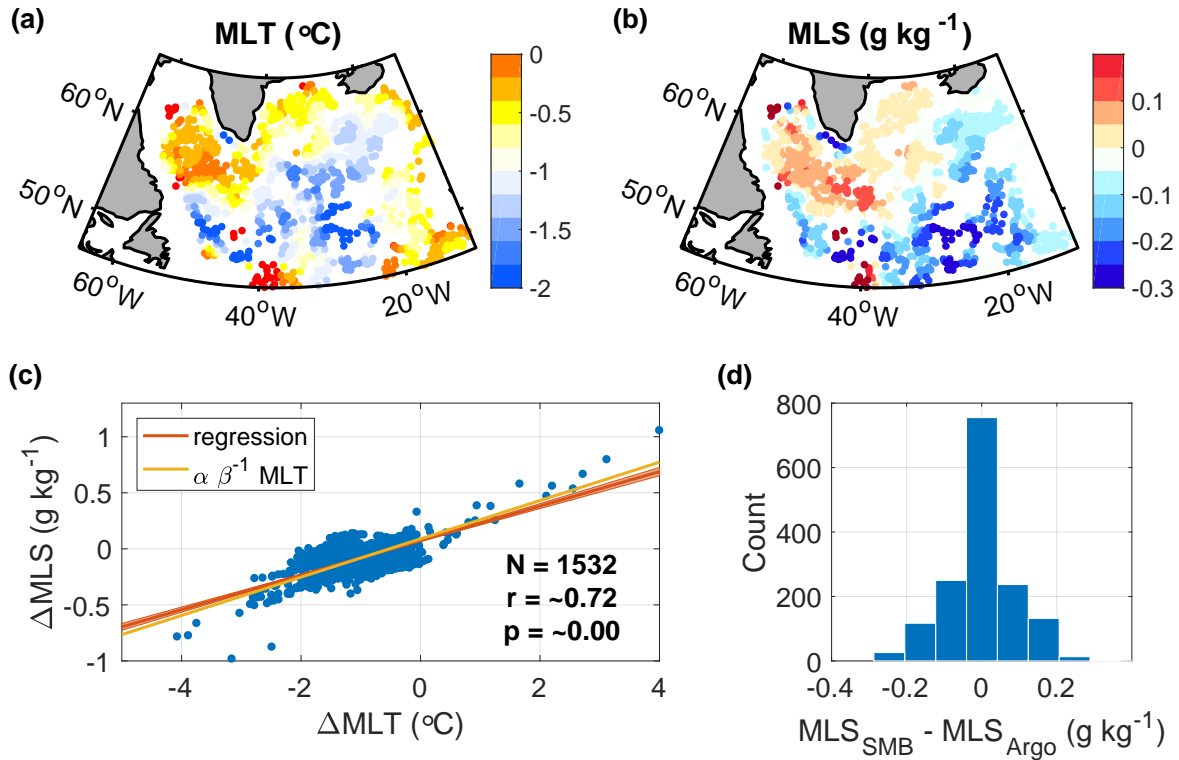
Figure A5. (a,b) Mixed layer temperature (MLT) and salinity (MLS) anomalies in the winters of 2015 and 2016 (January to April), derived from Argo profiles (Holte et al., 2017). The anomalies are relative to the climatological mean, estimated by averaging all other wintertime profiles within $2°$ longitude and $1°$ latitude. (c) Linear regression of the observed MLS anomalies on the MLT anomalies (red line), and the MLS estimate obtained by assuming density compensation (yellow line). (d) Differences between the estimated and observed MLS anomalies. The associated root mean square error is ~ 0.09 g kg^{-1}.

Appendix B: Robustness and significance tests

Appendix C: ~~Simulated atmospheric response to the freshwater-induced SST in winter~~

965 ~~To support the role of the SST pattern in driving the observed atmospheric response in winters after freshwater anomalies (Fig. 4b), we define an SST index that captures the time variability of the spatial SST pattern linked to freshwater anomalies. Specifically, we project the SST each winter onto the observed SST pattern after freshwater anomalies (Fig. B1a and b). The projection is obtained from a linear least-square fit of the SST each winter to the observed pattern after freshwater anomalies. We then regress the atmospheric streamfunction at different pressure levels onto this SST index , using 50 ensemble simulations~~

970 ~~from ECHAM5, performed with prescribed observation-based SSTs~~ In this section, we conduct sensitivity tests to assess the robustness of the indices F_E, F_W, and ΔSST. Considering the different weaknesses of each index, the analyses for each index are different. F_E only includes a low number of years. Thus, we will test the sensitivity of the results to including and excluding individual years. For F_W, the sample size is larger, such that adding or removing individual years has almost no effect on the results. Thus, we will test the sensitivity of the results to the number of years included in increments of 5 years. Finally, the

975 ΔSSS index is characterised by high autocorrelations. Thus, we will test if the results remain significant if we lowpass filter European summer weather and assume a lower number of degrees of freedom.

~~(a) Variability and (b) distribution of the freshwater-induced SST pattern in winter (January through March), obtained by projecting the SST each winter on the North Atlantic SST (north of 30 °N) after freshwater anomalies (Fig. 2a). Thus, SST$_{FW}$ represents the temporal variability of the spatial SST pattern linked to freshwater anomalies. (c,d) Regressions of the simulated~~

980 ~~stream function and winds in winter at (c) 500 hPa and (d) 250 hPa onto the normalised SST$_{FW}$ pattern shown in (a) and (b). The simulations were acquired from 50 ensemble members from ECHAM5, performed with prescribed observation-based SST over the period 1979–2018. Contours encompass regions that are significant at the 95% confidence level.~~

~~The SST-forced model simulations support that the SST pattern associated with freshwater anomalies leads to a significant atmospheric circulation anomaly over the North Atlantic, extending deep into the troposphere (Fig. B1c and d). As in the~~

985 ~~observations,~~ We start with the ~~simulated fields are characterised by a cyclonic circulation anomaly in the subpolar region and an anticyclonic circulation anomaly in the subtropical region. The winds at 250 hPa are still following the underlying SST gradients. Since the simulations were SST-forced, they imply that the obtained atmospheric circulation pattern is driven by the SST , although the SST is itself also the result of atmospheric feedbacks. While a detailed description of the involved diagnostics is beyond the scope of this study, the obtained atmospheric response is consistent with theoretical expectations~~

990 ~~(Eady, 1949), and the underlying dynamics are well-understood (O'Reilly et al., 2017; Omrani et al., 2019).~~

~~We point out that the SST$_{FW}$ pattern~~ F_E subset. If we include the outlier in 2019 (which was removed as part of the subsampling in Section 3), we still obtain similar ocean and atmospheric conditions in the subsequent summers, compared to those with the outlier excluded (Figure B1 and Figure 5). Specifically, we still identify an increased SST difference between the subpolar cold SST anomaly and the subtropical warm SST anomaly, with the location of the SST front being shifted northward

995 in the second summer relative to the first summer (Fig. B1a and b)~~is specific to the North Atlantic. It was obtained using a projection of the SST each winter onto the SST after freshwater anomalies~~. Moreover, we still identify northward deflections

of the jet stream and warm and dry anomalies over Europe (Fig. ~~2a), north of 30 °N. The results are not sensitive to the selected region as long as it includes the enhanced SST front between the subtropical and subpolar gyre. We do not find any significant links of the obtained SST$_{FW}$ pattern to the El Niño Southern Oscillation in the Pacific or to the SST in the South Atlantic.~~ B1c to h), with the locations closely resembling the regressions with the NAO$_S$ year in 2019 excluded (Fig. 5c to h). Likewise, if we only include the second anomaly in all consecutive anomalies, the results also remain similar and significant (Fig. B2).

Appendix C: ~~**Evolution and extent of the summer cold anomaly**~~

~~Section 4.7 showed that wind driven transports in summers after reduced NAO states are consistent with the associated SST signal and thus likely contribute to it~~

Next we examine the sensitivity of the results to the number of years included in the F_W subset. Since we find that the results do not change appreciably when we include or exclude single years, we show how the results are changing when we add or remove years in increments of 5 years. Thus, we show the regressions for $N = 7$ (Fig. ~~10a). We also examined the surface heat fluxes. While the surface heat fluxes may contribute to some cooling of the central North Atlantic in May and June, they are weakly positive over the cold anomaly region in July, when the cold anomaly is strongest~~ B3), $N = 12$ (Fig. B4), $N = 17$ (Fig. 6), $N = 22$ (Fig. B5), $N = 27$ (Fig. ~~C1)~~ B6) and $N = 32$ (Fig. B7), with N corresponding to the number of years included. The choice of years follows the same method as before (Section 3), with the objective of maximising the regression slope and the variance (resulting in high correlations). Thus, we rank all years according to the term $(y_i - y) \cdot (x_i - x_0)$ (Section 3.2) and then select the N highest terms. ~~A positive surface heat flux anomaly implies that the ocean anomalously cools the lower troposphere rather than the other way round, suggesting that the contribution of~~

The regression for the case, where no further subsampling is applied after excluding the F_E subset and the two outliers (corresponding to $N = 33$, not shown), do not change appreciably compared to the regression where $N = 32$. Likewise, if we exclude the only remaining consecutive year from the ~~surface heat fluxes to the cold anomaly may be limited.~~ case where $N = 7$ (not shown), the results do not change appreciably compared to the $N = 7$ case. Overall, we find: The lower the number of years, the higher is the amplitude of the correlations and regressions, which compensate for the reduced number of degrees of freedom in the significance estimates. In addition to the higher amplitudes, the location of the maximum warm and dry anomalies can shift in accordance of the location of the associated summer SST anomalies. However, in all cases we identify an increased SST difference between the subpolar cold anomaly and the warm North Atlantic Current, a northward deflection of the jet stream west of the European coastline, and warm and dry atmospheric anomalies over parts of western Europe or the eastern North Atlantic.

~~To assess the role of the atmospheric forcing for the development of the SST signal, we examined the vertical extent and evolution of the ocean signal with in-situ observations from Argo floats from the cold anomaly region (Fig. C2a). Due to the large spatial variability in this region, associated with shifts in the North Atlantic Current and eddies, it is not meaningful to construct time series of absolute temperature and salinity variability. The large spatial variability does not allow to deduce the temporal variability with sufficient accuracy. Therefore, we use vertical density gradients, representing stratification. Vertical~~
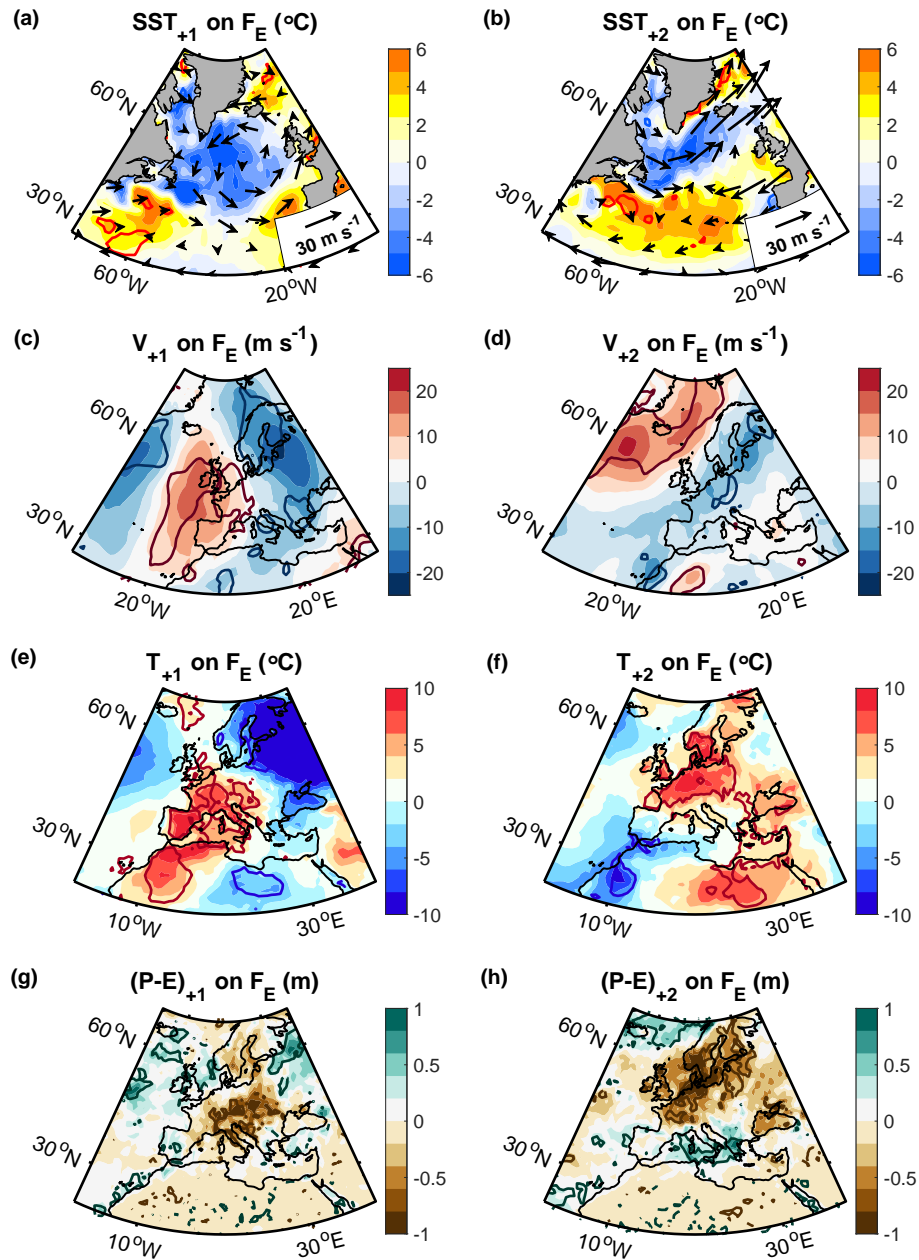
Figure B1. As in Figure 5 of the main manuscript, but with the NAO$_S$ index in 2019 included in the F$_E$ subset.
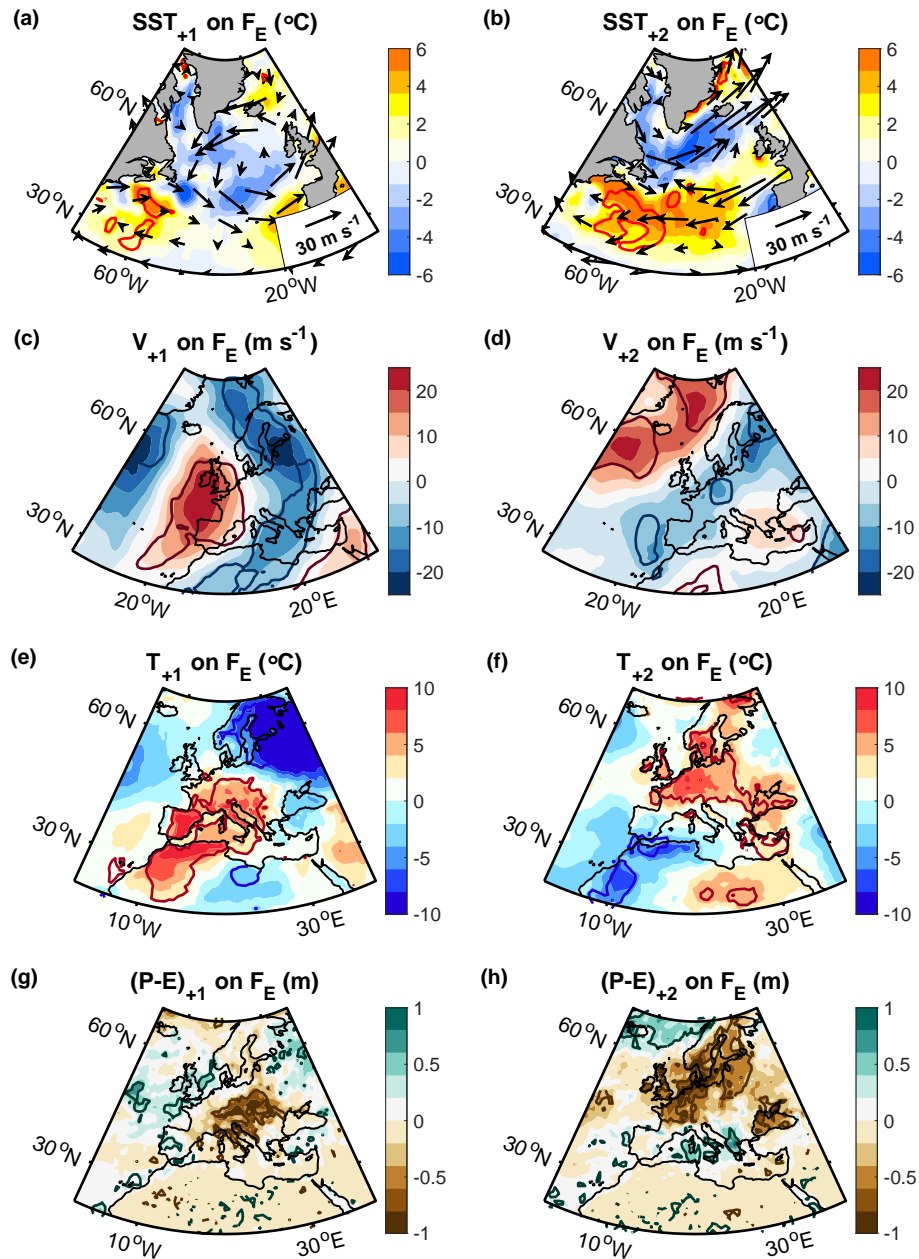
Figure B2. As in Figure 5 of the main manuscript, but excluding all consecutive years. Specifically, we only included the second year in all consecutive years. Thus, the regression is based on the NAO_S years 1980, 1993, 2009, 2012 and 2016.

Figure B3. (a) NAO$_S$ index with the years included in the F$_W$ subset shown in red. Years excluded prior to the subsampling (including the 8 F$_E$ years and the two outliers) are shown as faint blue bars. (b) Correlation between the F$_W$ subset (the red NAO$_S$ years in panel a) and the associated SSS anomaly in the subsequent winter (January to March), estimated from the surface mass balance by assuming density compensation. (c-f) Regressions as in Figure 6 of the manuscript but including only 7 years in the F$_W$ subset (shown in panel a). The thick contours encompass regions that are significant at the 95% confidence level.
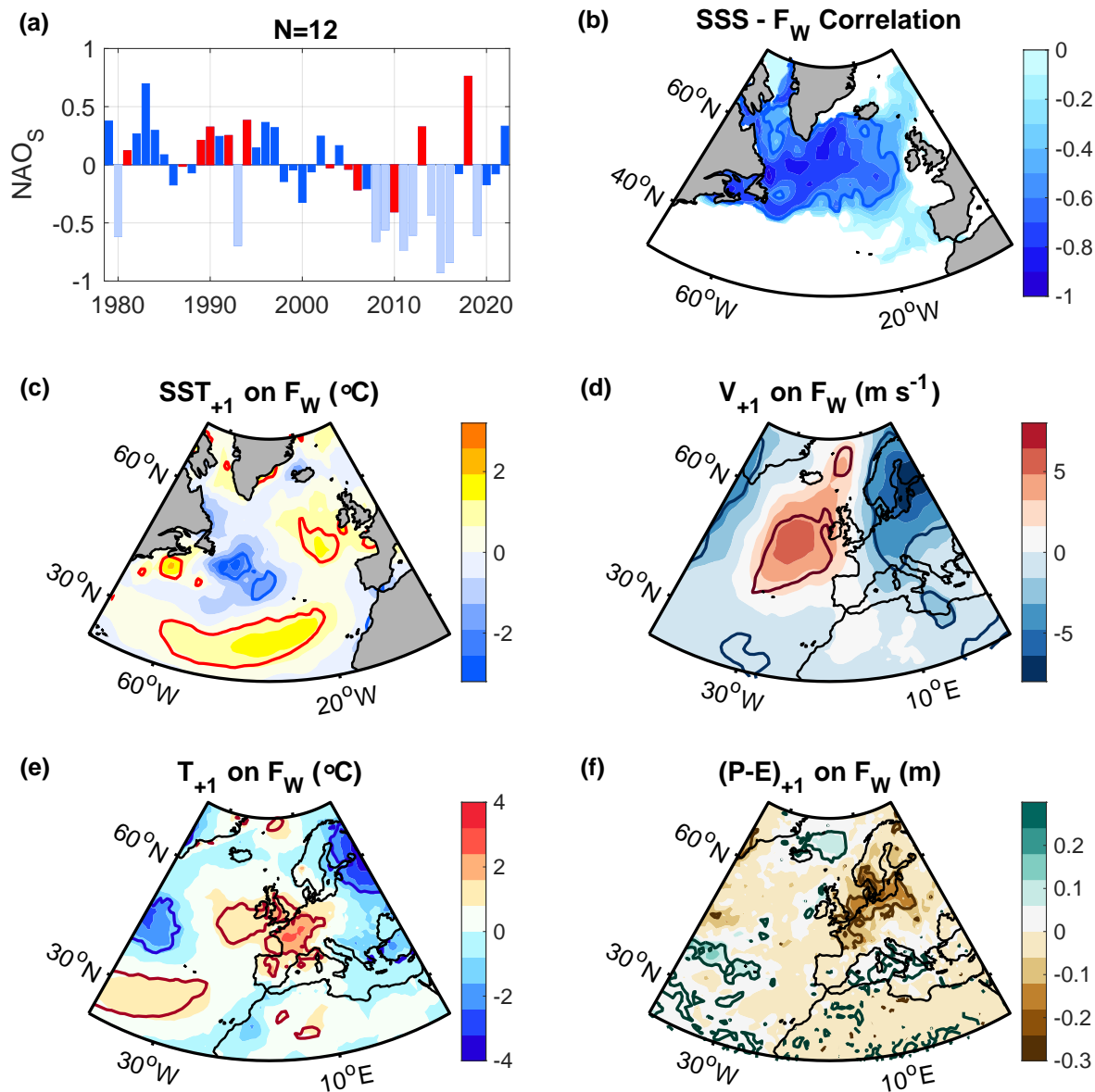
Figure B4. (a) Regression of the SST, averaged from May to August, onto ~NAO$_S$ As in July and August from the preceding year~Figure B3 but for $N = 12$ years.~(b) Time series of the vertical density gradient, obtained from Argo floats inside the box shown in (a), averaged within 2-week time windows, and smoothed by applying a 6-week running mean. (c) Regression of the time series in (b) onto ~NAO$_S$ from the preceding year. Thick contours encompass regions that are significant at the 95% confidence level.~

1030   ~gradients are spatially more uniform as they are typically linked to the surface forcing, which equally affects eddies, currents, or other spatially heterogenous regions. Thus, it is possible to construct continuous time series (Fig. C2b).~
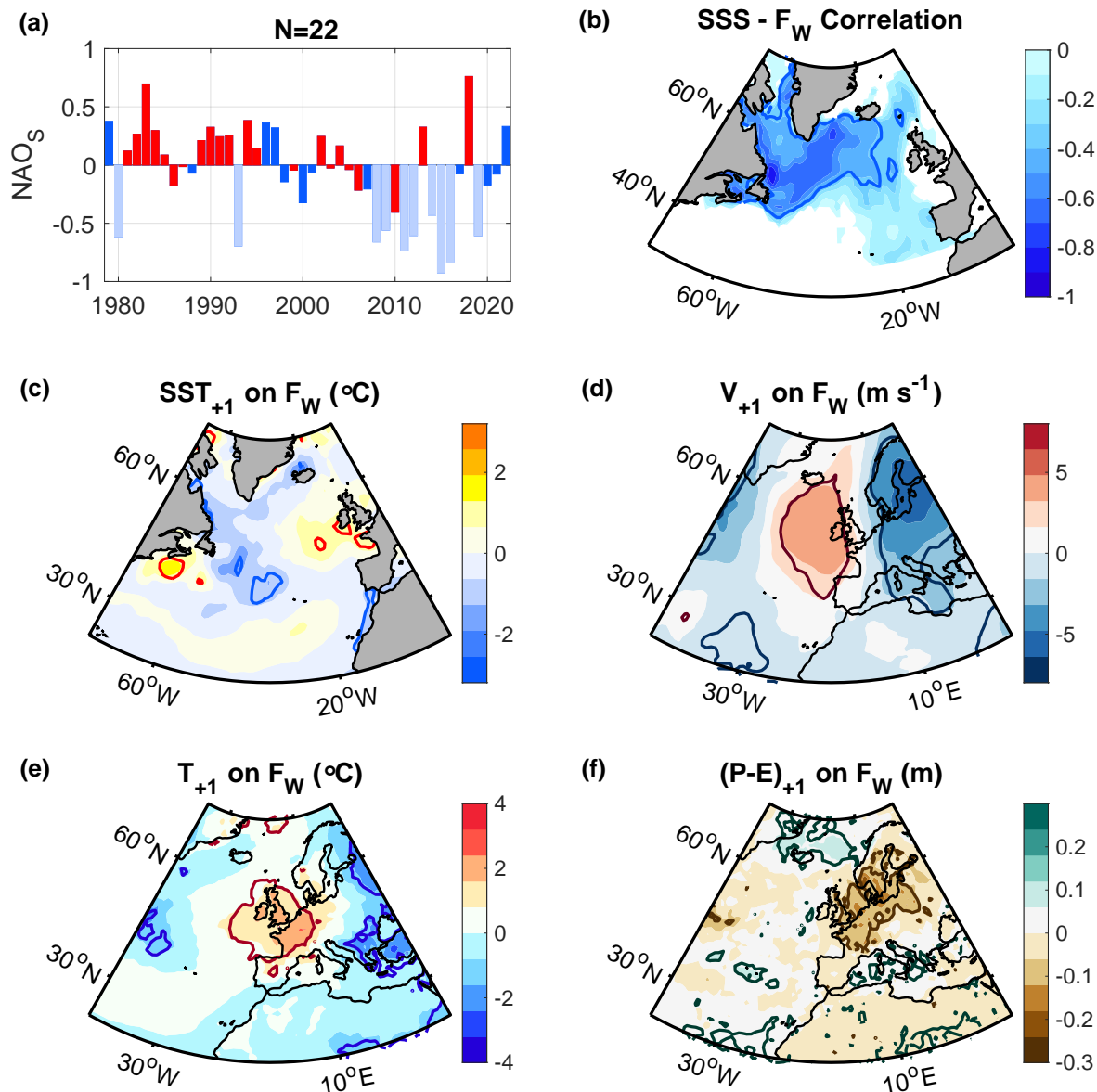
Figure B5. As in Figure B3 but for $N = 22$ years.

~~Next, we regress the obtained time series onto the summer NAO from the preceding year. We find a significant decrease in stratification that peaks near the surface, in the upper 50 m (Fig. C2c~~

Lastly, we tested if the results obtained with the ΔSST index (Fig. 7) remain significant if we lowpass filter the atmospheric anomalies in summer and assume a smaller number of degrees of freedom. In the lowpass filtering, we only consider the summer months (July and August). The ~~shallowness of the signal is consistent with wind-induced upwelling. Moreover, the~~
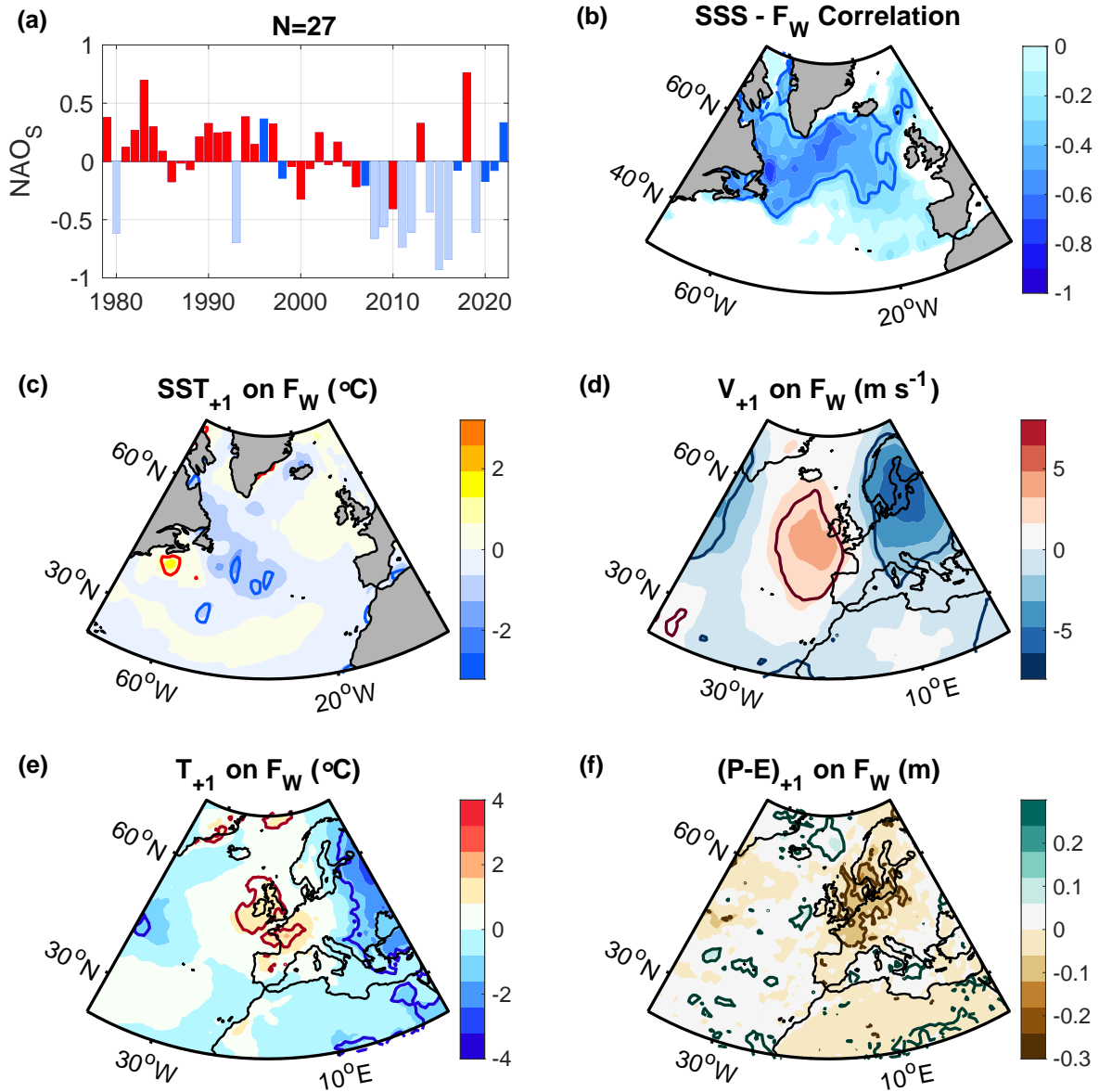
Figure B6. As in Figure B3 but for $N = 27$ years.
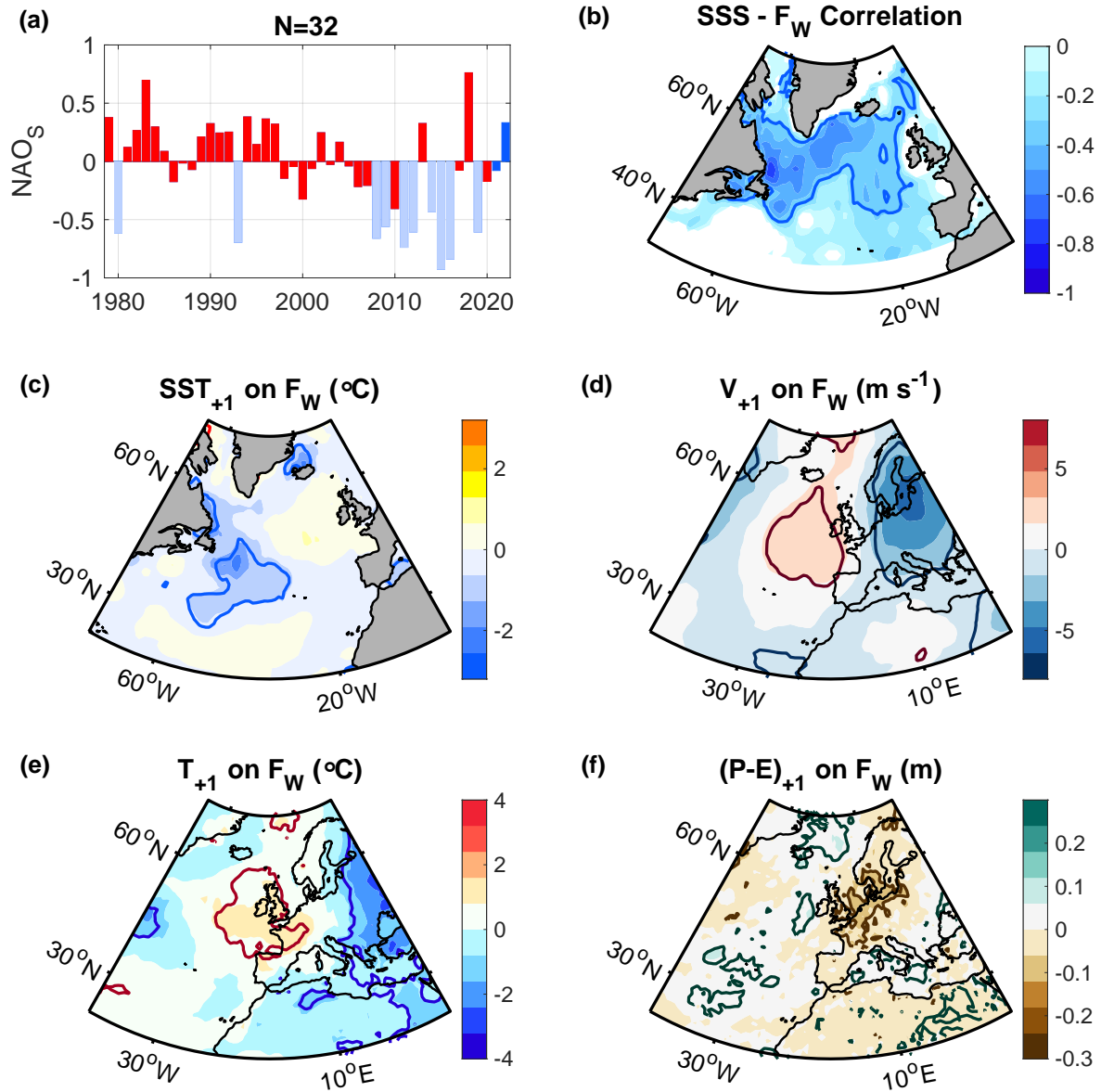
Figure B7. As in Figure B3 but for $N = 32$ years.

~~signal is strongest in July and August, when the temperature contrast across the coastline, and~~ filter does not include any other months. Thus, we lowpass filter the SST, winds at 700 hPa, the 2-m air temperature and precipitation minus evaporation variability with a 3-summer hanning filter. After the filtering, the resulting autocorrelations of European summer weather are still smaller than the one for the ΔSST index. Nonetheless, we estimate the number of degrees of freedom based on the ΔSST index, resulting in $N^* = \frac{N\Delta t}{2T_e} - 2$ degrees of freedom, where N here is the number of data points, Δt is the time interval between them, and T_e is the e-folding timescale of the autocorrelations (Leith, 1973), which is 2 years for the ΔSST index (Fig. 8a). While the regressions remain significant, their amplitude weakens (Fig. B8), indicating that the interannual variability, which has been filtered out, must have contributed to the increased relationship in the ~~temperature contrast between regions of upwelling and downwelling, is largest. Thus, the timing of the anomaly supports the role air-sea coupling in intensifying the cold anomaly signal (Section 4.7~~regressions obtained from the unfiltered time series (Fig. 7).
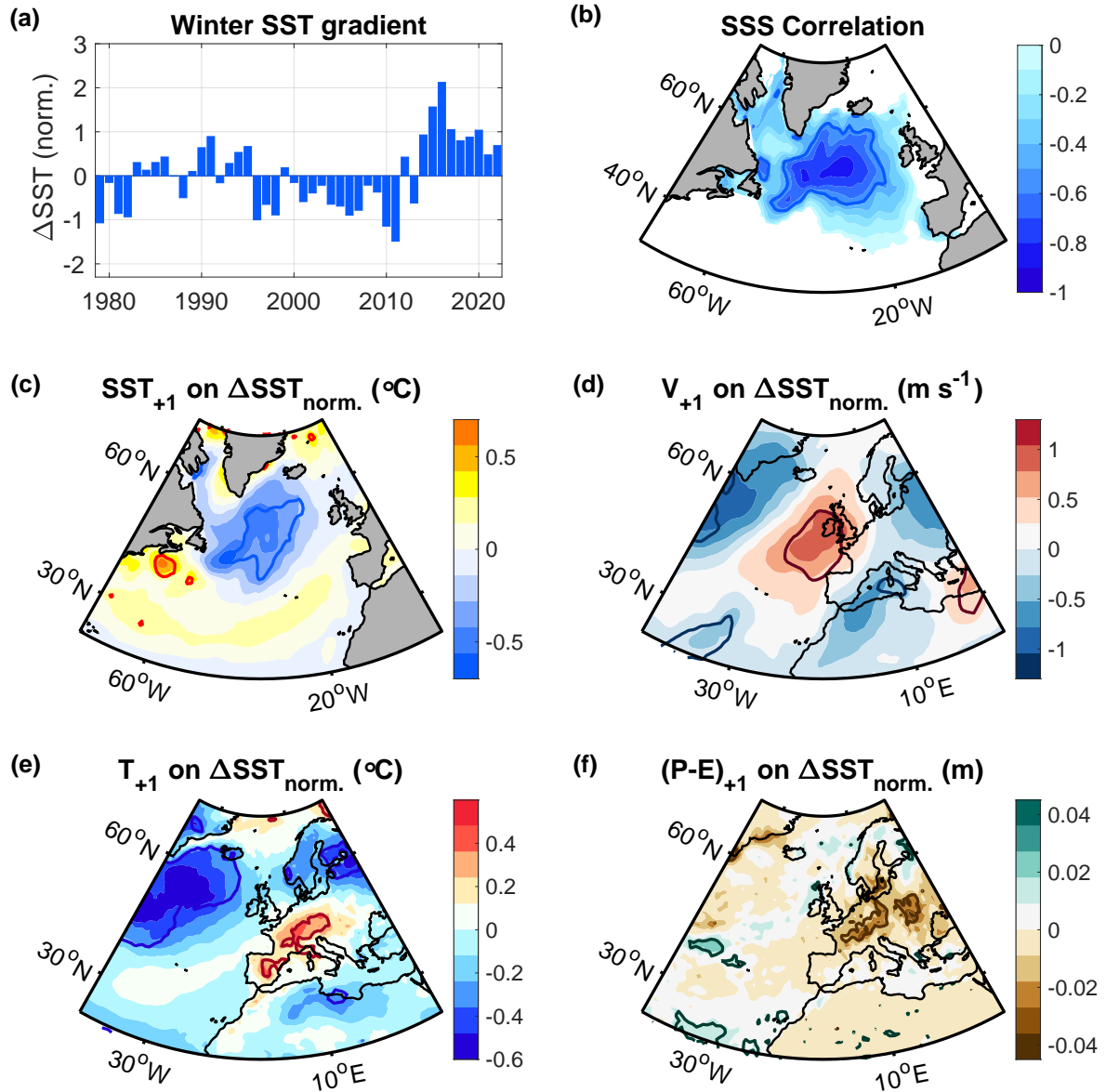
Figure B8. As in Figure 7 of the manuscript, after lowpass filtering the SST in summer (July and August), the 700 hPa winds in summer, and the 2-m air temperature and precipitation minus evaporation anomalies in summer, with a 3-summer hanning filter. The total number of degrees of freedom in the significance tests in all panels was estimated with $\frac{N\Delta t}{2T_e} - 2 = 9$, where N is the number of years (which is 44), Δt is one year, and T_e is the lag where the correlation drops to the e-folding value (~ 0.37), corresponding to ~ 2 years for the ΔSST index.

Table A1. List of years included in the three freshwater indices F_E, F_W and ΔSST. The years listed for F_E and F_W correspond to the years of the summer NAO index in July and August, while the period listed for ΔSST corresponds to the years of the SST anomalies in winter (January to March).

F_E	F_W	ΔSST
1980	1981	1979 – 2022
1993	1982	
2008	1984	
2009	1987	
2011	1989	
2012	1990	
2015	1991	
2016	1992	
	1994	
	1995	
	2003	
	2004	
	2005	
	2006	
	2010	
	2013	
	2018	

Author contributions. M.O. conceived the study, carried out the analyses and was lead writer of the text. P.H. facilitated the implementation of the study; J.S. provided guidance in the model analysis; S.B. helped to revise the paper.

Competing interests. The authors declare that they have no conflict of interest.

References

Amos, D. E. and Koopmans, L. H.: Tables of the distribution of the coefficient of coherence for stationary bivariate Gaussian processes, vol. 483, Sandia Corporation, 1963.

Arribas, A., Glover, M., Maidens, A., Peterson, K., Gordon, M., MacLachlan, C., Graham, R., Fereday, D., Camp, J., Scaife, A., et al.: The GloSea4 ensemble prediction system for seasonal forecasting, Monthly Weather Review, 139, 1891–1910, 2011.

Bamber, J., van den Broeke, M., Ettema, J., Lenaerts, J., and Rignot, E.: Recent large increases in freshwater fluxes from Greenland into the North Atlantic, Geophysical Research Letters, 39, 2012.

Bamber, J., Tedstone, A., King, M., Howat, I., Enderlin, E., van den Broeke, M., and Noel, B.: Land ice freshwater budget of the Arctic and North Atlantic Oceans: 1. Data, methods, and results, Journal of Geophysical Research: Oceans, 123, 1827–1837, 2018.

Bao, S., Wang, H., Zhang, R., Yan, H., and Chen, J.: Comparison of satellite-derived sea surface salinity products from SMOS, Aquarius, and SMAP, Journal of Geophysical Research: Oceans, 124, 1932–1944, 2019.

Barnes, E. A.: Revisiting the evidence linking Arctic amplification to extreme weather in midlatitudes, Geophysical research letters, 40, 4734–4739, 2013.

Barnston, A. G. and Livezey, R. E.: Classification, seasonality and persistence of low-frequency atmospheric circulation patterns, Monthly weather review, 115, 1083–1126, 1987.

Blackport, R. and Screen, J. A.: Insignificant effect of Arctic amplification on the amplitude of midlatitude atmospheric waves, Science advances, 6, eaay2880, 2020.

Böning, C. W., Behrens, E., Biastoch, A., Getzlaff, K., and Bamber, J. L.: Emerging impact of Greenland meltwater on deepwater formation in the North Atlantic Ocean, Nature Geoscience, 9, 523–527, 2016.

Booth, J. F., Naud, C. M., and Willison, J.: Evaluation of extratropical cyclone precipitation in the North Atlantic basin: An analysis of ERA-Interim, WRF, and two CMIP5 models, Journal of Climate, 31, 2345–2360, 2018.

Briner, J. P., Cuzzone, J. K., Badgeley, J. A., Young, N. E., Steig, E. J., Morlighem, M., Schlegel, N.-J., Hakim, G. J., Schaefer, J. M., Johnson, J. V., et al.: Rate of mass loss from the Greenland Ice Sheet will exceed Holocene values this century, Nature, 586, 70–74, 2020.

Carmack, E. C., Yamamoto-Kawai, M., Haine, T. W., Bacon, S., Bluhm, B. A., Lique, C., Melling, H., Polyakov, I. V., Straneo, F., Timmermans, M.-L., et al.: Freshwater and its role in the Arctic Marine System: Sources, disposition, storage, export, and physical and biogeochemical consequences in the Arctic and global oceans, Journal of Geophysical Research: Biogeosciences, 121, 675–717, 2016.

Cohen, J., Screen, J. A., Furtado, J. C., Barlow, M., Whittleston, D., Coumou, D., Francis, J., Dethloff, K., Entekhabi, D., Overland, J., et al.: Recent Arctic amplification and extreme mid-latitude weather, Nature geoscience, 7, 627–637, 2014.

Cohen, J., Zhang, X., Francis, J., Jung, T., Kwok, R., Overland, J., Ballinger, T., Bhatt, U., Chen, H., Coumou, D., et al.: Divergent consensuses on Arctic amplification influence on midlatitude severe winter weather, Nature Climate Change, pp. 1–10, 2019.

Czaja, A. and Frankignoul, C.: Observed impact of Atlantic SST anomalies on the North Atlantic Oscillation, Journal of Climate, 15, 606–623, 2002.

Davies, H. and Bishop, C.: Eady edge waves and rapid development, Journal of the atmospheric sciences, 51, 1930–1946, 1994.

Dierer, S., Schluenzen, K. H., et al.: Influence parameters for a polar mesocyclone development, METEOROLOGISCHE ZEITSCHRIFT-BERLIN-, 14, 781, 2005.

Dong, B., Sutton, R. T., Woollings, T., and Hodges, K.: Variability of the North Atlantic summer storm track: Mechanisms and impacts on European climate, Environmental Research Letters, 8, 034 037, 2013.

57

Duchez, A., Frajka-Williams, E., Josey, S. A., Evans, D. G., Grist, J. P., Marsh, R., McCarthy, G. D., Sinha, B., Berry, D. I., and Hirschi, J. J.: Drivers of exceptionally cold North Atlantic Ocean temperatures and their link to the 2015 European heat wave, Environmental Research Letters, 11, 074 004, 2016.

Dukhovskoy, D., Yashayaev, I., Proshutinsky, A., Bamber, J., Bashmachnikov, I., Chassignet, E., Lee, C., and Tedstone, A.: Role of Greenland freshwater anomaly in the recent freshening of the subpolar North Atlantic, Journal of Geophysical Research: Oceans, 124, 3333–3360, 2019.

Dunstone, N., Smith, D., Scaife, A., Hermanson, L., Fereday, D., O'Reilly, C., Stirling, A., Eade, R., Gordon, M., MacLachlan, C., et al.: Skilful seasonal predictions of summer European rainfall, Geophysical Research Letters, 45, 3246–3254, 2018.

Eady, E. T.: Long waves and cyclone waves, Tellus, 1, 33–52, 1949.

Ferrari, R. and Wunsch, C.: Ocean circulation kinetic energy: Reservoirs, sources, and sinks, Annual Review of Fluid Mechanics, 41, 253–282, 2009.

Fettweis, X., Box, J. E., Agosta, C., Amory, C., Kittel, C., Lang, C., van As, D., Machguth, H., and Gallée, H.: Reconstructions of the 1900–2015 Greenland ice sheet surface mass balance using the regional climate MAR model, The Cryosphere, 11, 1015–1033, 2017.

Francis, J. A. and Vavrus, S. J.: Evidence linking Arctic amplification to extreme weather in mid-latitudes, Geophysical research letters, 39, 2012.

Fratantoni, P. S. and McCartney, M. S.: Freshwater export from the Labrador Current to the North Atlantic Current at the Tail of the Grand Banks of Newfoundland, Deep Sea Research Part I: Oceanographic Research Papers, 57, 258–283, 2010.

Gervais, M., Shaman, J., and Kushnir, Y.: Impact of the North Atlantic Warming Hole on Sensible Weather, Journal of Climate, 33, 4255–4271, 2020.

Gill, A. E.: Atmosphere—ocean dynamics, Elsevier, 2016.

Griffies, S. M. and Greatbatch, R. J.: Physical processes that impact the evolution of global mean sea level in ocean climate models, Ocean Modelling, 51, 37–72, 2012.

Häkkinen, S.: Freshening of the Labrador Sea surface waters in the 1990s: Another great salinity anomaly?, Geophysical Research Letters, 29, 85–1, 2002.

Häkkinen, S. and Rhines, P. B.: Shifting surface currents in the northern North Atlantic Ocean, Journal of Geophysical Research: Oceans, 114, 2009.

Häkkinen, S., Rhines, P. B., and Worthen, D. L.: Warm and saline events embedded in the meridional circulation of the northern North Atlantic, Journal of Geophysical Research: Oceans, 116, 2011a.

Häkkinen, S., Rhines, P. B., and Worthen, D. L.: Atmospheric blocking and Atlantic multidecadal ocean variability, Science, 334, 655–659, 2011b.

Häkkinen, S., Rhines, P. B., and Worthen, D. L.: Northern North Atlantic sea surface height and ocean heat content variability, Journal of Geophysical Research: Oceans, 118, 3670–3678, 2013.

Hanna, E., Jones, J. M., Cappelen, J., Mernild, S. H., Wood, L., Steffen, K., and Huybrechts, P.: The influence of North Atlantic atmospheric and oceanic forcing effects on 1900–2010 Greenland summer climate and ice melt/runoff, International Journal of Climatology, 33, 862–880, 2013.

Hanna, E., Cappelen, J., Fettweis, X., Mernild, S. H., Mote, T. L., Mottram, R., Steffen, K., Ballinger, T. J., and Hall, R. J.: Greenland surface air temperature changes from 1981 to 2019 and implications for ice-sheet melt and mass-balance change, International Journal of Climatology, 41, E1336–E1352, 2021.

Hátún, H., Sandø, A. B., Drange, H., Hansen, B., and Valdimarsson, H.: Influence of the Atlantic subpolar gyre on the thermohaline circulation, Science, 309, 1841–1844, 2005.

Hersbach, H., Bell, B., Berrisford, P., Biavati, G., Horányi, A., Muñoz Sabater, J., Nicolas, J., Peubey, C., Radu, R., Rozum, I., et al.: ERA5 hourly data on single levels from 1979 to present, Copernicus Climate Change Service (C3S) Climate Data Store (CDS), 10, 2018.

1135 Heuzé, C.: North Atlantic deep water formation and AMOC in CMIP5 models, Ocean Science, 13, 609, 2017.

Holliday, N. P., Bersch, M., Berx, B., Chafik, L., Cunningham, S., Florindo-López, C., Hátún, H., Johns, W., Josey, S. A., Larsen, K. M. H., et al.: Ocean circulation causes the largest freshening event for 120 years in eastern subpolar North Atlantic, Nature Communications, 11, 1–15, 2020.

Holte, J., Talley, L. D., Gilson, J., and Roemmich, D.: An Argo mixed layer climatology and database, Geophysical Research Letters, 44,
1140 5618–5626, 2017.

Hurrell, J. W., Hack, J. J., Shea, D., Caron, J. M., and Rosinski, J.: A new sea surface temperature and sea ice boundary dataset for the Community Atmosphere Model, Journal of Climate, 21, 5145–5153, 2008.

Khan, S. A., Aschwanden, A., Bjørk, A. A., Wahr, J., Kjeldsen, K. K., and Kjaer, K. H.: Greenland ice sheet mass balance: a review, Reports on progress in physics, 78, 046 801, 2015.

1145 Kodama, C., Stevens, B., Mauritsen, T., Seiki, T., and Satoh, M.: A new perspective for future precipitation change from intense extratropical cyclones, Geophysical Research Letters, 46, 12 435–12 444, 2019.

Kostov, Y., Johnson, H. L., Marshall, D. P., Heimbach, P., Forget, G., Holliday, N. P., Lozier, M. S., Li, F., Pillar, H. R., and Smith, T.: Distinct sources of interannual subtropical and subpolar Atlantic overturning variability, Nature Geoscience, 14, 491–495, 2021.

Koul, V., Tesdal, J.-E., Bersch, M., Hátún, H., Brune, S., Borchert, L., Haak, H., Schrum, C., and Baehr, J.: Unraveling the choice of the
1150 north Atlantic subpolar gyre index, Scientific reports, 10, 1–12, 2020.

Kumar, A., Yadav, J., and Mohan, R.: Global warming leading to alarming recession of the Arctic sea-ice cover: Insights from remote sensing observations and model reanalysis, Heliyon, 6, e04 355, 2020.

Lashof, D. A. and Ahuja, D. R.: Relative contributions of greenhouse gas emissions to global warming, Nature, 344, 529–531, 1990.

Le Traon, P., Nadal, F., and Ducet, N.: An improved mapping method of multisatellite altimeter data, Journal of atmospheric and oceanic
1155 technology, 15, 522–534, 1998.

Leith, C.: The standard error of time-average estimates of climatic means, Journal of Applied Meteorology (1962-1982), pp. 1066–1069, 1973.

Lindzen, R. and Farrell, B.: A simple approximate result for the maximum growth rate of baroclinic instabilities, Journal of the atmospheric sciences, 37, 1648–1654, 1980.

1160 Liu, W., Xie, S.-P., Liu, Z., and Zhu, J.: Overlooked possibility of a collapsed Atlantic Meridional Overturning Circulation in warming climate, Science Advances, 3, e1601 666, 2017.

Marshall, J., Johnson, H., and Goodman, J.: A study of the interaction of the North Atlantic Oscillation with ocean circulation, Journal of Climate, 14, 1399–1421, 2001.

Marzocchi, A., Hirschi, J. J.-M., Holliday, N. P., Cunningham, S. A., Blaker, A. T., and Coward, A. C.: The North Atlantic subpolar circulation
1165 in an eddy-resolving global ocean model, Journal of Marine Systems, 142, 126–143, 2015.

McDougall, T., Feistel, R., Millero, F., Jackett, D., Wright, D., King, B., Marion, G., Chen, C., Spitzer, P., and Seitz, S.: The international thermodynamic equation of seawater 2010 (TEOS-10): Calculation and use of thermodynamic properties, Global ship-based repeat hydrography manual, IOCCP report no, 14, 2009.

Mecking, J., Drijfhout, S., Jackson, L., and Andrews, M.: The effect of model bias on Atlantic freshwater transport and implications for AMOC bi-stability, Tellus A: Dynamic Meteorology and Oceanography, 69, 1299 910, 2017.

Mecking, J., Drijfhout, S., Hirschi, J. J., and Blaker, A.: Ocean and atmosphere influence on the 2015 European heatwave, Environmental Research Letters, 14, 114 035, 2019.

Menary, M. B., Hodson, D. L., Robson, J. I., Sutton, R. T., Wood, R. A., and Hunt, J. A.: Exploring the impact of CMIP5 model biases on the simulation of North Atlantic decadal variability, Geophysical Research Letters, 42, 5926–5934, 2015.

Müller, V., Kieke, D., Myers, P. G., Pennelly, C., Steinfeldt, R., and Stendardo, I.: Heat and freshwater transport by mesoscale eddies in the southern subpolar North Atlantic, Journal of Geophysical Research: Oceans, 124, 5565–5585, 2019.

Munk, W. H.: On the wind-driven ocean circulation, Journal of Atmospheric Sciences, 7, 80–93, 1950.

Murray, D., Hoell, A., Hoerling, M., Perlwitz, J., Quan, X.-W., Allured, D., Zhang, T., Eischeid, J., Smith, C. A., Barsugli, J., et al.: Facility for Weather and Climate Assessments (FACTS): A Community Resource for Assessing Weather and Climate Variability, Bulletin of the American Meteorological Society, 101, E1214–E1224, 2020.

Neale, R. B., Chen, C.-C., Gettelman, A., Lauritzen, P. H., Park, S., Williamson, D. L., Conley, A. J., Garcia, R., Kinnison, D., Lamarque, J.-F., et al.: Description of the NCAR community atmosphere model (CAM 5.0), NCAR Tech. Note NCAR/TN-486+ STR, 1, 1–12, 2012.

Notz, D. and Stroeve, J.: The trajectory towards a seasonally ice-free Arctic ocean, Current climate change reports, 4, 407–416, 2018.

Oltmanns, M., Karstensen, J., Moore, G., and Josey, S. A.: Rapid cooling and increased storminess triggered by freshwater in the North Atlantic, Geophysical Research Letters, p. e2020GL087207, 2020.

Omrani, N.-E., Ogawa, F., Nakamura, H., Keenlyside, N., Lubis, S. W., and Matthes, K.: Key Role of the Ocean Western Boundary currents in shaping the Northern Hemisphere climate, Scientific reports, 9, 1–12, 2019.

O'Reilly, C. H., Minobe, S., Kuwano-Yoshida, A., and Woollings, T.: The Gulf Stream influence on wintertime North Atlantic jet variability, Quarterly Journal of the Royal Meteorological Society, 143, 173–183, 2017.

Osborne, J. M., Collins, M., Screen, J. A., Thomson, S. I., and Dunstone, N.: The North Atlantic as a driver of summer atmospheric circulation, Journal of Climate, 33, 7335–7351, 2020.

Overland, J., Francis, J. A., Hall, R., Hanna, E., Kim, S.-J., and Vihma, T.: The melting Arctic and midlatitude weather patterns: Are they connected?, Journal of Climate, 28, 7917–7932, 2015.

Piron, A., Thierry, V., Mercier, H., and Caniaux, G.: Gyre-scale deep convection in the subpolar North Atlantic Ocean during winter 2014–2015, Geophysical Research Letters, 44, 1439–1447, 2017.

Priestley, M.: Spectral analysis and time series, number v. 1-2 in Probability and mathematical statistics, Academic Press, 86, 328, 1982.

Proshutinsky, A., Dukhovskoy, D., Timmermans, M.-L., Krishfield, R., and Bamber, J. L.: Arctic circulation regimes, Philosophical Transactions of the Royal Society A: Mathematical, Physical and Engineering Sciences, 373, 20140 160, 2015.

Rayner, N., Parker, D. E., Horton, E., Folland, C. K., Alexander, L. V., Rowell, D., Kent, E., and Kaplan, A.: Global analyses of sea surface temperature, sea ice, and night marine air temperature since the late nineteenth century, Journal of Geophysical Research: Atmospheres, 108, 2003.

Reuter, M., Buchwitz, M., Schneising, O., Noël, S., Bovensmann, H., Burrows, J. P., Boesch, H., Di Noia, A., Anand, J., Parker, R. J., et al.: Ensemble-based satellite-derived carbon dioxide and methane column-averaged dry-air mole fraction data sets (2003–2018) for carbon and climate applications, Atmospheric Measurement Techniques, 13, 789–819, 2020.

Reynolds, R. W., Rayner, N. A., Smith, T. M., Stokes, D. C., and Wang, W.: An improved in situ and satellite SST analysis for climate, Journal of climate, 15, 1609–1625, 2002.

Roeckner, E., Bäuml, G., Bonaventura, L., Brokopf, R., Esch, M., Giorgetta, M., Hagemann, S., Kirchner, I., Kornblueh, L., Manzini, E., et al.: The atmospheric general circulation model ECHAM 5. PART I: Model description, Accessed March 2020., 2003.

Schmidt, S. and Send, U.: Origin and composition of seasonal Labrador Sea freshwater, Journal of Physical Oceanography, 37, 1445–1454, 2007.

Screen, J. A. and Simmonds, I.: Exploring links between Arctic amplification and mid-latitude weather, Geophysical Research Letters, 40, 959–964, 2013.

Sgubin, G., Swingedouw, D., Drijfhout, S., Mary, Y., and Bennabi, A.: Abrupt cooling over the North Atlantic in modern climate models, Nature Communications, 8, 14 375, 2017.

Simmons, A. J.: Trends in the tropospheric general circulation from 1979 to 2022, Weather and Climate Dynamics, 3, 777–809, 2022.

Spall, M. A. and Pickart, R. S.: Wind-driven recirculations and exchange in the Labrador and Irminger Seas, Journal of Physical Oceanography, 33, 1829–1845, 2003.

Stommel, H.: The westward intensification of wind-driven ocean currents, Eos, Transactions American Geophysical Union, 29, 202–206, 1948.

Talley, L. D.: Descriptive physical oceanography: an introduction, Academic press, 2011.

Tang, Q., Zhang, X., and Francis, J. A.: Extreme summer weather in northern mid-latitudes linked to a vanishing cryosphere, Nature Climate Change, 4, 45–50, 2014.

Tesdal, J.-E., Abernathey, R. P., Goes, J. I., Gordon, A. L., and Haine, T. W.: Salinity trends within the upper layers of the subpolar North Atlantic, Journal of Climate, 31, 2675–2698, 2018.

Timlin, M. S., Alexander, M. A., and Deser, C.: On the reemergence of North Atlantic SST anomalies, Journal of climate, 15, 2707–2712, 2002.

Vallis, G. K.: Atmospheric and oceanic fluid dynamics, Cambridge University Press, 2017.

Woollings, T., Hannachi, A., and Hoskins, B.: Variability of the North Atlantic eddy-driven jet stream, Quarterly Journal of the Royal Meteorological Society, 136, 856–868, 2010.

Wu, Y., Park, T., Park, W., and Latif, M.: North Atlantic climate model bias influence on multiyear predictability, Earth and Planetary Science Letters, 481, 171–176, 2018.

Wunsch, C. and Ferrari, R.: Vertical mixing, energy, and the general circulation of the oceans, Annu. Rev. Fluid Mech., 36, 281–314, 2004.

Xie, J., Raj, R. P., Bertino, L., Samuelsen, A., and Wakamatsu, T.: Evaluation of Arctic Ocean surface salinities from the Soil Moisture and Ocean Salinity (SMOS) mission against a regional reanalysis and in situ data, Ocean Science, 15, 1191–1206, 2019.

Yashayaev, I. and Loder, J. W.: Further intensification of deep convection in the Labrador Sea in 2016, Geophysical Research Letters, 44, 1429–1438, 2017.

Yu, H., Screen, J. A., Hay, S., Catto, J. L., and Xu, M.: Winter Precipitation Responses to Projected Arctic Sea-Ice Loss and Global Ocean Warming and Their Opposing Influences over Northeast Atlantic region, Journal of Climate, pp. 1–33, 2023.

Zhao, J. and Johns, W.: Wind-forced interannual variability of the Atlantic Meridional Overturning Circulation at 26.5 N, Journal of Geophysical Research: Oceans, 119, 2403–2419, 2014.